Micropatterns for surface potential mapping of biomolecules by kelvin probe force microscopy

Ruiz Ortega, Leonardo Ibor

Awarding institution:
King's College London

MICRO PATTERNS FOR SURFACE POTENTIAL MAPPING OF BIOMOLECULES BY KELVIN PROBE FORCE MICROSCOPY

By

Leonardo Ibor Ruiz Ortega

Student number: 1424918

A thesis submitted in partial fulfilment of the requirements for the degree of Doctor of Philosophy in Physics

to

King's College London
University of London

School of Natural & Mathematical Sciences
Department of Physics
Biological Physics and Soft Matter group

July 2018

DECLARATION OF AUTHORSHIP

I confirm that the following thesis does not exceed the word limit prescribed in the College regulations. I further confirm that the work presented in the thesis is my own and all references are cited accordingly. The copyright of this thesis rests with the author and no quotation from it or information derived from it may be published without proper acknowledgement.

To my parents, Irma and Leonardo

Acknowledgments

I would like to thank the national council of science and technology (CONACyT) in Mexico for the financial support provided through its student grant scheme for international PhD programs. My immense gratitude goes to my supervisor Dr. Patrick Mesquida for all the enormous support and advice provided in every single aspect that a PhD student might need. Without his permanent presence and attention this dissertation would not have been possible. I appreciate the great job he did as supervisor, mentor and friend during the period of my studies at King's. Throughout the time at King's I had the valuable opportunity of meeting outstanding PhD students, scientist and friends, who all at some point contributed to the development of my PhD project. My special thanks goes to Alix, Soraya, Yurema, Ankur, Jorge and Margoth, without them, the department of physics would not have been such a pleasant experience during the last few years. To a great extent, my work in the labs would not have been as smooth if it wasn't because of the help of William Luckhurst, since he always had a positive attitude and quick solutions to any problem that was encountered in the lab. Also, it is important for me to express great gratitude to the administrative staff at King's who were always to a large degree, very kind and helpful. Rowena Peake, James French, Paul Le Long and Megan Grace-Hughes, without them, finishing a PhD would not be humanly possible.

Abstract

Current methods to detect and quantify electrostatic properties of biomolecules, nowadays, still facing many challenges. For instance, they are not sensitive enough to meet the needs of more precise measurements, they require the use of external markers or antibodies, or rely on indirect calculations or models such is the case for zeta potential and electrophoretic mobility. However, Kelvin probe force microscopy (KPFM) have gained attention due to its expanding possibilities to asses electrostatic properties of biomolecules. Among the advantages that KPFM possess over other methods, stands out its high sensitivity and spatial resolution. Moreover, it does not require the use of external labels. In the interest of establishing a method for mapping surface potential of biomolecules by means of Kelvin probe force microscopy, two techniques of p*oly-dimethylsiloxane* (PDMS) soft lithography for micro-patterning (micro channel filling and micro contact printing) are studied. Similarly, the possibility of patterning biomolecules on different substrates (mica, glass and silicon dioxide) is explored. Primarily, poly-L-lysine was used as a model biomolecule due to the exposure of amino functional groups. Different physicochemical conditions on poly-Llysine micro patterns were tested in order to assess the suitability of soft lithography combined with KPFM to measure electrostatic properties of biomolecules. In this sense, continuous KPFM scans, immersions in water, lift height and time dependence were investigated. Moreover, due to the importance of the understanding of the effects of exposure of biomolecules to elevated levels of sugars, immersions in D-ribose were performed. A concentration dependent effect was observed, affecting drastically the surface potential of polyL-lysine. Electrostatically driven patterning of colloidal gold nanoparticles was also achieved on pol-L-lysine micro patterns,

resulting in a good method for marking the presence of pol-Llysine and opening the possibility to improve some properties of nanoparticle systems. Besides microchannel filling, micro contact printing of poly-L-lysine was successfully achieved on mica, glass and silicon dioxide, resulting in better quality micro patterns and understanding of the influence of using different substrates on surface potential. On this regard, continuous KPFM scans revealed a surface charge dynamic on mica, whereas on glass and silicon dioxide surface potential became more stable. Insulin, BSA and β-lactoglobulin were successfully patterned on mica by micro contact printing and imaged by KPFM. Response to pH and immersions in water was investigated showinga clear reversible shift on surface potential. Similarly, cross-patterning of different proteins on the same substrate for surface potential oneto-one comparison was successfully achieved. The classic case of avidin-biotin complex was also investigated byboth fluorescence optical microscopy and KPFM. Finally, in an attempt to stretch the applications of KPFM for surface potential mapping of biomolecules, insulin amyloid fibrils were co-fibrillated with highly charge nanoparticles. Surface potential maps of amyloid structures were achieved and the effect of continuous scanning on surface potential was assessed.

Table of contents

List of Figures

List of tables

Nomeclature

Symbol	Meaning
AC	Alternating current
AD	Alzheimer's disease
AFM	Atomic force microscopy
AGE's	Advance glycation end products
Ala	Alanine
AM-KPFM	Amplitude modulated Kelvin probe force microscopy
ApoE	Apolipoprotein E
APP	Amyloid precursor protein
Arg	Arginine
Asp	Aspartic acid
AuNp	Gold nanoparticle
Aβ	Amyloid beta
BSA	Bovine serum albumin
CAS	Chemical Abstracts Service
Cα	Alpha carbon
DC	Direct current
dH	Hydrodynamic radius
DLS	Dynamic light scattering

DNA	Deoxyribonucleic acid
EDL	Electric double layer
FM-KPFM	Frequency modulated Kelvin probe force microscopy
GCS	Gouy-Chapman model
Gly	Glycine
HMDS	Hexamethyldisilazane
Hz	Hertz
I	Isoleucine
IAPP	Isle amyloid polypeptide
k	Boltzmann's constant
*k*DA	Kilo Dalton
kHz	Kilohertz
KPFM	Kelvin probe force microscopy
mV	Millivolt
nm	Nanometre
OD	Optical density
PD	Parkinson's disease
PDMS	Polydimethylsiloxane
pH	Potential of hydrogen
pI	Isoelectric point
pKa	Negative logarithm of the acid dissociation constant
PLL	poly-L-lysine

PTM	Post-translational modification
q	Charge
QS	Quorum sensing
r	Radius
RMS	Root mean square
Rq	Roughness
SAP	serum amyloid P component
SDS	Sodium dodecyl sulphate
SEM	Scanning electron microscopy
SPM	Scanning probe microscopy
T	Temperature
TEM	Transmission electron microscopy
UV-Vis	Ultraviolet-visible spectroscopy
α-Syn	Alpha synuclein
γep	Electrophoretic mobility
ΔΦ	Surface potential difference
ζp	Zeta potential
η	Viscosity
μm	Micrometre

CHAPTER 1 :

Motivation and background

1.1 Motivation

The aim of this dissertation is to establish a method for determining electrostatic properties of biomolecules by a combination of micro construction techniques based on soft lithography and Kelvin force microscopy. At the same time, the possibilities of detecting the presence of molecules, nanoparticles and biochemical modifications on biomolecules is further explored.

Fabrication of biomolecular patterned structures on solid surfaces is of great importance for a variety of applications such as biosensors [1], tissue engineering and the understanding of fundamental biological phenomena [2]. Different methods for patterning biomolecules include photolithography, photochemistry, and self-assembled monolayers [3].

However, soft lithography, a technique based on the use of elastomeric stamps, mostly polydimethylsiloxane (PDMS), stands out from other techniques due to its versatility, facile preparation and low cost. While obtaining micro patterns and surface potential maps of biomolecules by a combination of PDMS soft lithography and KPFM is in the interest of different areas, in this case, the relevance resides on the possibility of studying fundamental phenomena of biological and chemical processes in relation to surface potential. Electrostatics plays an important role in biological phenomena.

For this reason, the development of techniques that are able detect biochemical changes and molecular interactions that cause alterations on electrostatic properties of biomolecules is crucial.

Existing approaches such as zeta potential [4], capillary electrophoresis [5], and molecular dynamic simulations [6], to name a few, have the purpose to understand electrostatic properties and interactions in biomolecules. Furthermore, from the analytical perspective, detection of compounds and biochemical modifications still faces many challenges in the area of biochemistry and biophysics.

This is to say, current methods are in most cases, not sensitive enough. They require the use of external markers or antibodies, and are not observable with spatial resolution in two dimensions. Specifically, these techniques rely on spectroscopic principles such as infrared spectroscopy [7] for detecting physicochemical modifications, UV-Vis, and fluorescence for biomolecular interaction visualization [8]. Commonly, antibodies are used to detect the presence of proteins, interactions and biochemical reactions complexes [9][10][11].

However, when using antibodies, the sample is greatly affected and generally cannot be used again for future experiments. Furthermore, electrostatic properties of proteins determine a wide variety of fundamental processes such as association of receptors with charged ligands [12][13], binding of substrates by enzymes, catalysis of reactions [14][15], formation of protein-protein, protein-nucleic acid complexes [16], transfer of electrons, selective transport of ions in protein channels [17], denaturation of proteins at high and low pH values, and also incorporation of proteins

into amyloid fibres. It is for this reason that the understanding of the role of electrostatics in biological and chemical processes is in need of additional approaches. Following existent knowledge on electrostatic properties of biomolecules and functional groups by KPFM[18][19], in this work, Kelvin probe force microscopy (KPFM) in combination with micro construction techniques based on PDMS soft lithography is proposed for the first time as a strong method not only to characterize electrostatic properties of biomolecules, but to detect the presence, distribution and surface behavior of compounds like sugars, receptors and free charges with high sensitivity and spatial resolution.

More specifically, the present investigation seeks to establish the bases for further experiments towards fundamental biophysical questions. In the following sections, important aspects of background and introductory information are presented.

1.2 Background

1.2.1 The concept of pH

The electrostatic charge of biomolecules in solution is highly dependent on pH or potential of hydrogen. For this reason, it is of great importance to present a brief description in this dissertation.

The first scientist to formulate the concept of pH was the Danish chemist S.P.L Sørensen. While working on problems related to beer brewing where the control of acidity is of great importance, it occurred to him to simplify the concentration of H^+

ions in a scale. As defined by Sørensen, pH is a logarithm (base 10) of the molar concentration of hydrogen ions. The sign is changed so pH values are positive [20].

$$pH = log\frac{1}{[H^+]} = -log[H^+] \text{ Eq. 1}$$

Normally, in water (H_2O), a small number of the molecules dissociate and some of them lose hydrogen to yield hydroxide ions (OH^-). The free hydrogen ions can be added up to water molecules and form hydronium ions (H_3O^+).

Whether a solution is acidic or basic is determined by the amount of hydronium ions dissolved. For practical reasons, hydronium ions (H_3O^+) can be referred to as hydrogen ions (H^+). In ultrapure water the amount of hydrogen and hydroxide ions is equal, for that reason, the solution is considered to be neither acidic nor basic.

An acidic substance donates hydrogen ions, resulting in a shift on the balance between hydrogen and hydroxide ions. When there are more hydrogen ions than hydroxide ions, the solution is considered to be acidic. In contrast, a basic substance accepts hydrogen ions. In this case, hydroxide ions outnumber hydrogen ions, so the solution is considered to be alkaline.

Usually, measuring scale of pH ranges from 0 to 14, where 0 corresponds to the most acidic, 7 to neutral and 14 to most alkaline. However, an acid that yields a concentration of hydrogen ions with a molarity greater than 1, can be considered to have a negative pH.

1.2.2 Basic structure of amino acids

In order to introduce what determines the charge of biomolecules it is important to briefly discuss the basic structure of amino acids, which are the building blocks of biomolecules, including proteins [21]. Amino acids always contain, in their general form, a carboxylic group (COOH) and an amino group (NH2). When carbon in an amino acid structure is the first atom that attaches to a functional group, it is referred to as α-carbon.

Correspondingly, amino acids that have an amino functional group attached to the α-carbon are known as alpha amino acids. As represented in figure 1, all alpha amino acids possess an alpha carbon (Cα) attached to a carboxylic acid (-COOH) group, and amino group (-NH2), a hydrogen atom (H) and an R group that is unique to every amino acid. Nonetheless, there is one exception to the general structure of amino acids. In glycine (gly), there is a hydrogen atom instead of an R group, which makes it in terms of structure, the simplest amino acid in nature [21].

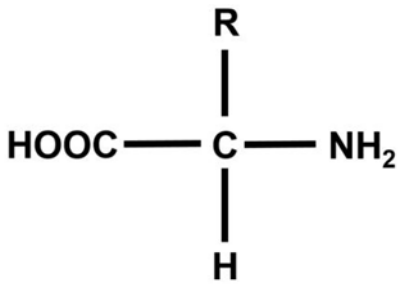

Figure 1. General structure of amino acids.

Amino acids, with exception of glycine, can occur in two isomeric forms. The mirrored configuration of amino acids, as observed in figure 1 for the case of alanine

(Ala) are also known as enantiomers. Configurations can be L (left handed) and D (right handed), as an example in 2-D see figure 2.

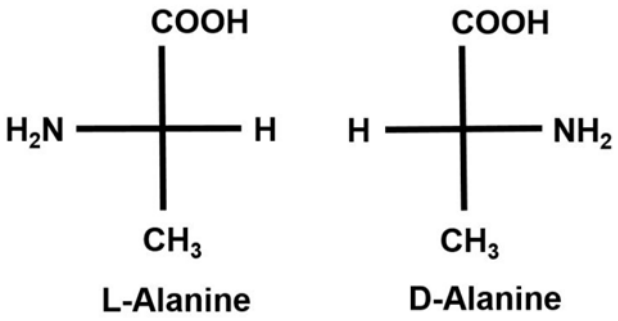

Figure 2. Optical isomers of alanine.

1.2.3 Charge of proteins, Hendersson-Hasselbalch equation and the isoelectric point

Single amino acids, peptides and proteins possess in their structure, acidic and basic functional groups. For instance in amino acids, as discussed, the basic building blocks of proteins, the charge is mostly determined by carboxyl and amino functional groups. Carboxyl groups, can be ionized and release H^+ ions into solution, hence, it is considered an acidic functional group.

On the other hand, amino groups can accept H^+ to form $NH3^+$. Since amino groups can take H^+ ions from the solution, they are considered to be basic functional groups. Accordingly, the predominant charge of an amino acid, peptide or protein, will depend on the pH of the solution. The *pKa* value of an amino acid or protein, determines the protonation and thus the charge of a residue at a given pH [22]. In order to understand the ionization conditions at certain pH present in an aqueous solution, the Hendersson-Hasselbalch (eq.2) equation is used.

$$pH = pKa + log_{10}\frac{[A^-]}{[HA]}$$ Eq.2

Where HA^- is the molarity of a given unassociated weak acid and $[A^-]$ is the acid's conjugate base. As the pH of a solution increases, both acidic and basic groups suffer from deprotonating. The isoelectric point (pI) of a protein is defined as the pH value in which the net charge is zero.

Biomolecules can contain both positive and negative charges and the net charge is determined by the pH of the surroundings. The pI is the pH value in which both negative and positive charges are equal. In the case of molecules containing dual charges, for instance an amino acid, that contains and amine and a carboxylic group, the pI is the sum of the *pKa* of the two groups divided by two.

As a consequence, when the pH is greater than the pI, a biomolecule will possess a negative net charge, and when the pH is lower than the pI, a biomolecule will possess a positive net charge. The isoelectric point varies on different biomolecules depending on the chain of amino acids or the distribution of charged functional groups. In figure 3, a hypothetic titration curve, adjusted in accordance to the Hendersson-Hasselbalch equation, the relationship between a titrant, pH, the pK of functional groups and isoelectric point can be determined. pK is understood as a dissociation constant and can be used to determine how strong or weak an acid is.

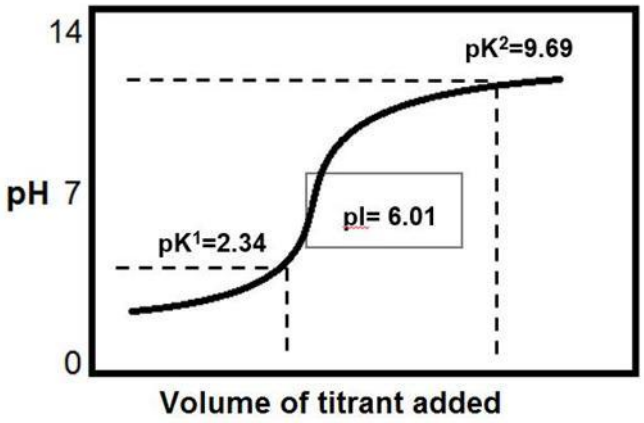

Figure 3. Representative titration curve for alanine.

In figure 4, ionization of alanine functional groups is represented according to the expected charge based on the titration curve. At low pH (below 2), amine groups are expected to be positively charged, whereas at its isoelectric point (around pH 6) as observed on figure 3 (titration curve), both functional groups are charged, resulting in a neutral net charge. At high pH (above 10), the carboxylic group is expected to possess a negative charge.

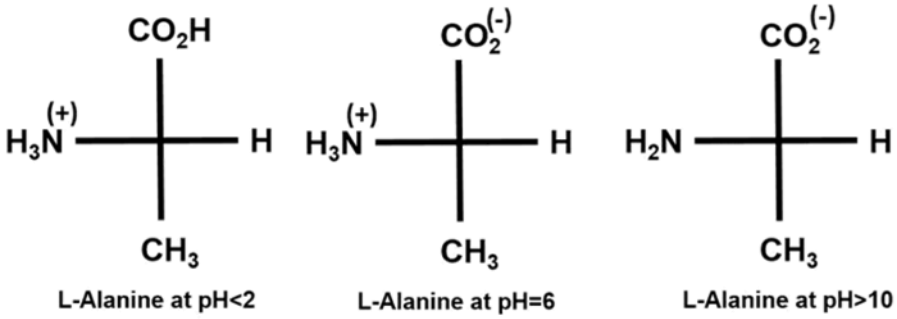

Figure 4. Expected charge of alanine functional groups at different pH according to its titration curve.

1.2.4 Electrophoretic mobility

An experimental approach that is commonly used to investigate the charge of biomolecules is by means of electrophoretic mobility. Electrophoretic mobility (γ) is referred to the velocity in which dissolved biomolecules in a solution displace or migrate as a response to an applied electric field. Electrophoretic mobility of dissolved biomolecules in a solution can also be defined as:

$$\gamma = \frac{q}{6\pi\eta r} \quad \text{Eq. 3}$$

where, q is the charge of molecules in a solution, η is the viscosity of the buffer and r is the radius. For a globular protein, the radius is related to the molecular mass. Electrophoretic mobility is highly dependent on charge and size of molecules. Molecules with high charges and smaller sizes will experience faster migration.

Furthermore, the direction of the movement will depend on whether molecules are negatively or positively charged. In this sense, cations and anions will migrate in opposite directions. Neutral solutes (q=0) will have the tendency to remain static (velocity=0) (See figure 5).

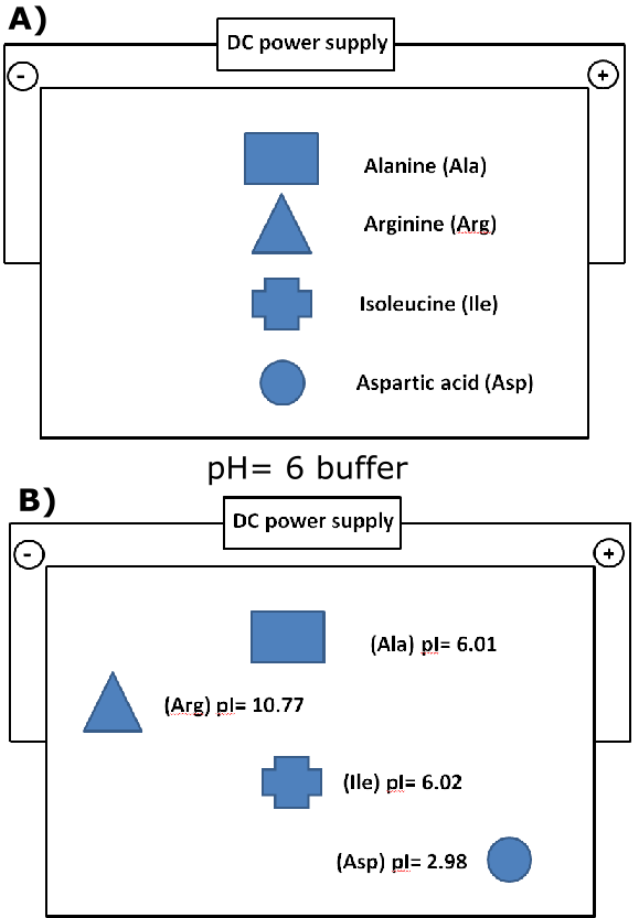

Figure 5. Electrophoretic mobility. Displacement of amino acids as a function of charge at pH 6.

1.2.5 Electrical double layer (EDL) and zeta potential

The understanding of electrostatic properties of surfaces is of great importance in areas such as colloids and electrochemistry. Moreover, is quite relevant in this dissertation to discuss commonly used model techniques to describe and measure electrostatic properties at interfaces. Such models and techniques include EDL and zeta potential. A simple way to describe the EDL is to consider a solid surface that is in contact with a solution containing ions.

As result of the difference of ionic affinity between the solid surface and the solution, the solid adopts a charge. In consequence, the charges at the interface arrange in a specific structure, known as the EDL (figure 6). To describe better the EDL, the Gouy-Chapman model (GCS) is used. Likewise, the GCS is composed of two layers; Helmholtz region (Stern layer) and a diffuse layer.

The Stern layer is the region at the interface of the solid surface where ions in the solution are compact and cannot experience movement. In the diffuse layer, ions in the solution can move freely randomly in all directions. Due to the importance of zeta potential and Stern layers concepts to determine electrostatic properties of biomolecules in general, these concepts will be briefly discussed in the following section

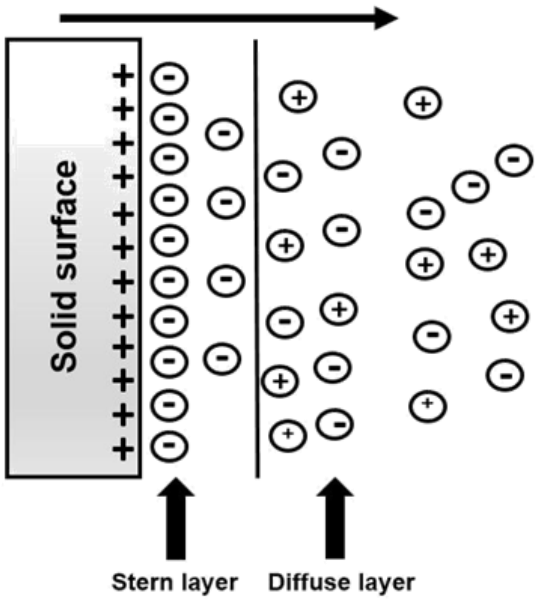

Figure 6. Visualization of the Double layer.

1.2.6 Dynamic light scattering

To measure zeta potential, optical devices use either dynamic light scattering (DLS) or image analysis for extracting information on the speed of the particles motion in the electric field. DLS is commonly used to measure particles in the size on the micrometer region. The working principle relies on the fact that particles suspended in liquids undergo Brownian motion. Velocity of Brownian motion of particles within a solution is directly related with the size of the particle.

DLS monitors Brownian motion based on scattered light. Other uses beyond particle sizing include zeta potential and estimation of molecular weight of organic compounds. The particle size is given in terms of hydrodynamic radius (*dH*), which is the diameter of a sphere that has the same translational coefficient as the particle.

1.2.7 Stokes-Einstein equation:

The hydrodynamic radius (*dh*) is determined by the Stokes-Einstein equation. Where *k* is Boltzmann's constant, *T* is the absolute temperature, η is the viscosity of the liquid and *D* is the translational diffusion coefficient.

$$d(h) = \frac{kT}{3\pi\eta D} \quad \text{Eq.4}$$

Analytical instruments based on dynamic light scattering to perform measurements on particle size and Z-potential are suitable to be used only on diluted solutions. Instrument design should prevent liquid from thermal motion, which usually

restricts high limit of the ionic strength. In optical devices, laser light scattering is used to measure diffusion coefficients of small colloidal particles by measuring the Doppler broadening of the frequency of the scattered light due to the velocity of the scattering centres. If an electric field is placed at the right angles to the incident light and in the place defined by the incident and observation beam, the line broadening is unaffected but the centre frequency of the scattered light is shifted to an extend determined by the electrophoretic mobility [23].

1.2.8 Soft lithography

Soft lithography is a form of micro construction that is quite versatile. In its origins, photolithography was intended to be used in semiconductor's industry and is nowadays utilized for a variety of disciplines such as microelectronics, biophysics and cell biology. In addition, patterning of surfaces is one of the strongest motivations to develop micro and nano construction techniques.

An important key aspect to soft lithography is the use of an elastomeric block with patterned relief structures on its surface, which serves as either a stamp or a mold. For this purpose, commonly polydimethylsiloxane (PDMS) is used. PDMS is a viscous fluid at room temperature. However, it can be easily converted into a solid by cross-linking to create a stamp. PDMS and its curing agents are commercially available being Sylgard 184 the most frequently employed.

In order to prepare an elastomeric stamp, a solution of PDMS is poured over a master possessing the desired structure for the stamp on the surface. Subsequently, the

solution is cured by heating and it is peeled off from the surface of the master. To fabricate the master, microlithography techniques such as photolithography, micromachining and e-beam writing are commonly used.

Elastomers are quite convenient to perform soft lithography for various reasons. For instance, when they are in contact with a substrate, elastomers adapt to it albeit the substrate is not planar in the micrometer scale. Additionally, the material is elastic enough so it allows being easily detached from rigid masters and complex three dimensional surfaces. Among other physical characteristics that make PDMS advantageous for soft lithography are optical transparency, chemical stability and low adherence.

There are different types of soft lithography. However, for purposes of this dissertation only micro contact printing and microchannel filling (microfluidics) are described. In micro contact printing the surface of a PDMS stamp is functionalized by the molecule that is required to be patterned on a substrate, which will function as ‘’ink’’. Then, the stamp is placed in contact with the substrate so the ‘’ink’’ initially placed on the stamp is transferred to the substrate.

Usually, micro contact printing generates patterns of self-assembled monolayers. Micro channel filling utilizes a PDMS stamp as well. However, instead of printing molecules through contact between the stamp and a substrate, it relies on a capillary flow of a solution over the open channels of the stamp. To this end, a PDMS stamp is placed over the substrate, leaving a confined space between the substrate and the capillary channel of the stamp. Subsequently, a solution is pipetted at one end of the

open channels in the stamp. After all the fluid has filled up the channels, the stamp can be removed, leaving a pattern of the molecules contained in the solution. Low viscosity solutions are preferable. Both methods for soft lithography share several advantages. For instance, fabrication of stamps does not require the use of complex lab equipment or a clean room, each stamp can be used multiple times. Nevertheless, micro contact printing is probably the simplest form of soft lithography. A detailed description of micro channel filling and micro contact printing soft lithography procedure is described in a subsequent section on this dissertation.

CHAPTER 2 :

Introduction

One important aspect in this dissertation is investigating the effect of sugar exposure on biomolecules in relation to electrostatic changes. The exposure of biomolecules to sugars and the effect on its electrostatic properties has many medical implications. The effect of sugar concentration in blood and methods to detect it and quantify it are greatly needed, being one of the reasons the high incidence of diabetes as a chronic disease in public health [27].

Prediabetes and the early stages of type 2 diabetes are characterized by the absence of symptoms, which prevent early diagnosis. It is of great importance to develop ways to detect and monitor sugar levels in blood and urine in an efficient way so patients can start treatment before symptoms are evident.

The ability to detect and monitor sugar levels in a patient is the most important tool to treat and control diabetes. In addition, these methods should be also accessible for the population, from cities to remote areas and at the lowest cost possible. This represents a challenge in biological detection methods.

In general, detection of sugar levels is normally done by two principal tests in urine: Benedict's test and Fehling's test. The concentration of sugar, mainly glucose, is determined by a scale of colour (colorimetric assay), where the range is from absence of sugar up to 2% or more [28]. This method obviously is not sensitive enough to

detect low concentrations, it is not time efficient, labels are needed (reagents), and it neglects the presence of other biologically relevant sugars. In blood, the most popular method for measuring sugar concentration is by glycated haemoglobin test (haemoglobin bA1c level) [29].

It is clear that it has become increasingly important to use label free detection and analysis methods for biological compounds. Among these methods, plasmonic based [30], optical fibre sensors [31], and optical biosensors based on interferometry [32] are under intense investigation.

In this case, using KPFM as a detection method represents a strong possibility to avoid using labels, which could alter physicochemical properties of the sample. KPFM in combination with micro patterning by soft lithography could give insights into the possibilities of fully take advantage of the capabilities of KPFM to develop highly sensitive bio sensing techniques.

Moreover, it has been already proven that KPFM possess, by far, enough resolution and sensitivity to be applied on biomolecules and detect changes in surface potential with high sensitivity in the order of a few millivolts [33][19][18].

Besides, detection purposes, the combination of PLL patterns, immersions in D-ribose solutions and KPFM measurements, could represent as well, an alternative method to detect post-translational modifications on biomolecules, specifically non-enzymatic glycation with high spatial resolution and high

sensitivity. To this date, there are no reported techniques that could address non-enzymatic glycation methods with these peculiarities.

2.1 Post-translational modifications

Post-translational modifications directly modify physicochemical properties of biomolecules, and it is sensible to think that electrostatic properties might suffer alterations as well. It is for this reason of vital importance understanding protein modifications and their impact on their function. Either covalent or enzymatic modifications in proteins after or during protein biosynthesis are known as post-translational modification (PTM). PTMs affect protein structure and function. Relevant PTMs include phosphorylation, acetylation, glycosylation, non-enzymatic glycation, ubiquitination and hydroxylation.

Protein folding, and refolding play a critical role in protein function. However, the modification of amino acids and their side chains contributes significantly to the structural and functional diversity of the proteins. Furthermore, their effect on proteins would include enzyme activity, protein turnover, protein-protein interactions, modulation of signalling, DNA repair, and cell division among others.

2.2 Glycation

Protein and peptide glycation with reducing sugars by means of the Maillard reaction is one of the most critical and fundamental reactions in food chemistry and in the human body. Hence, this investigation focuses on the possibility of glycation

of biomolecules after exposure to sugars. The general definition of non-enzymatic glycation is a non-selective modification of proteins that occurs via covalent bonding between a carbonyl group of sugars and amino group of proteins. Glycation is generally associated to a loss of function of the target protein due to modifications of its native structure. In contrast, glycosylation is a well-controlled cellular mechanism driven by specific enzymes [34].

The chemical reactions leading to the non-enzymatic glycation on proteins is termed as Maillard reaction or advanced glycation. Specifically, the targets of glycation on proteins are side chains of arginine and lysine, the N-terminus of amino group, and thiol groups of cysteine residues [34]. All sugars are believed to participate in glycation reactions. Nevertheless, D-ribose is the most active and abundant reducing sugar within the cell. Intra-cellularly, D-glucose is the least reactive and its concentration is rather low. D-ribose levels in the blood are estimated to be around 20 mg/L, whereas D-glucose around 6-10 g/L [34].

2.3 Maillard reaction

The process of glycation is described by the Maillard reaction. This reaction was named after the French scientist Louise Camille Maillard (1878-1936) who first published a paper reporting the reaction between amino acids and reducing during heating.

The initial step on the Maillard reaction is the condensation of a reactive carbonyl group from a reducing sugar such as glucose or ribose and a nucleophilic free amino

group, normally the epsilon amino group of lysine residues on proteins. This reaction results in the formation of an unstable Schiff base that spontaneously rearranges to form a more stable ketoamine, which is also known as Amadori product, a simplified reaction pathway. Amadori products are reversible at high pH or in the presence of phosphate [35].

This set of reactions eventually leads to the formation of several products such as furfurals, reductones and fragmentation products (carbonyl and hydroxycarbonyl compounds). The reaction of these intermediate products with amino groups in proteins, leads to what is known in food science as melanoidins. They were defined by John Hodge (1914–1996) as "brown, nitrogenous polymers and copolymers" [36], due to the fact that these compounds are responsible for browning in food during cooking process. It is worth mentioning that despite the number of articles published on glycation and the Maillard reaction in recent years [37], these products are poorly defined. Rates of these reactions are quite slow and particularly proteins with long half-lives and containing lysine residues, such as collagen under high sugar concentrations undergo this glycation [38].

The dominant factor in protein glycations is the half-life of individual proteins. However, at high concentration of reducing sugars, the extent of glycation is determined by the intrinsic glycability of the protein, for instance, number of lysine residues [39]. Regarding the biomedical aspects of glycation, it has been considered an age related problem influencing mainly extracellular proteins, such as collagen and elastin, which are located outside the cells and provide strength and flexibility to the tissues [34].

Moreover, proteins in amyloid deposits are found often glycated suggesting a direct correlation between protein glycation and amyloidosis [40]. Structural proteins such as collagen and elastin undergo continual non-enzymatic cross-linking during aging and in diabetic individuals (hyperglycaemia) [38]. Owing to the impact of glycation on disease and nutrition, there is an ongoing interest in understanding the biochemical pathway of the Maillard reaction, defining advanced glycation end products (AGE's), and understanding physicochemical changes on glycated peptides and proteins.

2.4 Poly-L-lysine patterns on mica by micro channel filling

As an initial step, soft lithography is used to micro fabricate two-dimensional patterns of poly-L-lysine (PLL) on mica and investigate the dependence of surface potential on different parameters such as re-immersions in water, temperature and lift height. Similarly, investigating the effect of repeated scans by KPFM and different substrates on the surface potential results of significant importance. The motivation for this set of experiments relies on standardizing the combination of poly-L-lysine patterning and KPFM as a foundation for detecting and quantifying electrostatic properties of biomolecules in relation to different physicochemical settings relevant for biophysical studies.

Initially, it is critical to describe the effect of scanning continuously poly-L-lysine or functional groups adsorbed on mica. Since most biochemical reactions and biological processes occur in aqueous media, it is important to investigate the

structural and surface potential stability of the patterned structure after experiencing continuous re-immersions in water.

In other words, PLL micro patterns on mica should be tested under aqueous conditions and remain stable, to replicate the conditions in which many biological and chemical reactions occur. Moreover, most relevant reactions in protein biophysics and in biology, in general, occur above room temperature (37℃). Besides, it is also well known that proteins and amino acids can be greatly affected by high temperature [41][42]. For these reasons, it is necessary to understand how PLL adsorbed on mica behaves in both, topography and surface potential when heated above room temperature. Specifically, PLL in solution can suffer structural transitions when heated or at different pH, that could be in turn, be accompanied with alterations in surface potential [43].

Finally, the distance between the AFM tip and the sample has an important effect on both spatial resolution and sensitivity, hence, it is essential to determine the range of distance in which a strong surface potential difference between PLL and the substrate can be obtained with a good degree of confidence.

As a model biopolymer, poly-L-lysine was selected due to its lysine functional groups, which is a relevant amino acid present in various proteins and biomolecular structures. For instance, lysine is the most repeated residue on type I collagen which is also the most abundant structural protein in vertebrates [44].

Additionally, lysine residues are particularly targeted by different post translational modifications such as acetylation, methylation, ubiquitation and sumoylation. Likewise, they have been identified to be a target for non-enzymatic post translational modifications such as phosphorylation and glycation, which adds biomedical relevance to this amino acid.

The selected substrate to perform this experiment is muscovite, which is worth briefly describing. Muscovite is the most common mineral of the family of mica. Muscovite is a widely used substrate for AFM studies for the reason that in can be perfectly cleaved, leaving a clean fresh surface available to place the sample to be under study. Another reason is that at the micro and nano scale is a flat substrate, making it easier to image small objects under AFM.

The chemical classification of Muscovite is under silicates and it is transparent. Regarding the chemical composition, Muscovite is quite rich in potassium and the general chemical formula is $KAl_2(Si_3AlO_{10})(OH)_2$ [45].

PLL is a synthetic polymer, which in this case, is composed of repeated L-lysine groups, as shown in figure 7. It contains two amino groups, which in solution at pH 7, one amino group is expected to be positively charged. In biological sciences is commonly used to improve attachment of proteins and cells to substrates[46][47].

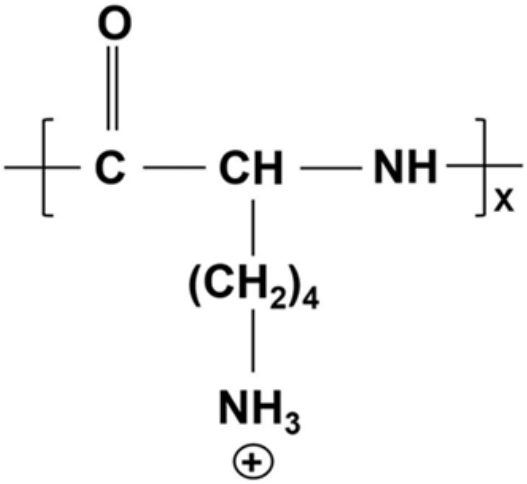

Figure 7. Chemical structure of poly-L-lysine.

Mica is a negatively charged surface with a consequent strong electrostatic attraction between the surface and the polyelectrolyte. Figure 8 is a schematic representation of a mica surface containing adsorbed poly-L-lysine.

Following adsorption of the first few segments of polyelectrolyte, partially neutralizing the available (negatively charged) binding sites on the mica surface, a positively charged 'atmosphere', balanced to some extent by counter ions, is formed above the surface due to the extended configuration of the polymer, this mechanism has been hypothesized on the cited research article. However, adsorption on mechanisms of PLL on mica was not characterized on this dissertation. Unusually, PLL forms monolayers of no more than 1 nm on thickness and can be easily characterized by AFM topography measurements [48].

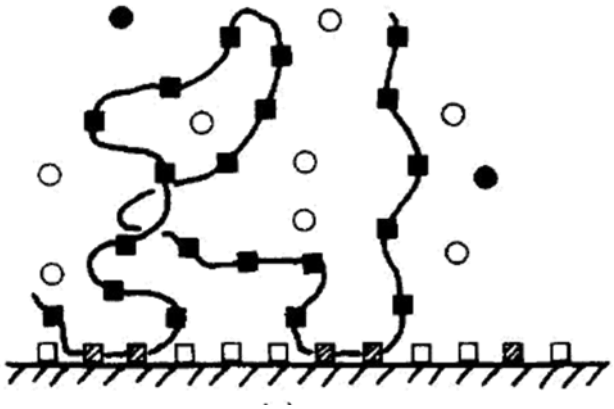

Figure 8. Schematic figure of proposed adsorption of PLL on mica. White squares represent negatively charged binding sites on mica; black square represent positively ionisable monomer; dashed squares represent surface binding sites neutralized by counterion or ionized monomer [49]

2.5 Electrostatic adsorption of colloidal gold nanoparticles on poly-L-lysine patternn

A major issue observed when imaging poly-L-lysine patterns in both topography and KPFM modes, is that the topographic height of a monolayer of poly-L-lysine, in most cases, is very low (less than 1 nm). Therefore, in the presence of other objects such as debris or dust located within the image, it is difficult to confirm the presence of poly-L-lysine molecules in the pattern. As a solution，to confirm the presence of poly-L-lysine in the surface that would reinforce potential images, it was resolved to explore the use of colloidal gold nanoparticles of opposite charge (negative) as markers. In addition to locate the presence of strong positively charge regions (poly-L-lysine pattern), interesting advantages can be observed and studied.

For instance, fabrication of nanoparticle patterns by a combination of PDMS soft lithography and electrostatic driven self-assembly from solution, is a simple method that do not require time consuming and complicated procedures for sample

preparation. Moreover, all the required materials needed such as PDMS, poly-L-lysine and mica are low cost and very common materials in labs in a wide range of disciplines.

The system offers a straightforward way to create well defined micro patterns with different desirable properties such as semiconducting, conducting or plasmonic micro patterns, depending on the surface properties of the nanoparticles.

The major requirement is the surface charge difference between the substrate and the colloidal nanoparticles. Fabrication of self-assembled systems with biomolecules for nano and biotechnological applications have been widely reported [50][51][52].

Existent methods for nanoparticle patterning include the fabrication silica and gold nanoparticle from suspension on a fluorocarbon film by using the AFM tip to write charges on the substrate achieved in previous reported experiments [53][54][55].

Similarly, gold and silver nanoparticles have been successfully aligned in patterns with desired periodicity at the micrometre scale by a simple self-assembled system [56]. However, the addition of information about the surface potential of patterned colloidal nanoparticles, in general, would be beneficial for the understanding of self-assembled systems and different applications.

2.6 Micro-contact printing of proteins for surface potential mapping by KPFM.

Up to date, analytical techniques for the study of electrostatic properties of proteins are quite restrictive. For instance, existing techniques use indirect models to calculate surface potential values of biomolecules (zeta potential), cannot create a spatially resolved map of electrostatic properties, require the use of label (dyes or antibodies), and the sample cannot be reused for further studies.

Furthermore, the possibility to pattern proteins on surfaces and record the electrostatic environment with high sensitivity and spatial resolution, is crucial for the development of more advantageous detection of biochemical modifications and sensing techniques for small compounds (biosensors). In the same way, an experimental set up which consists of complex proteins adsorbed on a surface and its corresponding electrostatic properties measured by KPFM after adsorption, may give important insights on electrostatic properties of proteins at interfaces on different substrates. The practice of patterning biomolecules is not new in the scientific community. Patterning of extracellular matrix fibronectin on glass by means of PDMS soft lithography has been reported [57].

Similarly, micro arrays of proteins by micro contact printing have been successfully achieved to grow neurons into networks of controlled geometry, representing an advancement in the fields of biosensors, neuroelectronic circuits, neurological implants and pharmaceutical testing [58].

Nevertheless, the novelty of this set of experiments relies on the combination of reliable, clean and efficient patterning techniques by micro contact printing, and surface potential mapping by KPFM, which represents the opening of new possibilities on protein biophysics. Patterning of different proteins is achieved on mica without the need of micro fabricating complex substrates such as chemically functionalized gold thin films as substrates.

2.7 AFM tip assisted triboelectric surface charge on mica: detection by KPFM and dissipation

The generation of triboelectric surface charge created by friction between the AFM tip and mica is described. Although, the initial goal was to micro fabricate a patterned surface by removing material within a defined area on the surface by scratching, the observation of the presence of a surface charge created by friction is worth of studying for to several reasons.

The study of electrostatic free charges on dielectric surfaces such as mica is of increasing importance in nanotechnology. For instance, the development of antistatic materials and tracking of free charges in electronics. Nevertheless, most studies are resolved at the macroscopic and mesoscopic level. KPFM may have a great impact in this area due to the capacity to resolve two dimensional maps in the micro and nano metre range with high sensitivity.

Although, the main goal was to create a patterned surface by removing material within a defined area on the surface by scratching the AFM tip against mica surface, the presence of triboelectric generated surface charge was observed. In consequence, the effect of continuous scans by KPFM, condensation and time dependence were

explored. Beyond the application of this methodology for the study of free charges to technological ends, this type of experiments could give valuable information about electrostatic dynamics on mica, which is widely used and accepted as a suitable substrate for the study of biomolecules by SPM techniques.

2.8 Insulin amyloid fibrils: Aggregation dynamics, effect of highly charged gold nanoparticles and surface potential mapping by KPFM

So far, in this dissertation surface potential mapping of biomolecules was performed on micro constructed patterns, gaining important knowledge on technical aspects of surface potential mapping by KPFM. Nevertheless, in order to move a step further, surface potential mapping of biomolecules was applied to biomolecular structures with important relevance not only in protein biophysics but in medicine in general.

In this sense, amyloid fibrils are structures that are of immense importance and intense research for its implication in neurodegenerative diseases. Here, the relationship between aggregation kinetics, surface charge, co-incubation with highly charged nanoparticles and finally surface potential mapping by KPFM was explored.

Amyloid fibrils are formed by normally soluble proteins, which assemble to form insoluble fibers that are resistant to degradation. They are highly linked with disease and each disease is characterized by a specific protein or peptide that aggregates (Figure 9) [59]

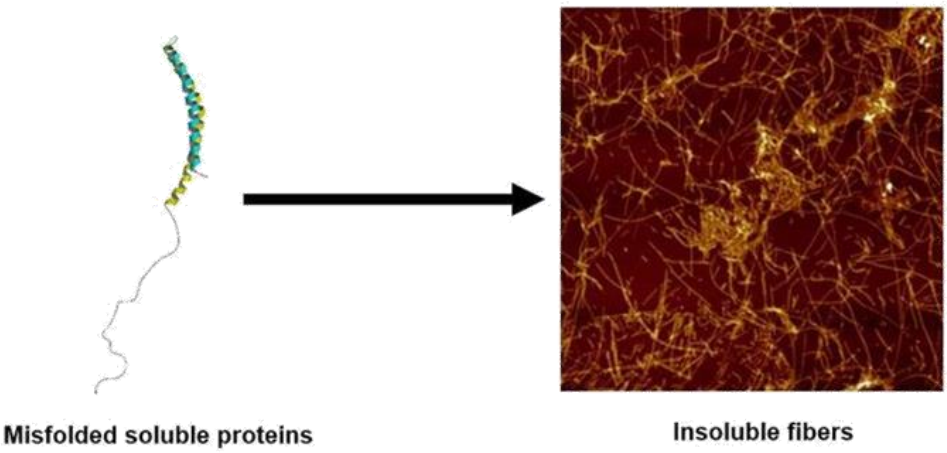

Figure 9. Transition of a misfolded soluble protein (left) to a heterogeneous insoluble fibers (right, AFM image) resistant to degradation.

Amyloid fibrils are mainly deposited in the extracellular spaces of organs and tissues as a result of a sequence of changes in protein folding, leading to cytotoxicity. Nowadays it is well known that regardless the protein that is forming amyloid-like fibrils, they all share a common 'cross-β' core [60].

Fibrils are formed by numerous repeats consisting of β-strands that are oriented perpendicular to the fibre axis form what is known as a cross-β pattern, with diameters of 6-12 nm wide and up to 10 micrometers long (figure 10-B). These peptide strands appear to be "stacked" in either parallel or antiparallel directions [61]. The interstrand and intersheet stacking distances of the cross-β core has been demonstrated by X-ray diffraction and is known to be around 4.7 Å and 10 Å respectively (Figure 10-A)[62].

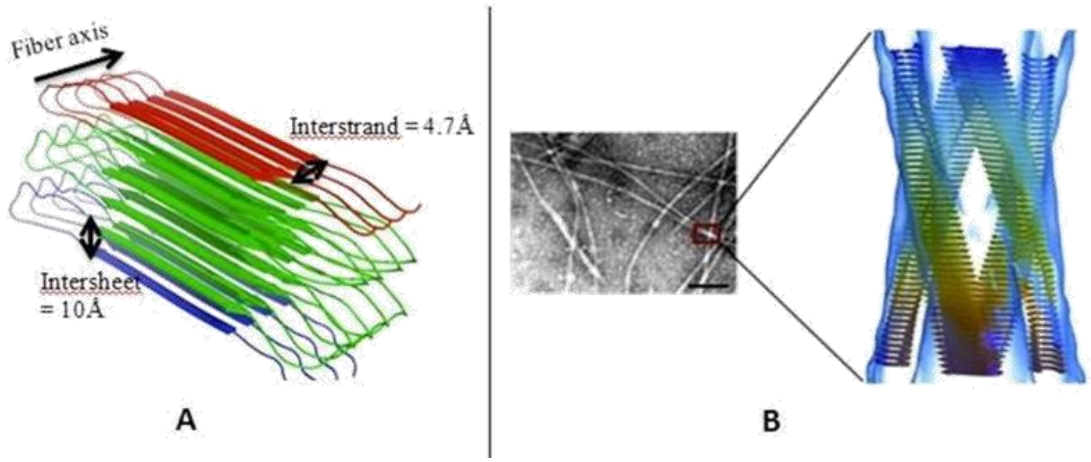

Figure 10. β-sheet core of amyloid fibrils. A) Interstrand and intersheet distances determined by X-Ray diffraction[82]. B) Amyloid fibril structural dimension by electron microscopy.

Intermolecular interactions such as non-polar Van der Waals and hydrogen bonds stabilizes the structure. In regards of the fibrillation kinetics, figure 11 summarizes several studies that show the mechanism of fibrillation in which amyloid proteins form insoluble polymeric fibrils: a monomeric form of protein precedes formation of oligomers, which then serve as seeds for accelerated fibril growth [63][64][65].

Amyloid formation consists of two phases or stages. The first stage is a nucleation phase/lag time, in which monomers undergo conformational change and associate to each other to form oligomeric nuclei.

The second stage consists of an elongation phase/growth phase, in which the nuclei rapidly grow by further addition of monomers and form larger polymers/fibrils until saturation

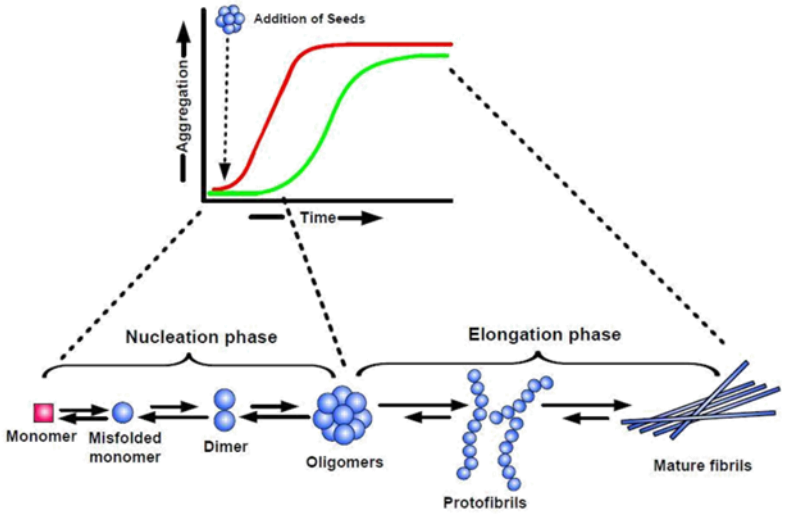

Figure 11. Polymerization model of amyloid aggregation [66].

The nucleation phase, is thermodynamically unfavourable and occurs gradually, whereas elongation phase, is much more favourable process and proceeds quickly. Consequently, kinetics of amyloid formation is well represented by a sigmoidal curve with a lag phase followed by rapid growth phase (figure 11).

The rate limiting step in the process is the formation of seeds to promote aggregation. Thus, amyloid formation can be substantially speedup by the addition of preformed seeds. Amyloid fibrils are highly associated with different diseases.

It has been proposed that altered metabolism of amyloid precursor protein (APP) is the causative of Alzheimer's disease (AD), when it leads to aggregation of Aβ protein and formation of fibrils and plaques in the brain. These plaques are believed to later cause pathological changes including the formation of neurofibrillary tangles compromising synaptic function resulting in brain cell death and dementia. This is known as the amyloid cascade hypothesis [67]. Nevertheless, later it was found that there is no correlation between the density of plaques and tangles and the

severity of AD. On the contrary, there was a strong correlation between the amount of soluble Aβ and cognitive impairment [68][69][70]. These studies suggests that soluble non-fibrillar intermediates, such as oligomers (20 To >50 kDa globular aggregates, including ADDLs) and protofibrils (curvilinear structures 4–11 nm in diameter and ≤200 nm long) are the actual initiators of AD pathogenesis and that mature fibril formation represents the end point of the disease.

Another condition involving amyloid fibrils is diabetes mellitus type 2, in which islet amyloid deposits are a characteristic pathologic feature in the pancreas. Islet amyloid polypeptide (IAPP) is co-localized with insulin in the islet β-cells and is co-secreted with insulin in response to β-cell stimulation by both glucose and non-glucose [71].

The physiological function of IAPP is still not completely understood. Proposed biological functions of IAPP include suppression of food intake, gastric emptying, and glucagon secretion stimulated by arginine from pancreatic β-cells.

However, several studies *in vitro* have demonstrated that both intracellular and extracellular accumulation of human IAPP is associated with β-cell death, although the mechanisms are likely different. For instance, overexpression of amyloidogenic human IAPP has been shown to induce apoptosis in COS-1 cell. Interestingly, it has been found that only the aggregated (fibrillar) form of IAPP kills β-cells, whereas the soluble form of the peptide is not toxic.

In Parkinson's disease (PD), dementia is caused mainly by the fibrillation of α-synuclein (α-Syn). However, a more complex co-fibrillation process occurs involving Aβ, α-Syn and TAU proteins, that fibrillate together to form Lewy bodies.

Disease	Protein	Abbreviation
Alzheimer's disease	Beta amyloid	Aβ
Diabetes mellitus type 2	IAPP (Amylin)	IAPP
Parkinson's disease	Alpha-synuclein	none

Table 1. Principal proteins involved in amyloid related diseases.

It has become evident that the more research is done, the more proteins are found to fibrillate together. In other words, disease related amyloid forming proteins does not act in isolation; in many cases, fibrillation is driven by a complex system of co-fibrillation involving different proteins. This is the case, for instance, of diabetes mellitus type 2, where IAPP deposits contain a variety of proteins including serum amyloid P component (SAP), apolipoprotein E (ApoE), and the heparan sulfate proteoglycan perlecan [71].

The role of these components in islet amyloid formation is not completely understood, the finding that these molecules are also present in other types of amyloid deposits such as senile plaques in Alzheimer's disease, suggests that similar mechanisms might underlie amyloid formation in different pathologic states.

Similarly, in PD, fibrillary deposits are found to be causative of brain cell loss and are referred to as Lewy bodies. Lewy bodies appear as spherical masses that displace other cell components. The two morphological types are classical (brain stem) Lewy bodies and cortical Lewy bodies. These deposits are composed of the protein alpha-synuclein associated with other proteins, such as ubiquitin, neurofilament protein, and alpha B crystallin.

Tau proteins may also be present, and Lewy bodies may occasionally be surrounded by neurofibrillary tangles. Moreover, some investigations suggests that there might exist a synergistic interaction of α-Syn, TAU and even Aβ causing these proteins to mutually promote each other's aggregation [72][73]. Existent research suggests that the simultaneous accumulation of different proteins in the central nervous system is a common feature in many degenerative diseases, uprising the importance to understand the basic biophysical mechanisms underlying both inhibition and promotion of protein co-fibrillation. Furthermore, the understanding of self-assembled nanofibers could gain more relevance due to its potential applications recently found as in tissue engineering [74], templates for metallic nanowires [75], and biomedical sciences in general [76]. Studying mechanisms of protein aggregation on model systems is extremely useful for a better understanding of the molecular mechanisms of disease associated amyloid genesis.

To prepare preliminary fibrils as a generalized model of amyloid assembly is very common due to the fact that several proteins are known to easily aggregates and produce fibrils in vitro. Among these proteins, insulin, β-lactoglobulin and lysozyme are the main proteins used as models for fibrillation.

However, this study focuses on insulin since their fibrillation kinetics in vitro is well known. Insulin is a 51-amino acid protein (Figure 12) hormone produced *in vivo* in the pancreatic cells. The precursor protein (preproinsulin) contains a 23-30 amino acid signal peptide attached to the amino terminal of proinsulin. Insulin is the primary hormone responsible for controlling the cellular uptake, utilization and storage of glucose, amino acids, and fatty acids while inhibiting the breakdown of glycogen, protein, and fat.

Bovine insulin differs from human in only three amino acid residues, and porcine insulin in one. Insulin can aggregate and form fibrillar interdigitated beta-sheets and has been used extensively for protein fibrillation studies. Hence, its aggregation kinetics and fibril characteristics are quite well known [74][77][78][79]. Insulin fibrillates in vitro and has been used as a model for amyloid fibril forming protein [80] [81][82][83].

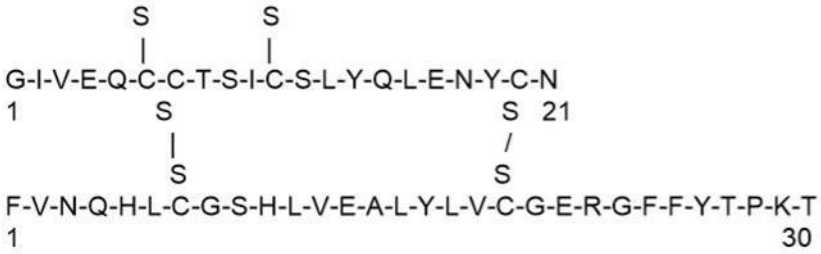

Figure 12. Structure of insulin [84].

2.8.1 Influence of nanoparticles on protein fibril formation

Even though many molecules are proven to function as chaperons and alter kinetics of amyloid fibrils formation, nanoparticles have the advantage of being excellent candidates for the ability to cross through the blood brain barrier, which acts

very effectively to protect the brain from many common bacterial infections, and only small peptides and nanoparticles are known to be able to cross [85]. Nanoparticles are under intense investigation for this ability and are believed to be able to transfer drugs and possibly inhibit or retard fibril formation.

Furthermore, in the opposite case, when they promote fibril formation, can be used to study fundamental mechanisms of fibril formation, as they can be easily tailored in terms of physicochemical properties such as surface chemistry, morphology and size, in order to be incorporated on incubating systems as models.

The principal approaches to study the influence of nanoparticles on the speed of amyloid fibril are scanning electron microscopy (SEM), transmission electron microscopy (TEM), and atomic force microscopy (AFM) to characterize the morphology of the fibrils.

In order to track the speed of amyloid formation and conformational changes optical spectroscopy is used [86][87][88][89][80][77][90][91]. The characteristics and aggregation dynamics of fibrils have been extensively reported. However, due to the high complexity and number of variables involved in the systems, well defined mechanisms of the effects of nanoparticles on protein fibrillation has not been established, nor are completely understood.

For this reason, a number of studies have attempted to address this matter. For instance, tt is well known that gold nanoparticles can either promote or inhibit

aggregation of fibril forming proteins depending on characteristics such as size, shape, temperature or pH [92][90][93].

According to simulation studies, smaller nanoparticles decrease the aggregation speed of fibril forming proteins [92]. Similarly, it was found by thioflavin-T fluorescence and SEM studies that fibrillation speed of α-synuclein, a relevant fibril forming protein related to neurodegenerative diseases, was increased by smaller (10 nm) nanoparticles and decreased by bigger nanoparticles (22 nm) [94].

Another important physicochemical aspect that influneces aggregation kinetics of amyloid fibrils is pH. Interestingly, insulin-coated gold nanoparticles show high sensitivity to pH changes. For this reason, they can be spontaneously aggregated or disaggregated by changing values of pH [93].

2.8.2 Influence of surface charge of nanoparticles on protein fibril formation

Recent studies suggest that surface charge on nanoparticles may have an influence on amyloid fibril formation. For instance, it has been found that negatively charged bare gold nanoparticles, not only inhibited fibrillation, but also promoted fibril dissociation of Aβ fibrils as a function of concentration [95]. Likewise, gold nanoparticles coated with anionic curcumin converted to monocarboxylic acid derivative (curcumin-COOH) dissolved amyloid fibrils without any external agent or force when co-incubated with lysozyme [89]. Gold nanoparticles possess a negative surface charge when are coated with citrate [96].

In this sense, the presence of citrate-coated gold nanoparticles can effectively accelerate the formation of small aggregates of gold nanoparticles and Aβ peptides, however, inhibit the formation of aggregates and further protofribrils and fibrils, the localization of nanoparticles into fibrils was possible by KFM microscopy due to the difference of surface charge between the fibrils and the nanoparticles [97].

On the other hand, it was shown that the presence of nanoparticles in the process of protein fibrillation particularly does not inhibit the formation, but can promote fibril growth. Maghemite (γ-Fe2O3) nanoparticles surface can be positively or negatively charged depending on the pH [98].

Hence, the predominant charge at low pH, where amyloid protein fibrillation usually occurs *in vitro*, would be positive. The co-incubation of human insulin and 15 nm maghemite at high temperature and low pH resulted in an acceleration and promotion of the formation of fibrils, as it was observed by AFM, TEM and supported by optical density measurements of absorbance at 600 nm as a function of time [91]. To support the idea, that nanoparticle surface charge could play a role in the inhibition or promotion of fibril formation, recent studies have suggested that negatively charged particles have an inhibitory effect, while positively charged particles have the opposite effect.

Fibril formation was accelerated by iron oxide nanoparticles coated with Aβ, yielding a net positive charge, while the same nanoparticles inhibited the formation of fibrils when coated with the anionic beta sheet breaker Leu-Pro-Phe-Phe-Asp (LPFFD) [99].

Similarly, when the cationic surfactant cetrimonium chloride (CTAC) and the anionic surfactant sodium dodecyl sulfate (SDS), were co-incubated with Aβ at a concentration of 1mg/ml, the inhibition of fibrils forming caused by the effect of charged (anionic) micelles and the reduction of time for fibrils to form caused by cationic micelles was confirmed [100].

Nevertheless, studies regarding the influence of surface charges are scarce and the existent knowledge is not conclusive. The generation of knowledge in this specific topic would give insights not only for the potential prevention and treatment of neurodegenerative diseases related with protein fibrillation, but could also serve as a precise model for understanding the nature of synergistic co-fibrillation involving differently charged entities, for instance a-synuclein and TAU.

For this purpose, a systematic study involving a family of differently charged nanoparticles and at least two different proteins known to form amyloid fibrils is needed. Based on the existent literature, the addition of gold nanoparticles influences the aggregation kinetics of amyloid fibrils.

However, the effect of surface charge of gold nanoparticles on fibrillation kinetics has not been previously investigated. The proposed hypothesis behind this experiment is that in a co-fibrillation system of nanoparticles and a fibril forming protein, insulin in this case, inhibition or promotion of amyloid fibril formation depends on the difference of surface charge between nanoparticles and native fibril forming protein (see figure 13).

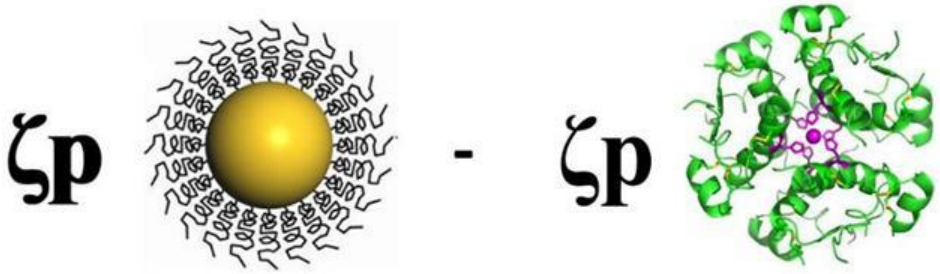

Figure 13, shows a representation of a nanoparticle with a specific surface charge, and a protein with different surface charge, which might lead to an effect on the protein aggregation.

CHAPTER 3:

General methods and experimental details

3.1 Patterning by sof lithography 3.1.1 PDMS stamp fabrication

Prior PDMS fabrication, a mold with the desired pattern was produced by UV-photolithography (London Centre for Nanotechnology, London, UK) (see figure 14). The patterns utilized were stripes (linewidth was 10 μm or 30 μm with a periodicity of 40 μm).

The mould consisted of a spin-coated layer of Megaposit photo-resist (Dow Chemical Co., Midland MI, USA, (Megaposit SPR 955-CM) on silicon dioxide wafers. Before spin coating, the wafers were polished and cleaned with ultrapure water and then heated to eliminate humidity.

As an adhesion promoter, hexamethyldisilazane (HMDS) was applied by spin coating. Subsequently, a 1.5 μm thick Megaposit resist film was applied to the wafer by spin coating at 3500 rpm. Thereafter, it was heated to eliminate excess of solvent by evaporation. UV-photolithography and development were carried out according to the protocol for Megaposit. As a final stage, baking was carried out at 150^{o}C for at least 15 minutes [101][102].

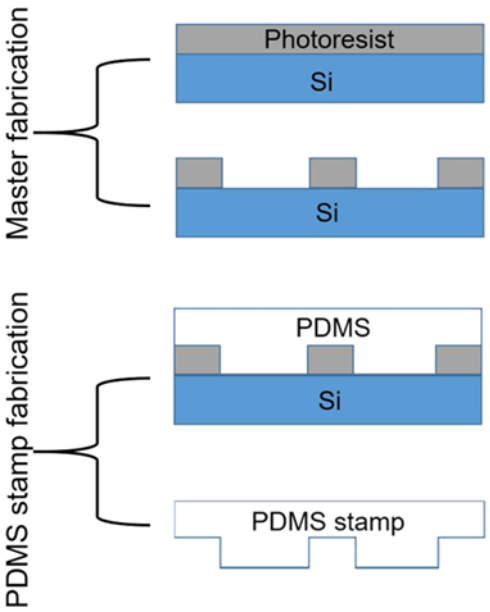

Figure 14. PDMS stamp fabrication using masters as templates.

To fabricate the PDMS stamp, a mixed solution of pre-polymer and curing agent was prepared (Sylgard 184, Dow Corning Co., Midland, MI, USA). To prepare the mixture, both, the silicon elastomer and the curing agent were mixed together in a proportion of 10:1. As shown in figure14, once the solution was transparent and free of bubbles, it was poured over the substrate (masters).

Afterwards, the entire structure is heated around 50 ℃ for a few hours in a hot plate until the PDMS is completely cross linked and the solution is solidified. Finally, the stamp can be peeled off from the master, resulting in a PDMS stamp with desirable features.

When the stamp is peeled off, it should possess the opposite features as the master. In figure 15, AFM micrographs of both the master and the produced stamp are shown. In some cases, the AFM image does not allow observing the edge; hence, obtaining its corresponding profiles is needed. In figure 16, where the corresponding profiles are

shown, it is possible to notice that the topography of both the master and the stamp are exact opposites and share the same dimensions at the planar edge, which corresponds to the end of the 10 µm ridges of the PDMS stamp. Nevertheless, the profile of the master (in black), shows a tip artefact, for which, in appearance the master possesses a curvature in the upper region.

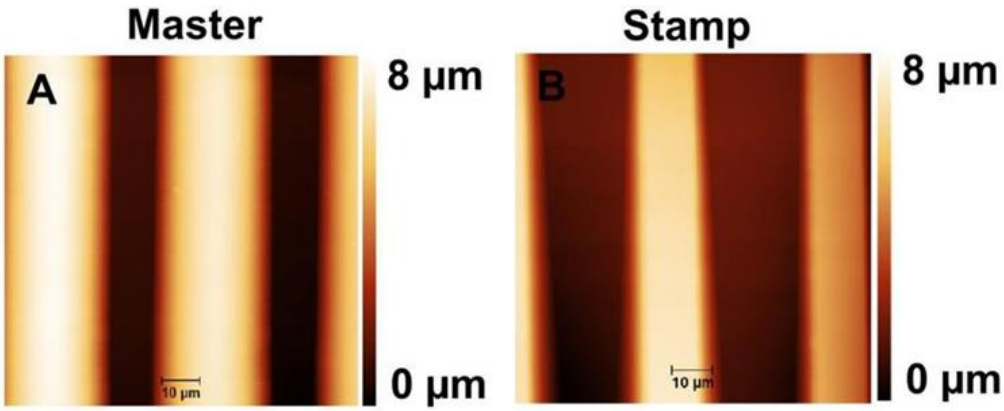

Figure 15. AFM topographic images of A) a master showing 10 µm ridges and about 30 µm gaps in between, B) resultng PDMS stamp showing channels around 10 µm with and 30 µm gaps in between.

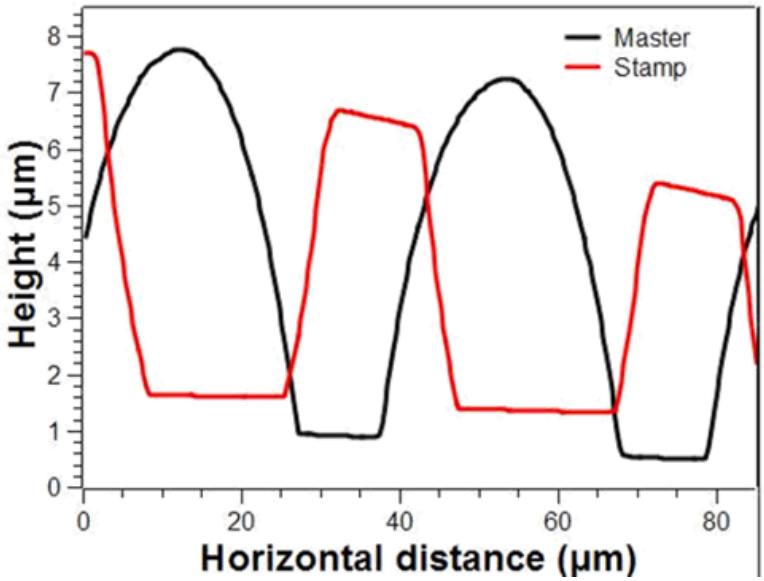

Figure 16. Height profiles of the master and its corresponding PDMS stamp after fabrication.

If the opposite features are desired, a different master showing the opposite features should be used. However, a prefabricated stamp can also be used as template to fabricate a new stamp with the opposite features.

3.2 Micro channel filling patterning for KPFM measurements

A fresh PDMS stamp (10 μm channels, 30 μm ridges) was situated on a freshly cleaved piece of mica. Micro channels were brimmed over by pipetting around 40 μL of poly-L-lysine (Sigma-Aldrich, CAS: 25988-63-0, 0.01% w/v in H2O) at the edge of the channels of the stamp. After 5 minutes, when the channels were visually brimmed over with poly-L-lysine solution, ultrapure water was flushed into the micro channels and the stamp was removed to displace remaining poly-L-lysine.

The whole procedure was carried out avoiding lateral movements as much as possible. Finally, the sample was washed with ultrapure water and dried either with nitrogen, if available, or a hand-held air blower.

To observe the patterns and obtain potential maps, tapping mode and KPFM images were produced simultaneously. Several conductive silicon tips (Veeco antimony doped Si) were used with a typical oscillation frequency around 360 kHz. In the interleave mode, a drive amplitude between 1000 mV and 2500 mV and a lift height of 25 nm was used (except for the lift height experiment). Lock-in phase was typically found around -90 °and optimized for each tip by detecting an artificial square signal applied to the sample [103]. Despite all measurements were carried out in air, the sample was subjected to different conditions such as immersions in water. These were carried out

by immersing the sample in water, drying the sample with air, and re-scanning in the same area.

Similarly, prolonged exposure to water was tested by immersing the sample in water for 20 minutes, then drying the sample out and re-scanning in the same area. Immersions in water were repeated at least 6 times. The effect of potential difference versus lift height was tested by locating a clear poly-L-lysine pattern and performing surface potential scans repeatedly at different scan lift heights.

After obtaining the first potential image at a distance of 1 nm from the sample, the lift height parameter in the interleave mode was adjusted to a different distance, and the resulting images were recorded. This procedure was repeated until reaching 1000 nm.

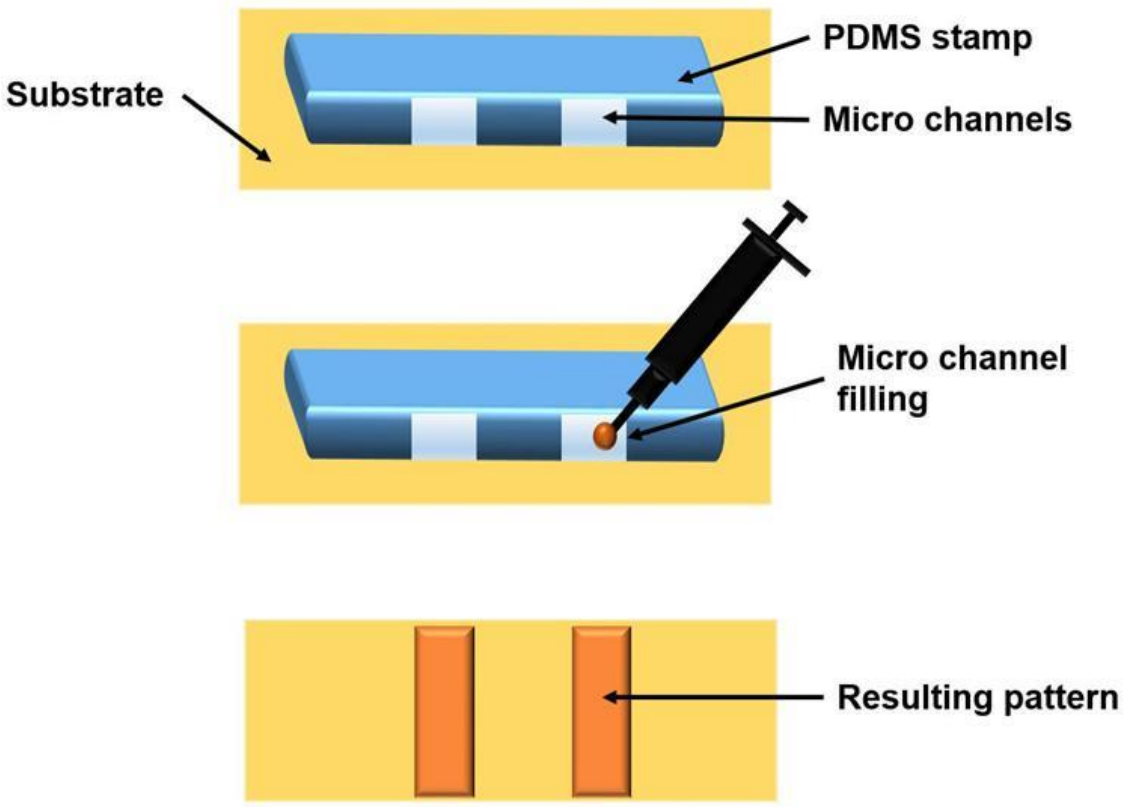

Figure 17. Representation of microchannel filling technique.

To obtain better values of surface potential difference of patterned poly-L-lysine on mica, AFM images were taken in the same scanning area and by aligning the patterns at 90,º as shown in figure 18. Surface potential difference (ΔΦ) was calculated by substracting the average surface potential of the substrate from the average surface potential of the patterned PLL.

For this reason, it is convenient to scan the sample perpendicularly to the orientation of the patterns. In this way, bigger areas can be selected using the software to obtain average surface potentials and calculate the surface potential difference (ΔΦ). Moreover, the term samples/line (figure 18) determines how many points are going to be considered per each scanned line within the image, and it determines in the same way the resolution of the image.

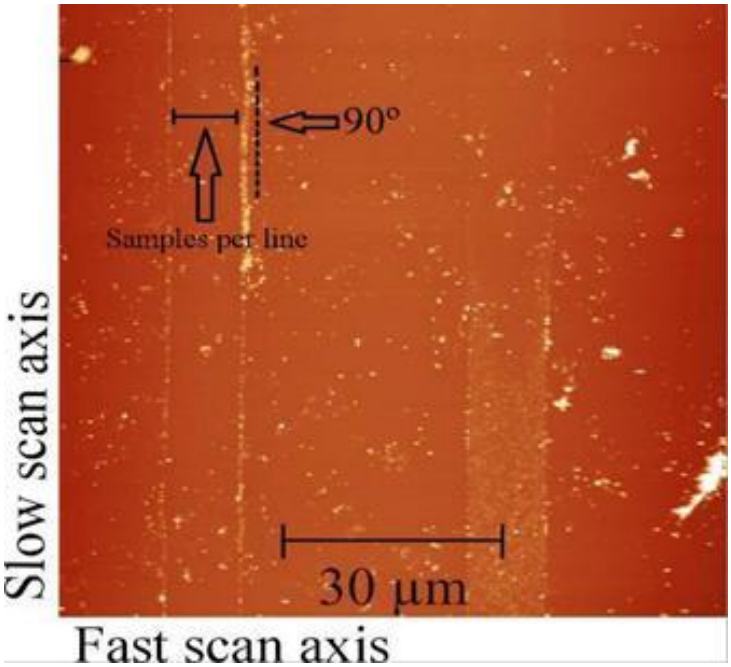

Figure 18. 90 º alignment of patterned poly-L-lysine.

3.3 Micro-contact printing of proteins for surface potential mapping by KPFM.

Protein micro patterns on a solid substrate were achieved by placing a drop protein in solution on top of the PDMS stamp. Globular proteins lyophilized powder of bovine serum albumin (BSA), lyophilized powder of β-lactoglobulin from bovine milk, and lyophilized powder of insulin from bovine pancreas, were all obtained from Sigma-Aldrich. Solutions of these proteins were prepared at a concentration of 2 mg/mL in ultrapure water.

Once the drop was placed on the stamp, it was left there for about 10 minutes. Subsequently, the stamp was dried with air. The stamp was then, placed in contact with the substrate (mica, glass, and silicon dioxide) avoiding drifting the stamp as much as possible. As a last step, the pattern was observed on an optical microscope to confirm the formation by creating water condensation on the sample by exhaled breath.

In order to assess the effect of pH on surface potential of the protein micro patterns, buffers were utilised. A buffer solution pH 4.0 composed by citric acid, sodium hydroxide, sodium chloride and red colour (Fulka analytical) was used.

Avidin from egg white, expressed in corn (Sigma-Aldrich CAS: A8706) was dissolved in water 1 mg/mL. A few drops of the resulting solution were placed on a clean PDMS stamp for 5 minutes. Subsequently, the PDMS stamp was dried with nitrogen.

The stamp was placed in contact with previously washed coverslips. To determine whether a pattern was formed or not, a condensation test was performed under an optical microscope.

3.4 Immersion of poly-L-lysine patterns on D-Ribose solutions

3.4.1 Immersions in D-Ribose solutions

Poly-L-lysine patterns were immersed repeatedly in D-ribose (Sigma) solutions at 6 mM and 6 M concentrations. The patterns were immersed in D-ribose solutions repeatedly up to 8 times and the solution was left in contact with the pattern for 1 minute.

After each immersion in D-Ribose, the sample was washed with ultrapure water and dried with air. In the case of 6 mM D-ribose solution, AFM and KPFM images were taken before and after washing and drying the sample, allowing to get the surface potential of the pattern in the presence of sugar and after the washing. In the case of 6 molar D-ribose solution, only images after washing the sample were taken.

The practical reason for this action to be taken was due to the excessive amount of sugar in the surface, which makes obtaining meaningful images difficult. The tip used was from the same batch as in the previous sections, with very similar parameters as in control experiments.

3.5 Electrostatic adsorption of colloidal gold nanoparticles on poly-L-lysine patterns

Poly-L-lysine pattern was prepared by placing a preformed PDMS stamp on mica as previously described [104]. A drop of poly-L-lysine solution was added at the end of the PDMS stamp. Subsequently, the channels were flushed with ultrapure water, the stamp was mechanically removed, and the sample was washed again with ultrapure water. Finally, the remaining water was dried out using air. The sample was taken to the AFM for further characterization. The nanoparticle patterns were formed by immersing the sample into a colloidal solution of 10 nm gold nanoparticles coated with lipoic acid (nanoComposix .05 mg/mL). Lipoic acid is a disulphide compound that is well known for its antioxidant activity.

Nevertheless, there are numerous reports in which it is used for functionalizing gold nanoparticles [105][106]. The immersion was carried out on the AFM by retracting the scanner, immersing the sample and washing it with ultrapure water, then air dried. The same area was successfully localized to perform measurements before and after nanoparticle adsorption.

The tip used were from the same batch as previous section and the parameters used for the AFM and KPFM measurements were as follows: topographic image was recorded in tapping mode using a drive amplitude of 850 mV while the amplitude set point was about 450 mV.

The scan rate was .8 Hz. The lift height on the lift mode was 25 nm, the drive amplitude 2500 mV, the optimum value for the lock-in phase on the tip was found to be -75^0. Utilized nanoparticles possess a hydrodynamic radius of 10 nm, and a -40 mV zeta potential in solution.

Due to the presence and exposure of highly negative charge functional groups (OH^-), a selective and spontaneous electrostatic attachment to amino groups of poly-L-lysine is expected.

3.6 AFM modes

3.6.1 Contact Mode:

The simplest AFM form of operation is contact mode. In this set up, the AFM tip interacts in close contact with the surface of the sample. It is also the most common mode utilized in force microscopy. In contact mode the cantilever is pushed against the surface by a piezoelectric element.

The most important parameter in the feedback system is the deflection of the cantilever, which is detected and adjusted with a DC feedback amplifier to match the desired value of deflection (deflection set point). In order to keep the desired deflection set point, the feedback system applies a voltage to the piezoelectric element to either move higher or lower the position of the sample in the Z axis in order to restore the desired deflection set point.

Hence, the voltage applied by the feedback amplifier corresponds to the physical height or specific features on the sample. Contact mode can be performed in different experimental conditions such as high vacuum, liquids and air. A major disadvantage of contact mode is the excessive force applied to the sample, in which, depending on the material to be studied, can result in sample destruction or damage. To overcome this problem, the forces applied to the sample can be minimized. However, this aspect still a practical limiting factor.

Moreover, as in any other AFM mode, typically the sample is covered by of adsorbed gases, primarily water. This condition affects the interaction between the tip and the surface within the regime of attraction forces. When the tip is in contact with the water molecules, a meniscus is formed and the cantilever is pulled towards the sample by surface tension forces.

By immersing the whole sample and the cantilever in liquid the surface tension and other attractive forces are minimized. Samples such as semiconductors and insulators (mica included) have also the capacity to hold electrostatic charges. These phenomena will be addressed further in this dissertation.

The combination of different forces such as electrostatic charges and attractive forces caused by the presence of water on the surface result in a final highly frictional force over the surface when scanning in contact mode.

Moreover, many of substrates and samples cannot be immersed in liquids in order to be imaged by AFM. To overcome this issue another mode of atomic force

microscopy was developed: non-contact mode. Figure 19, represents the general components of AFM imaging.

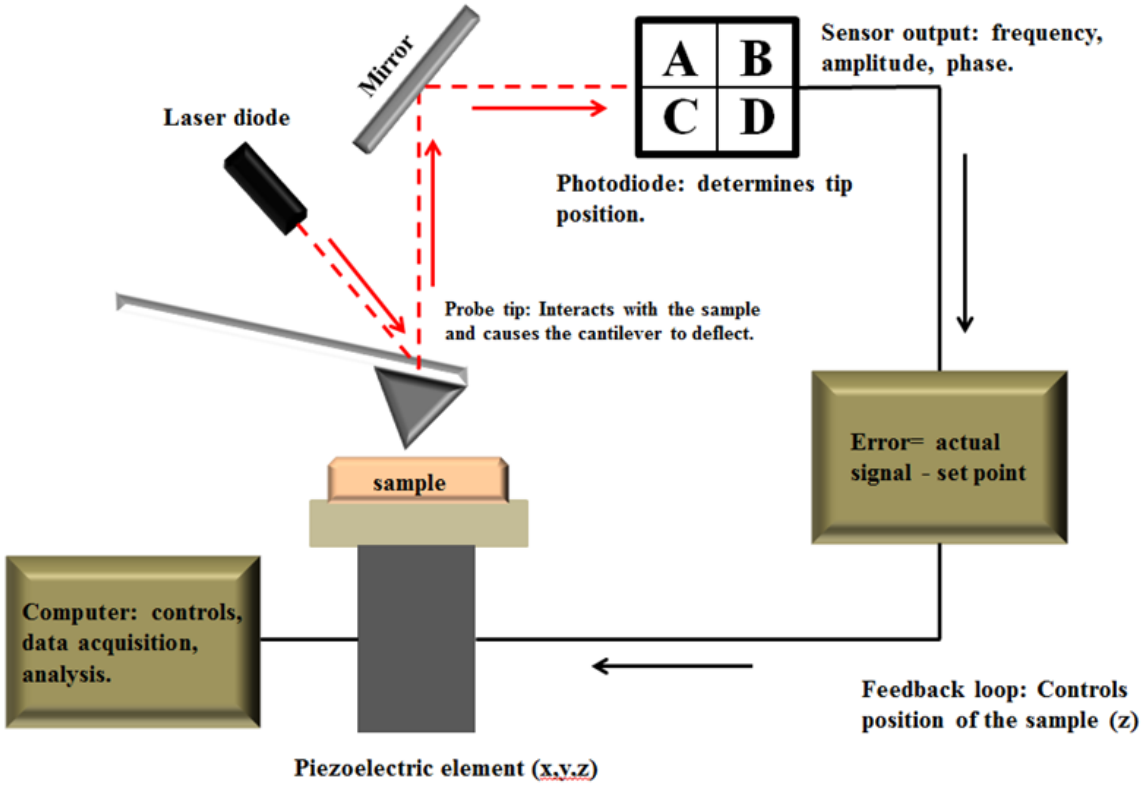

Fig 19. Diagram of the general components of atomic force microscopy imaging.

3.6.2 Non-contact mode

Non-contact mode was developed to overcome situations when the sample is likely to be affected by the interaction with the AFM tip. During the scanning in this specific mode, the tip oscillates over the surface with a slight separation in the order of a few Ångström. At this distance, attractive forces act on the tip, and are detected and translated into, for instance, topographical features.

The attraction forces in non-contact mode are weaker than contact mode, for this reason, a small alternating current (AC) has to be applied to the tip, to let the feedback system measure changes in amplitude, phase or frequency of the oscillation in the cantilever as response to forces in the sample. Unfortunately, the distance between the tip and the sample still lower (within the range of the Van der Waals forces) than the actual thickness of the layer of water which is usually present in substrates. It is for this matter, that the water meniscus stills a major problem even in non-contact mode. Non-contact mode is represented in figure 20.

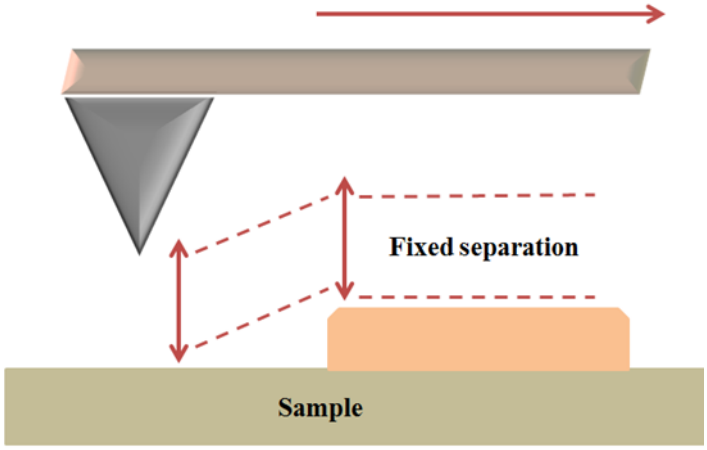

Figure 20. Non-contact mode representation.

3.6.3 Tapping mode:

Tapping mode is probably the most utilized AFM mode and it represents a substantial advancement in atomic force microscopy. Among the advantages, high resolution on topographic images that are easily damaged, low adherence to the substrate, or the capacity to scan samples that are too demanding to study under other AFM modes stands out. In other words, tapping mode overcomes difficulties related to friction,

adhesion, electrostatic forces, among others. In tapping mode, the tip is placed in contact over the sample in an intermittent manner.

By lifting the tip from the surface after making a brief contact, dragging across the surface is minimized; hence, usually higher resolution than other AFM modes can be achieved. Similar to contact mode, tapping mode can be implemented either in air or liquids by oscillating the cantilever near its resonant frequency using a piezoelectric element. When a voltage is applied to the piezoelectric element, the motion causes the cantilever to physically oscillate at a high amplitude (usually above 20 nm) when the tip is not in contact with the sample. This amplitude is known as free oscillation (original amplitude) and it occurs approximately at a frequency of 50,000 to 500,000 Hz. The behavior of the cantilever when it is driven in a sinusoidal motion can be comparable to a damped spring or a single harmonic oscillator. As the cantilever approaches the surface of the sample, the amplitude of the oscillation is reduced.

When the cantilever reaches contact with the surface, the oscillation decreases its amplitude due to energy loss as an effect of the tip getting in close contact with the sample. The reduction in the cantilever oscillation (reduced amplitude) is adjusted by the feedback system loop, by maintaining a constant cantilever amplitude (adjusted amplitude). Hence, in tapping mode amplitude is the most important feedback parameter. The main characteristic of the feedback loop during tapping mode imaging is that it tries to maintain constant oscillation amplitude. Amplitude information is then used to determine topographical features of the sample Tapping mode is exemplified in figure 21.

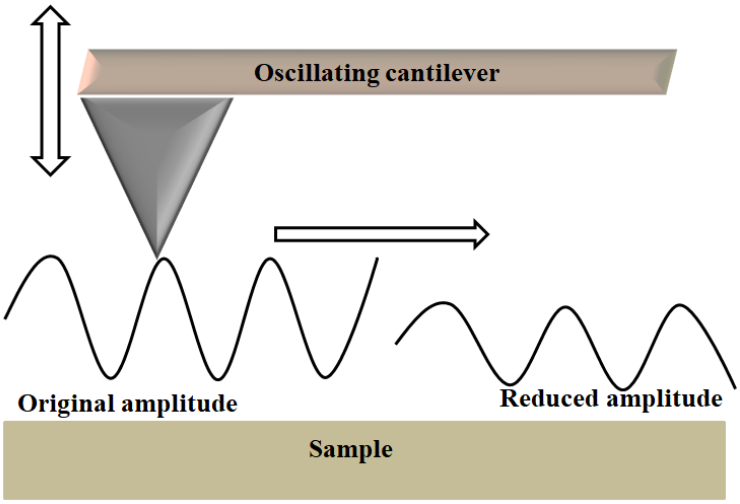

Figure 21. Tapping mode representation.

The presented description corresponds to amplitude modulated tapping mode or dynamic mode. The most important parameters to be optimized in this mode are the cantilever spring constant, free oscillation amplitude and amplitude set point. The cantilever stiffness should be correctly selected. If a cantilever is quite stiff, it might destroy; damage the sample or the tip itself.

The free oscillation amplitude determines the amplitude of the vibration of the cantilever when is not in contact with the sample. It is measured in voltage with a correspondence in nanometers if calculated. The amplitude set point is the target reduced amplitude.

The set point is expressed as a percentage of the free oscillating amplitude. In principle, the lower the amplitude set point, a higher force will be applied on the sample by the tip when in contact. Besides amplitude modulated tapping mode, there is also phase imaging mode. Phase imaging is a form of tapping mode

which is more sensitive to mechanical properties of the material. During this mode of operation, the signal from the phase channel is collected. An oscillating cantilever may experience a phase shift when interacting with the sample. The phase shift φ is described by the following equation:

$$d = Asin(2\pi ft + \varphi)$$ Eq. 5

where d = deflection of the cantilever; A = amplitude; f = frequency; t = time; and φ = phase shift.

3.6.4 Kelvin force probe microscopy

KPFM is becoming a very useful and well established technique in different areas such as nanotechnology and material sciences. Depending on manufacturers and brands, KPFM can be referred to with various names and working modes. Nevertheless, there are in principle two different modes of operation: lift mode and dual frequency mode. In this dissertation only amplitude modulated (AM-KPFM) lift mode is used.

3.6.5 AM-KPFM

In this dissertation, only AM-KPFM is used to perform surface potential readings. AM-KPFM is a dual AFM mode in which each line is scanned twice. During the first pass, the topography of the sample is recorded. On second pass, the cantilever is elevated to a given constant scan lift height, the mechanical oscillation applied to

the tip is turned off and an oscillating voltage $U_{AC}sin(\omega t)$ with a direct current (U_{DC}) offset is applied directly to the AFM tip.

$$U(t) = U_{AC}\cos(\omega t) + U_{DC} \text{ Eq.6}$$

Then the cantilever scans the recorded surface topography at a specific lift height above the sample while responding to electric forces on second pass (interleave) scan. When there is a DC voltage difference between the tip and sample (contact potential difference), results on an oscillating electric force acting on the AFM tip at the frequency ω (F_ω). Since KPFM is a nulling technique, the ω component is used as feedback signal to adjust U_{DC} so that F_ω=0, where

$$F_\omega = \frac{\partial C}{\partial h} U_{AC}(U_{DC} - \Phi_s)\cos(\omega t) \text{ Eq. 7}$$

In experimental conditions, the AFM tip has its own surface potential (Φ_t) depending on the material. U_{DC} signal corresponds to the local contact potential difference (Φ_s):

$$U_{DC} = \Phi_t - \Phi_s \text{ Eq.8}$$

If the tip and sample are at the same DC potential, there is no force on the cantilever at frequency ω and the cantilever amplitude will be equal to zero. The voltage applied to the probe tip is recorded by the controller to construct a voltage map of the surface.

3.6.6 Resolution and sensitivity

Lateral spatial resolution on KPFM is understood as the ability to distinguish adjacent regions on a sample which possess different surface potential properties separated by a given *d* distance. In figure 22, the distance is represented by the letter *d*. The area referred to as *d*, represents the distance at where electrostatic forces from the sample are acting on the tip.

Geometry of the tip plays an important role on the lateral resolution on KPFM, however, it is also affected by the separation distance (z) between the AFM tip and the sample. In figure 22 lift distance is represented by the letter ‘’H’’. In order to increase lateral resolution, lift distance is required to be minimized. This would result in reducing the distance in which electrostatic forces acts on the tip.

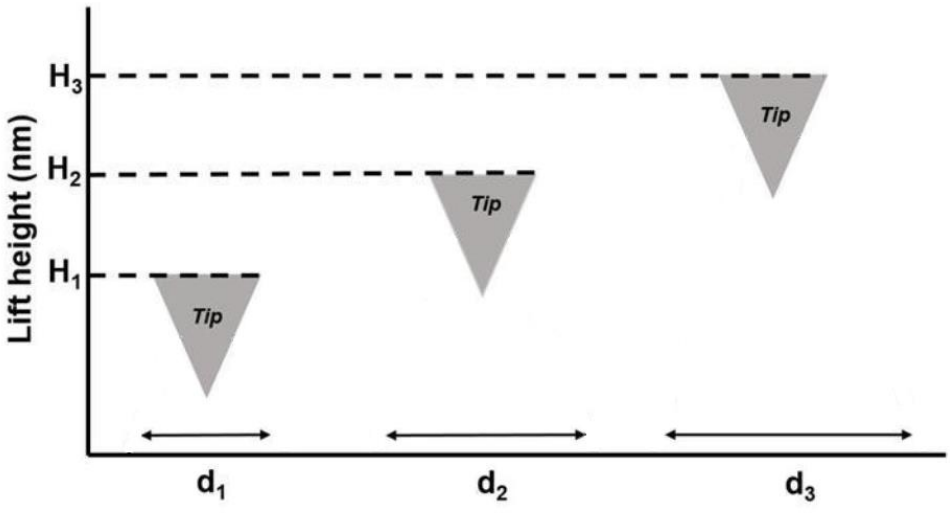

Figure 22. Effect of lift height on surface potential difference and resolution.

3.6.7 Image processing

All atomic force microscopy and Kelvin force microscopy images were processed using the SPM data visualization and analysis tool Gwyddion 2.38. Some images required to remove polynomial background and this was done by applying 2^{nd}-order polynomial in horizontal direction to compensate scanner bow artifacts. Similarly, images were levelled by applying mean plane subtraction. In topographic images dark areas represent smaller features in the vertical direction (height), whereas in surface potential images darker areas represent lower or negative values on surface potential.

3.7 AFM tip assisted triboelectric surface charge on mica: detection by KPFM and dissipation

In this experiment, an uncoated conductive tip (Veeco antimony (n) doped Si), with a resonant frequency of 361.01 Khz and a deflection sensitivity of 27.69 nm/V was used. To scratch mica surface with the AFM tip, contact mode was used with a deflection set point of 1 V, 10 μm scan size and a 3 Hz scan rate taking 512 samples per line. Subsequently, the AFM was switched to tapping mode in the same area increasing the scan size to 40 μm, leaving the initial scanned area (in contact mode) in the centre of the frame.

A drive amplitude of 30 mV and a set point of 450 mV was used. Whereas, in the lift mode, an electrical drive amplitude of 2500 mV and lift height of 25 nm was used. The lock-in phase for the used tip was found to be -90.° All measurements were carried out at 39% relative humidity and a temperature 25 ℃. After obtaining the first simultaneous

complete image on tapping and KPFM of the scratched area, 5 subsequent continuous scans were performed.

After the last continuous scan, condensation was induced by exhaled breath to saturate the sample with water and dissipate remaining surface charge, and a last scan was performed. Ultimately, a different area was "scratched" using the same parameters as previously, and different scans were performed at various times: 0, 30, 60, 90 and 120 minutes.

3.8 Principles of direct measurement of protein aggregation by ultraviolet-visible spectroscopy (UV-Vis)

Proteins display a broad peak in the 250- to 300-nm region of their UV spectrum. This is composed of multiple overlapping bands arising primarily from the aromatic residues phenylalanine, tyrosine, and tryptophan. In addition to the ability of UV-absorption spectroscopy to detect alterations in protein conformation and dynamic fluctuations, both of which could lead to protein aggregation, this technique has been widely employed to directly probe protein aggregation as well as analyse aggregation kinetics and identify the presence of intermediates and the underlying mechanisms involved.

Such analyses often include time-dependent turbidity measurements to monitor the formation of aggregates or probing time dependent protein monomer loss. Herein, we use the term aggregation to refer to any process including fibrillation, polymerization, gelation, etc. that leads to the formation of multimeric non-native protein species [107].

Turbidity *(τ)* is defined as:

$$\tau = -\ln(I/I0) \qquad \text{Eq.9}$$

where *I*0 and *I* are the intensity of the incident and transmitted light, respectively. The measured optical density (OD) signal is related to turbidity according to:

$$\tau = 2.303\ \text{OD} \qquad \text{Eq. 10}$$

Note that OD = *A* + *S*, where *S* is the light extinction due to scattering and any other process that blocks light from being detected. Thus, when *A* = 0, the OD is the loss due to scattering under common circumstances.

Furthermore, τ is a coefficient that reflects attenuation of the light passing through the sample. Such attenuation of light is often due to the presence of larger particles (multimers and aggregates) approaching 1/50–1/20 or above of the wavelength of incident light in size [107].

3.9 Insulin incubation:

Insulin from bovine pancreas was purchased from Sigma-Aldrich. pH was adjusted by adding a few drops of HCl at 32% concentration in milli-Q water, until the desired pH was reached. bPEI (bPEI/AuNp) and lipoic acid coated gold nanoparticles (lipoic acic/AuNp) dispersed in milli-Q water were purchased from nanoComposix (San Diego, CA, U.S.A). Water used to perform the experiment was ultrapure. Insulin solutions were prepared to a final concentration of 1mg/ml in 32% HCl pH 2.0

ultrapure water. Subsequently, solutions were sonicated for 15 minutes to eliminate visible aggregates. All solutions were prepared by triplicate and placed on 2 ml Eppendorf tubes. Incubation was carried out at 75 ±.5 ℃ using an aluminium heating block for Eppendorf tubes, docked on a Thermo-Scientific block heater. Temperature was measured with a digital thermometer and constantly observed.

3.10 Fibrillation kinetics:

Insulin fibrillation kinetics was measured by UV-Vis absorbance assay. Absorption readings were performed at wavelengths ranging from 600 nm to 250 nm by triplicate and averaged.

However, the maximum absorbance value for insulin occurs around 280 nm, and has been extensively used in various investigations to track insulin fibrillation kinetics [65][108][109].

Spectroscopic measurements were performed on a Perkin Elmer LAMBDA 800 UV-VIS spectrometer. Samples analysed were prepared by taking 200 µl aliquots from the incubated insulin solution and diluting the resulting solution into ultrapure water adjusted to pH 2 with HCl.

3.11 Observation of fibrils by AFM:

Diluted samples of fibrils for AFM were directly taken from the samples prepared for UV-Vis measurements. One drop of each solution was deposited on freshly cleaved

mica. The samples were washed several times with ultrapure water to remove unattached fibrils or impurities and were nitrogen dried. Uncoated antimony doped AFM tips (Bruker, model NCHV) with a resonant frequency of 359.30 kHz were used to perform AFM in tapping mode.

3.12 Nanoparticles characterization:

Table 2, summarizes the physical properties of bPEI/AuNp and lipoic acid/AuNp coated gold nanoparticles. The average particle size for both nanoparticle systems, as measured by TEM as dried powder is around 12 nm, displaying a homogenous spherical morphology (figure 23). As presented in Table 2, zeta potential (mV) of the nanoparticles is greatly affected by pH.

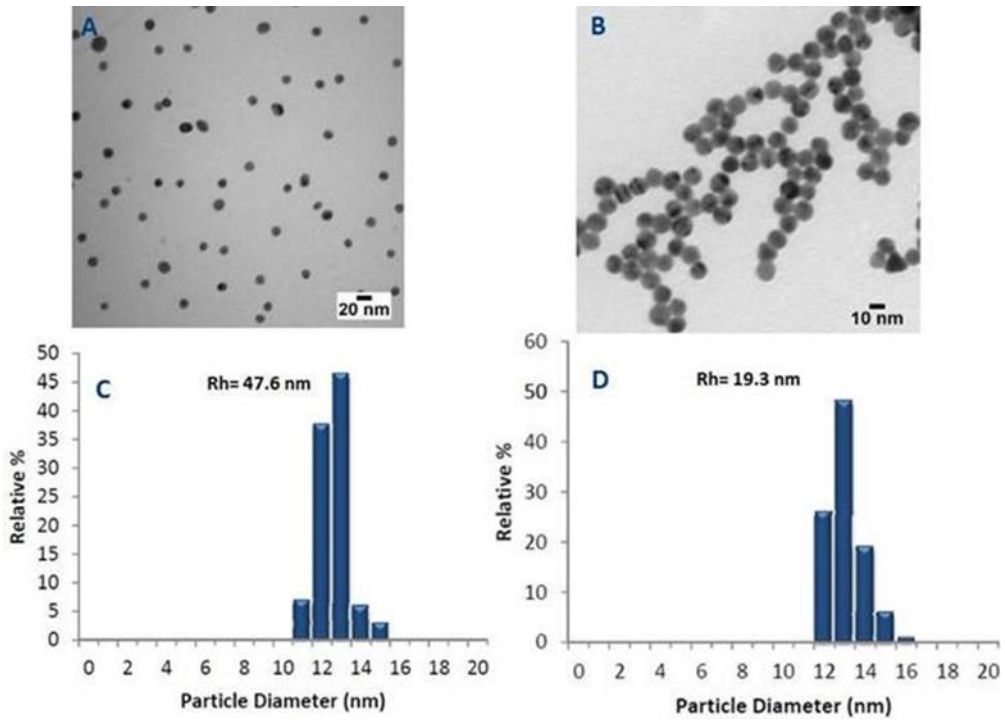

Figure 23. TEM micrographs of; A) bPEI/AuNp; B) Lipoic acid/AuNp. Hydrodynamic radius (Rh) distribution of gold nanoparticles with different coatings. C) bPEI/AuNp; D) Lipoic acid/AuNp (Nanocomposix technical data sheet).

Type	pH	Zeta potential	Size (TEM)	solvent
bPEI/AuNp	pH 7.4	46.3 mV	12.1 ± 0.8 nm	DI water
bPEI/AuNp	pH 2	22.3 mV	12.1 ± 0.8	DI water/HCl
Lipoic acid/AuNp	pH 7.4	-47.5 mV	12.6 ± 0.8 nm	DI water
Lipoic acid/AuNp	pH 2	13.1 mV	12.6 ± 0.8	DI water/HCl

Table 2. Gold nanoparticle characteristics

CHAPTER 4:

Results and discussion

4.1 Micro channel filling patterning for KPFM measurements

For all types of micro-printing (contact, channel filling) on mica, patterns at the micro scale can be observed by creating condensation on the surface. As a general example, figure 24, portrays the pattern as it should be visible under an optical microscope.

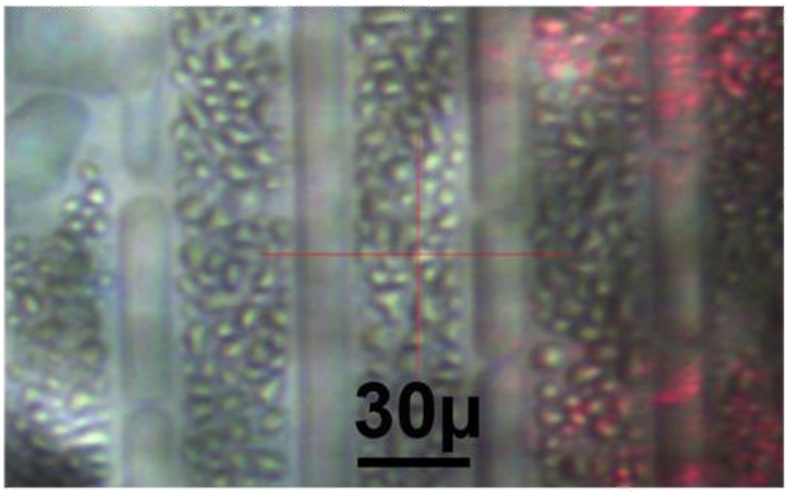

Figure 24. Image of the condensation pattern obtained by the built-in optical microscope (scale bar at 30µm).

Condensation is used to observe the presence of patterns when the pattern itself is not visible under optical microscopy.

However, in some cases, condensation patterns are observed under optical microscopy while AFM confirms that there is no presence of poly-L-lysine. A

probable reason could be that simple contact between the substrate and the stamp alters the surface by leaving traces of PDMS or dust.

In either way, the observation of a condensation pattern is the first step towards successfully imaging with AFM and KFPM patterned poly-L-lysine. As an example, figure 25 shows how ideally poly-L-lysine patterns should present a clear contrast and delimitation with the mica substrate.

In addition, it demonstrates the dimensions of the gap between patterned poly-L-lysine, corresponding to the expected values from the morphology of the stamp used (10 μm channels, 30 μm ridges). Similarly, both topographic and surface potential profiles are in accordance.

PLL patterns on this sample (Figure 25) are very well defined, and the distribution of the PLL layer can be easily observed in both the topographic and potential image. Figure 25-A and 25-C, shows clearly the presence of patterned PLL, which has an approximate height of less than 1 nm, which is in accordance to the expected high of random coil biomolecules on mica [48].

On the other hand, figure 25-B and 25-D, show the surface potential mapping of patterned PLL on mica. It can be observed a very well-defined pattern with a surface potential difference in respect to the substrate of approximately 240 ± 10 mV

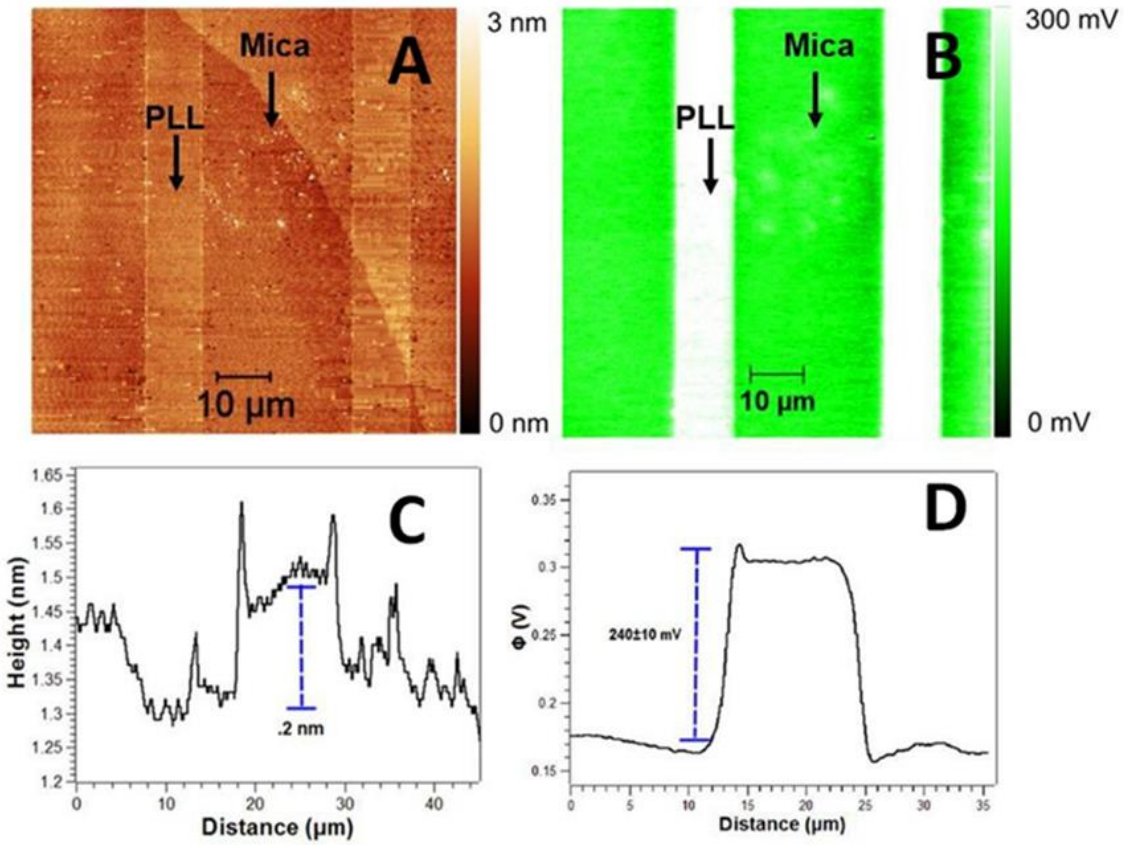

Figure 25. Good poly-L-lysine pattern fabricated by microchannel filling. A) Topography image, B) Potential image, C) topography profile, D) potential profile.

Once good patterns were produced, and a potential mapping was obtained, further experiments under different conditions were tested. Initially, the effect of multiple KPFM scans is described Figure 26 shows the effect of continuous scans. Figure 26 show qualitative images of topography and surface potential of poly-L-lysine patterns of after a 1st and the 8th consecutive scans.

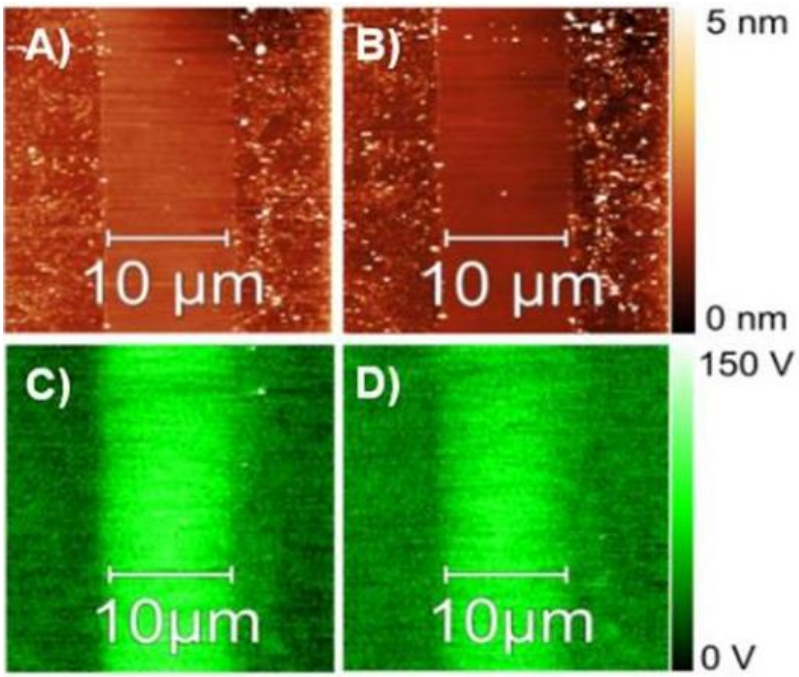

Figure 26. Continuous scans. A) Topographic image of a PLL pattern at initial time, B) Topographic image of a PLL pattern after 8 scans, C) Surface potential image of PLL pattern at initial time, D) Surface potential image of a PLL pattern after 8 scans.

Nevertheless, figure 27, shows the quantitative surface potential difference of 8 continuous scans on the same area corresponding to the area shown in figure 26. Furthermore, a 9th scan on the same area after 48 hours showed a surface potential difference decay (Figure 27).

The observed result suggests that a PLL pattern on mica produced by micro channel filling can be scanned up to 8 times without a significant decay in surface potential. However, the substantial decay on surface potential after 48 hours is likely to be caused by change on mica over time.

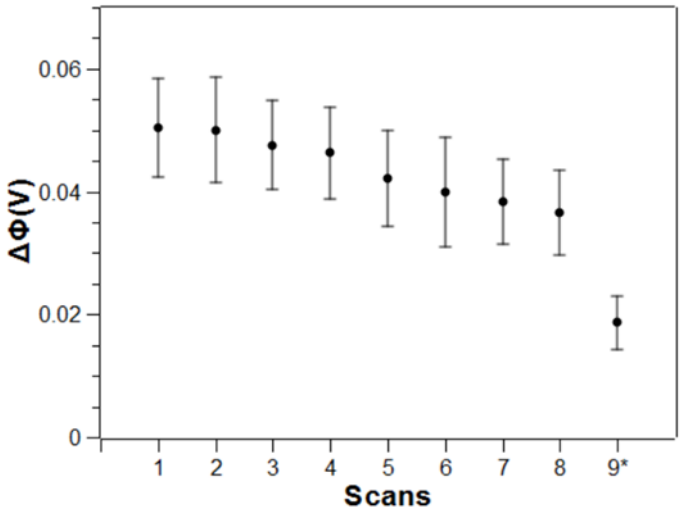

Figure 27. Continuous scans. *Represents potential difference in the same areameasured 48 hours after the last scan.

In protein biophysics, most reactions and process occur in fluid. Likewise, it is the case for bio sensing devices, which are expected to perform under near biological conditions.

For these reasons, it is important to investigate how stable the patterns and the KFM readings are when it comes to re-immersions in liquids.

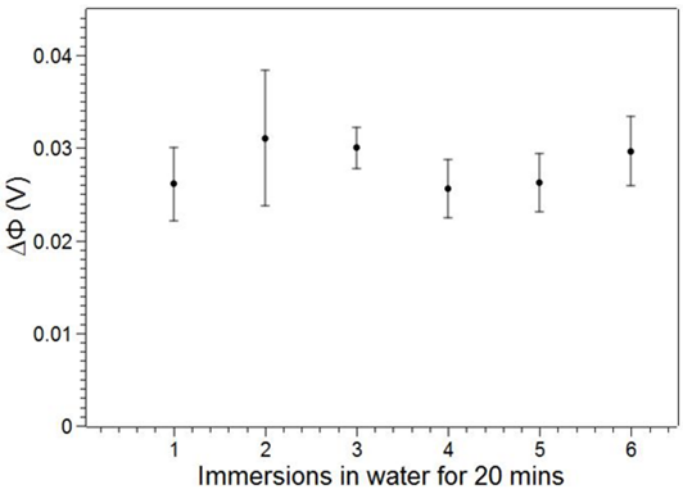

Figure 28. Immersions in water for 20 mins. Control experiment.

Figure 28, demonstrates that when immersing the sample in water for 20 minutes, air drying it and re-scan it repeatedly, the surface potential difference between patterned

PLL and the substrate, in this case mica, do not change significantly. We can conclude from this graph that, in fact, the fabricated PLL patterns can be used to investigate biochemical processes involving biomolecules in solution with high repeatability.

Lift height, as discussed in the methods section, is a very important parameter in KPFM readings [110]. In order to investigate how it influences both sensitivity and resolution on the fabricated PLL patterns, surface potential mappings were obtained at different lift heights from the sample. Figure 29, demonstrates the effect of lift height on surface potential difference of a poly-L-lysine pattern, starting at 5 nm until 1.5 μm.

It can be observed that a considerable surface potential difference can be detected up to 1000 nm above the sample, which corresponds to ~2 times the dimensions of the PLL patterned surface (10 μm). Moreover, it can be determined that any value under 100 nm of lift height can be used with strong confidence since, there is no apparent strong effect on the sensitivity at that height.

On the other hand, scanning at lift heights in the order of 1 nm to 5 nm increases the chances of the tip being in contact with the sample, creating cross talk and possible artifacts on the surface potential image, whereas using lift heights in the order of 10 nm to 25 nm, resulted in stable images with a good degree of sensitivity and standard deviation. Standard deviation, as it can be seen on the error bars, is constant because the highest standard deviation of all measurements was selected and applied to every point.

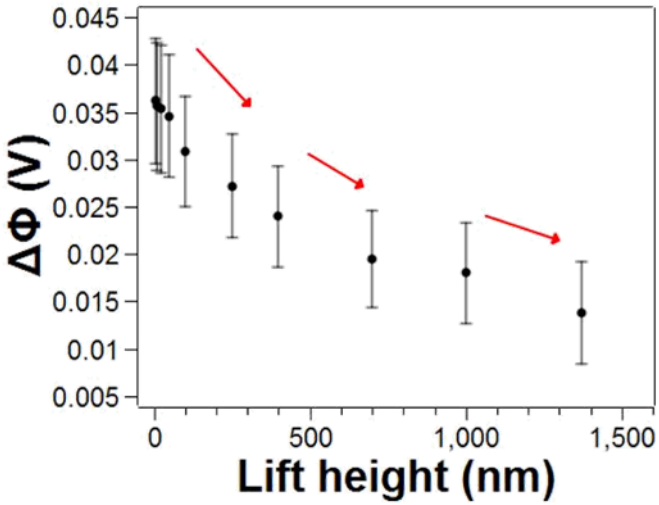

Figure 29. Surface potential difference (ΔΦ) versus lift height.

Subsequently, after 48 hours, lift heights of 50 nm, 25 nm, 10 nm and 5 nm re-scanned respectively are shown in figure 30. Values of surface potential difference are around 10 mV lower after 48 hours, however, they still show lift height dependence.

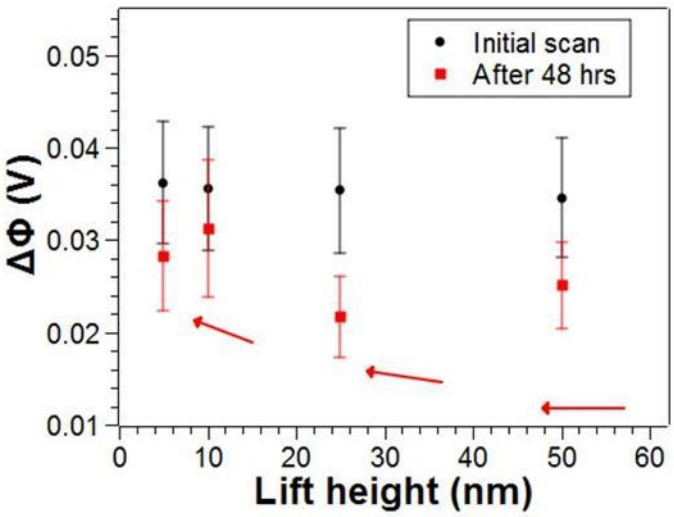

Figure 30. Comparison of initial values of ΔΦ on the initial scan versus same lift heights after 48 hours.

Patterning with micro channel filling present high variation from one sample to another and from one area to other (figure 31). To overcome the effect of high variation, experiments were performed in the same

scanning area. Possible reasons for the high variation from sample to sample and area to area are discussed in the next pages.

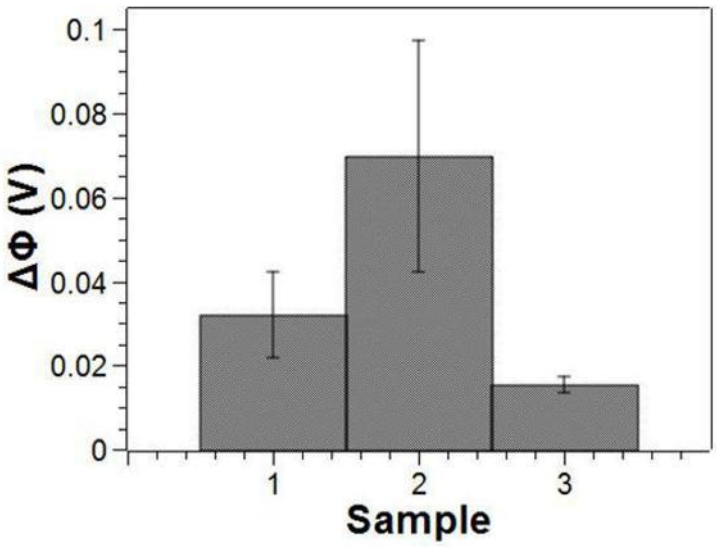

Figure 31. Average potential difference in three different samples.

4.1.1 Common defects while patterning by micro channel filling

In general, micro channel filling presents some difficulties, resulting in time consuming, low repeatability and high variation. When patterning by microchannel filling, sometimes different defects can be observed. For instance, when micro channels are blocked on the PDMS stamp, the appearance of empty channels can be observed when studied by AFM (figure 32). As an opposite case, due to the highly hydrophilicity of both PLL and mica, and their clearly opposite surface charge, PLL has the tendency to adsorb and spread evenly on mica (figure 33). When the PDMS stamp is not properly sealed against the substrate, PLL can be found distributed outside of the pattern very often, yielding lower surface potential difference between the region of the pattern and the substrate. For this reason, it is

important to consider a different method of soft lithography, such as micro contact printing, which results in higher quality of the patterns.

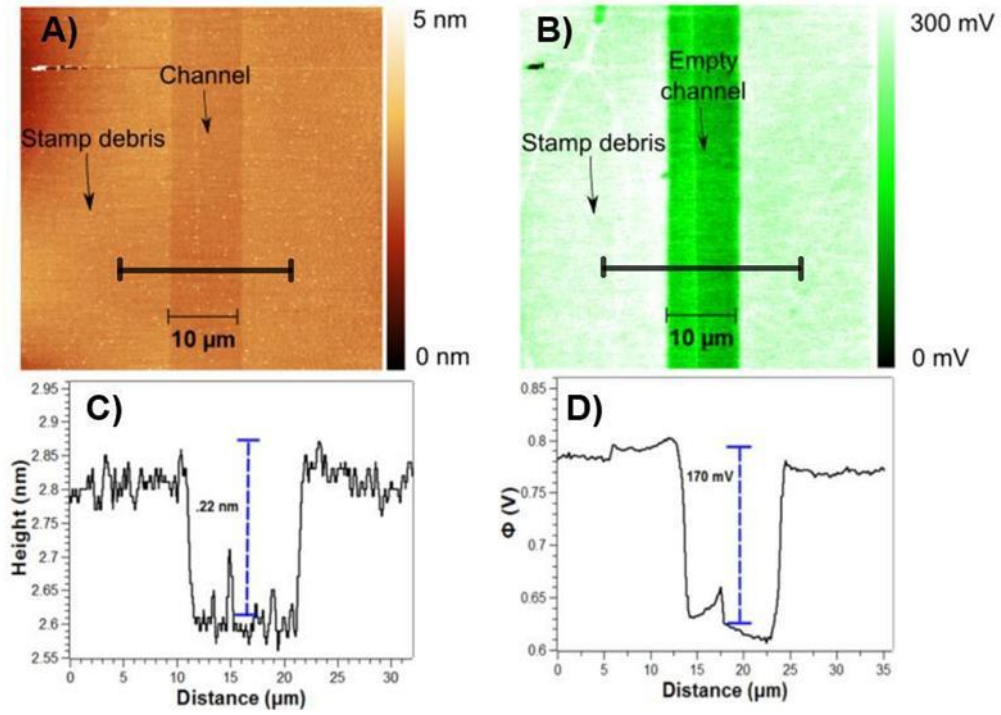

Figure 32. A) Topography of an empty channel by microchannel filling, B) Surface potential image of an empty channel by microchannel filling, C) topography profile of an empty channel, D) surface potential profile of an empty channel.

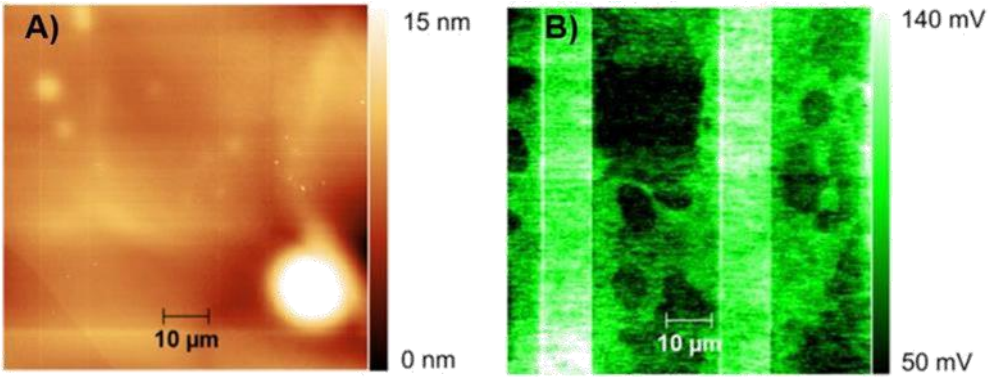

Figure 33. Poly-L-lysine distributed outside of the pattern. A) Topography image, B) potential

The observed results on surface potential readings under different factors such as repeated scans, immersions and lift distance, suggest this patterning method in combination with KPFM is reliable for further and more complex experiments regarding surface potential properties of biomolecules and its relationship with external

factors such as physiochemical and biochemical modifications. However, this approach has shown to be poor in the sense of good topographic resolution.

This is attributed to the fact that there is a high contact area between the stamp and the substrate, which results in deposition of dust or stamp residues. Another drawback is that high variation narrows experiments to be carried out in the same scanning area, obtaining reliable data with a maximum of 50 μm^2.

Furthermore, this technique possesses a low probability of success when preparing samples, due to the presence of various defects on sample preparation, which makes it highly difficult to perform experiments on a regular basis and with a good degree of efficiency.

4.2 Immersions in 6 mM D-Ribose solutions

After repeated immersions of poly-L-lysine patterns in ultrapure water have shown that the surface potential difference is not altered, a subsequent step towards the study of sugar accumulation and possible biochemical changes on the patterns was tested. In this experiment, freshly prepare PLL patterns by microchannel filling were immersed repeatedly in 6 mM and 6M D-ribose solutions. In regards the low concentration solution (6 mM), samples were scanned after immersions in sugar solution, and after washing the sample with ultrapure water. The initial observed effect was a clearly inverted surface potential (negative).

The effect seems to be reversible, since the surface potential returned repeatedly near to the initial value (positive) after the sugar content was washed away with water from the surface (immersions in water). Qualitative images are displayed on figure 34.

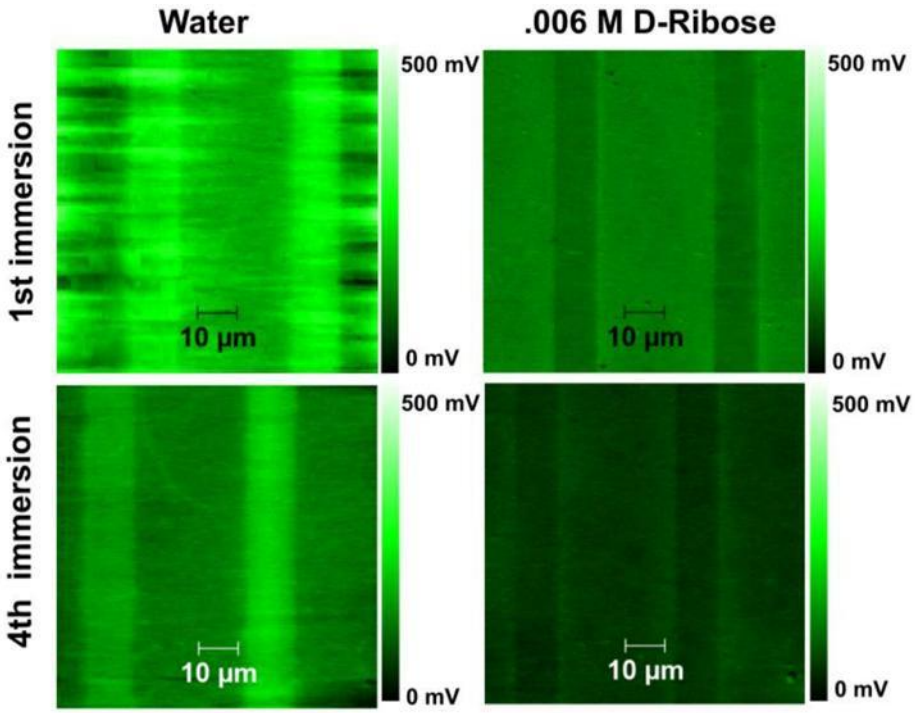

Figure 34. Surface potential micrographs of repeated immersions in water and .006M D-ribose solutions.

Figure 35, presents quantitative data extracted from potential images before and after immersions in .006M D-ribose solutions. When the patterns are exposed to the presence of sugar, a drastic drop in surface potential difference down to negative values is observed (black dots). Nevertheless, by washing the sample with ultrapure water, it was possible to reversibly return to positive values (red squares).

However, after repeating the process up to four times, it was no longer possible to reach the initial positive value, leaving the last reading about 50 mV below the original value (red squares). Likewise, after the immersions in .006M D-ribose solutions, a slightly

positive increment on surface potential difference is observed after each subsequent immersion (black dots).

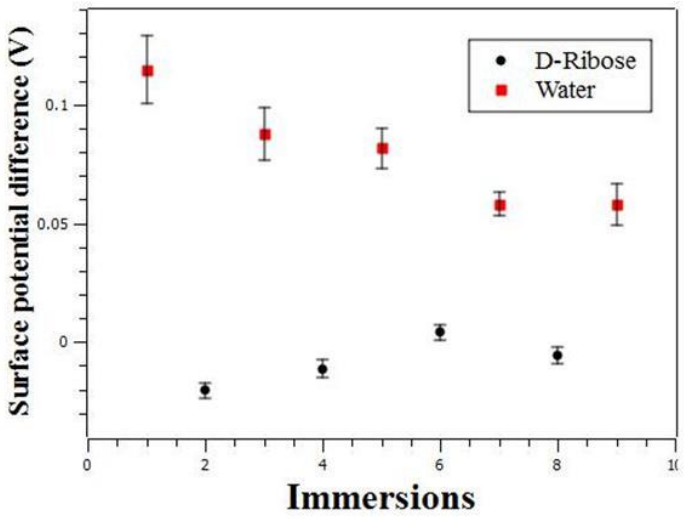

Figure 35. Surface potential difference after repeated immersions in water and .006M D-ribose solutions.

These results suggest that there could be a deposition of sugar molecules over the poly-L-lysine pattern that remain on the surface after washing it with ultrapure water (red squares). Sugar molecules could have the tendency of accumulation after each immersion in sugar solution, yielding a constant decrease on the surface potential difference. Up to this point, there is not enough evidence suggesting a biochemical modification on the poly-L-lysine pattern.

4.3 6 molar D-Ribose

Since using a 6 mM sugar concentration was arbitrary, an extreme concentration (6M) was also tested to observe the effect of surface potential. The concentration of D-ribose in this set of experiments was quite high. The excess of sugar on the surface made both topographic and potential imaging very difficult.

Hence, all the samples had to be washed with ultrapure water prior imaging after each immersion in 6 molar D-ribose solutions. It can be observed that the surface potential is no longer reversible after immersions in ultrapure water and there is a clear accumulation of sugar on the poly-L-lysine pattern, observed in the topographic profiles (Figure 36), where the increment on height is evident after re-immersions in sugar solution

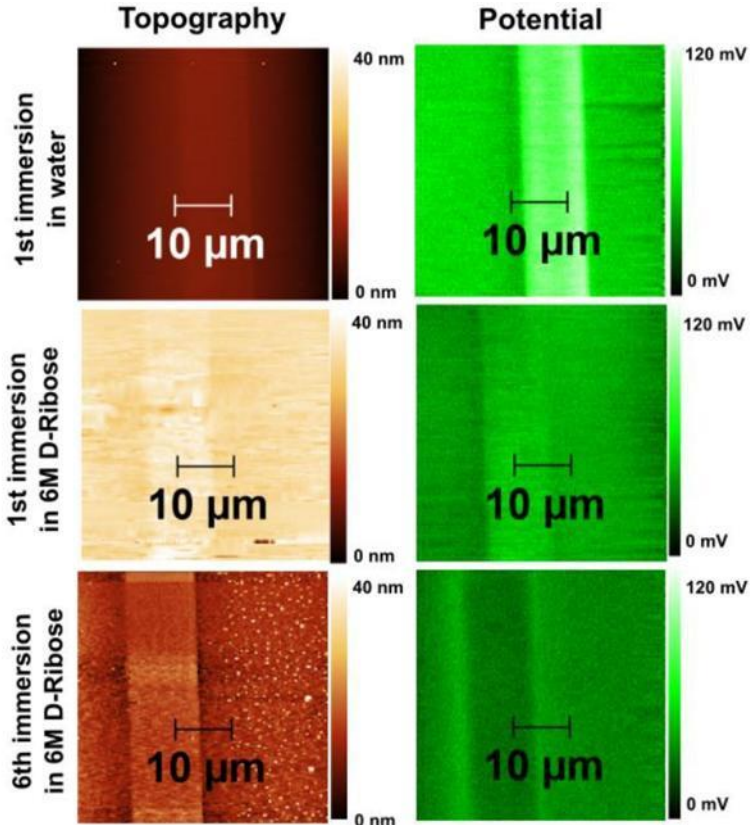

Figure 36. Qualitative images of both topography and surface potential after a first immersion in ultrapure water and subsequent immersions in 6M D-ribose solutions.

Besides qualitative images, it is interesting to analyse the corresponding topography and potential profiles. Figure 37, represents topography (37-A) and potential (37-B) profiles of the immersions of poly-L-lysine patterns in 6 molar D-ribose solutions. In the topographic profiles after the first immersion in D-Ribose solution 37-A), a layer of about 2 nm is present on the surface.

Poly-L-lysine molecules usually display topography heights below 2 nm, which suggest an accumulation of sugar aggregates from the first immersion in 6 molar D-ribose solutions (see figure 37-A). After up to six subsequent immersions, the layer in the same area is increased to around 8 nm.

This fact, may also reveal some possibilities of functionalizing surfaces for different purposes. Quorum sensing (QS) is a system of stimuli and response correlated to bacterial population density. For instance, recently has been found that D-ribose deposition can interfere QS and inhibit biofilm formation [111].

For instance, in the previously mentioned case, it would be very helpful to fabricate a surface in which deposition of sugar is patterned and suitable for AFM and KPFM imaging. In the case of potential profiles (37-B), after the first immersion in D-ribose a positive potential of about 12 mV exists in the poly-L-lysine pattern.

This potential, in the same area, is shifted to around -14 mV after six subsequent immersions. It is important to consider that between each immersion at 6 molar concentration, the sample is washed with water and dried with air, meaning that both the accumulation of sugar in the pattern and the inversion of surface charge in the potential, are no longer reversible.

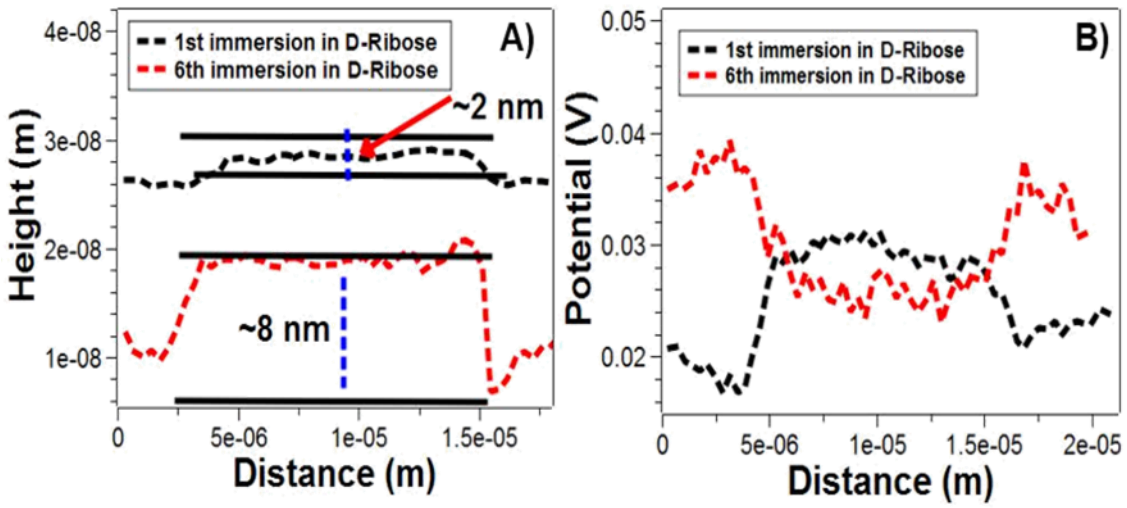

Figure 37. A) Topographic and B) surface potential profiles comparing the first immersion in 6M D-ribose and the last immersion.

After an overlook of images and profiles, a more rigorous statistical analysis is shown in figure 38. After the first immersion in in 6M D-ribose solution and followed by washing with ultrapure water, the surface potential difference is dropped to nearly zero. Subsequent immersion and washings results in a decrease in surface potential around -20 mV.

We can conclude with this, that at higher concentrations of sugar, the process is irreversible, and the highly negative surface potential difference would be attributable to either sugar deposition or the effects of a biochemical modification on the PLL patterns such as non-enzymatic glycation. Nevertheless, without an alternative method to confirm biochemical changes, it is difficult to state the event of glycation.

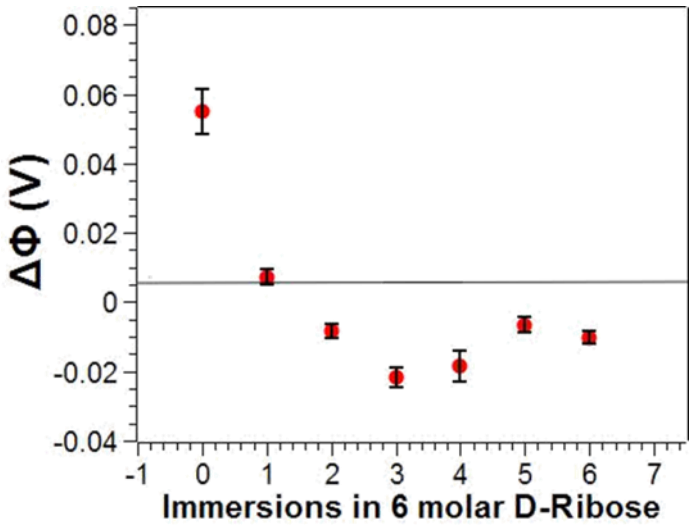

Figure 38. Surface potential difference between the pattern and the substrate (mica) after each immersion in 6M D-ribose and washing with ultrapure water; 0 denotes the value after an initial immersion in ultrapure water.

4.4 Electrostatic adsorption of colloidal gold nanoparticles on poly-L-lysine patterns

Both topographic and potential changes before and after the addition of nanoparticles are qualitatively observable in figure 39. Topographic features of a thin layer of poly-L-lysine are difficult to be observed by the Z sensor on the AFM.

However, on the potential channel (KPFM), the positive charge of functional groups of poly-L-lysine (amino) creates a sharp contrast with mica surface (figures 39-A and 39-B). When negatively charged nanoparticles in colloidal solution are in contact with patterned poly-L-lysine, preferential arrangement of nanoparticles on the poly-L-lysine pattern is possible due to an electrostatic driven auto assembly mechanism.

After the solution of nanoparticles is washed away from the sample, a small number of nanoparticles remain absorbed to mica. Nevertheless, the nanoparticle density is enormously higher within the poly-L-lysine pattern (figure

39-C). As a result, the potential detected on the poly-L-lysine pattern covered by nanoparticles, appears to be negative in respect to mica (figure 39-D).

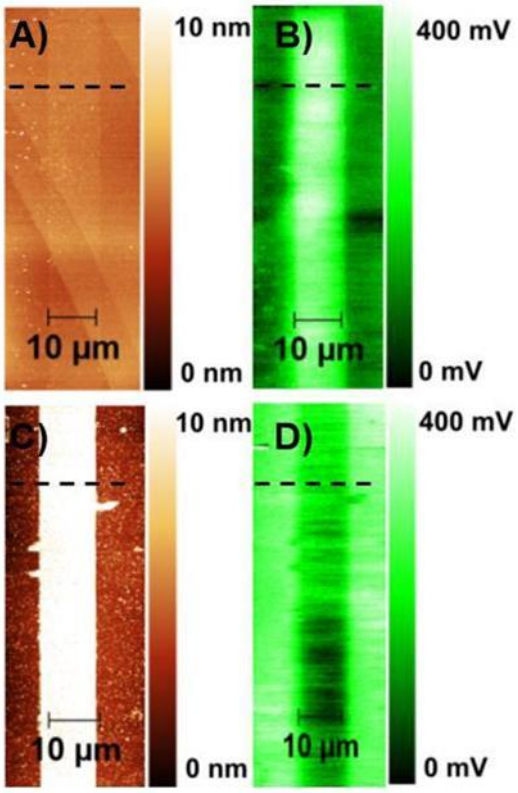

Figure 39. A) Topographic image of PLL patterned by microchannel filling on mica, B) surface potential image of the PLL pattern, c) topography image of the PLL pattern after immersion in colloidal gold nanoparticles, D) surface potential image of the PLL pattern after immersion in colloidal gold nanoparticles.

Figure 40, shows topographic and potential profiles extracted from figure 39 images.

The approximate height of the poly-L-lysine pattern is about approximately .40 nm, which is in accordance with similar studies on adsorption of poly-L-lysine on mica [35].

Furthermore, after immersion in a solution of colloidal gold nanoparticles (figure 40-C), a height of about 8 nm is observed, corresponding this value, to the approximate diameter of the nanoparticles in solution. In the same sense, surface potential profiles show a meaningful change after the immersion in solution of colloidal gold nanoparticles (Figures 40-B and 40-D).

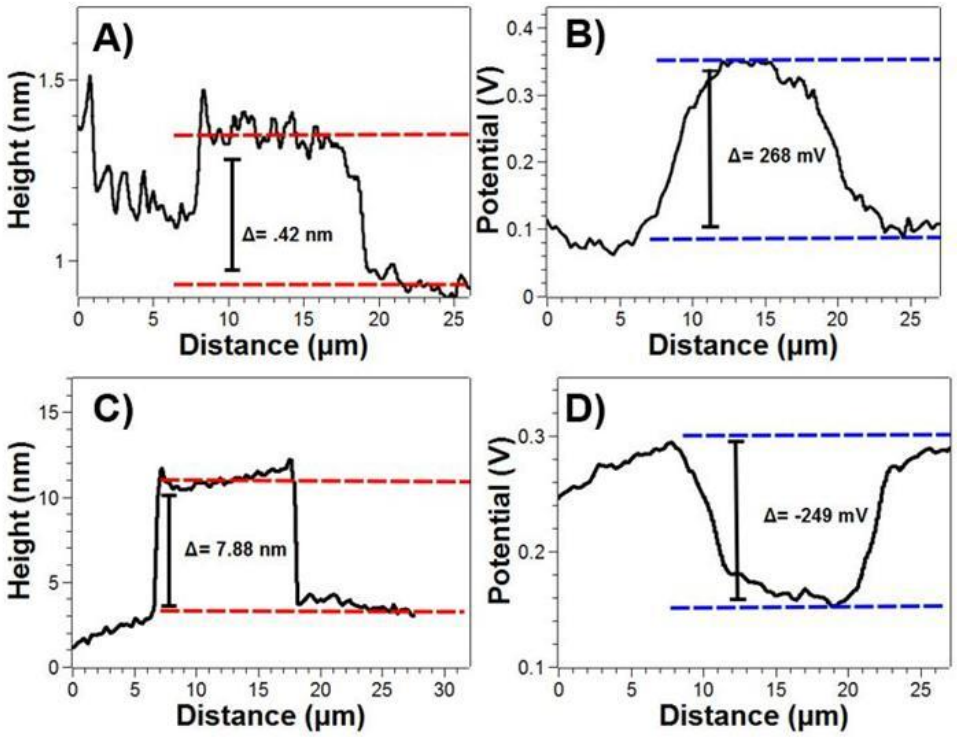

Figure 40. A) Profile of the topographic image of PLL patterned by microchannel filling on mica, B) profile of the surface potential image of the PLL pattern, c) profile of the topography image of the PLL pattern after immersion in colloidal gold nanoparticles, D) profile of the surface potential image of the PLL pattern after immersion in colloidal gold nanoparticles.

Additionally, when a statistical analysis is performed, a drop of more than 100 mV is observed after the poly-L-lysine pattern is exposed to the solution of colloidal gold nanoparticles (figure 41).

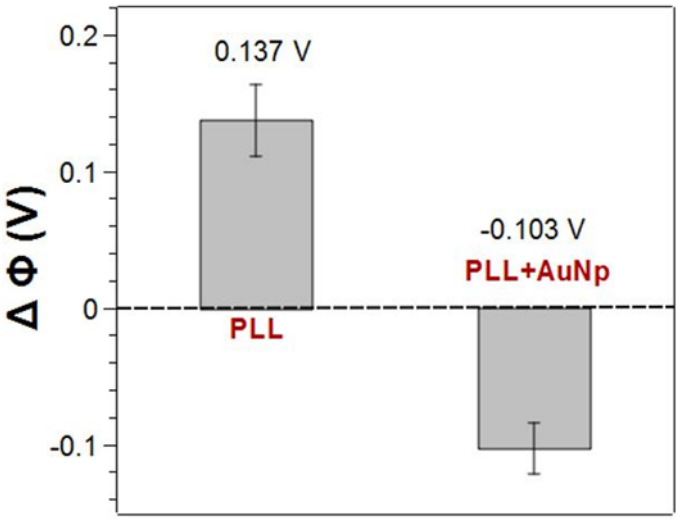

Figure 41. Statistical potential difference of PLL patterned by micro contact printing before and after immersion in colloidal gold nanoparticles.

4.5 Micro contact printing on different substrates

4.5.1 Mica

Initially, a control experiment was carried out to observe the effect of making contact between a fresh PDMS stamp and the freshly cleaved mica (figure 42). The control experiment confirms that no alterations on the topography or potential image is detected on the surface after being in contact with a fresh PDMS stamp.

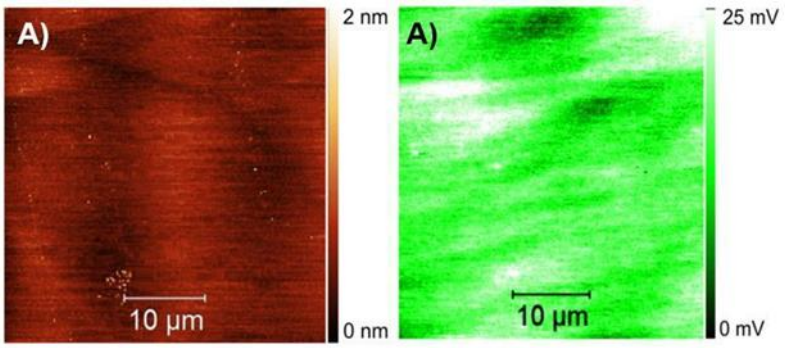

Figure 42. Control stamping with fresh stamp on mica. A) Topography and B) surface potential.

Nevertheless, when the stamp is placed in contact with a poly-L-lysine solution, molecules are clearly printed on the surface and they are observable by both topographic and surface potential images (figure 43). Interestingly, surface potential of poly-L-lysine patterns on mica fabricated by micro contact printing is less stable than patterns fabricated by micro channel filling.

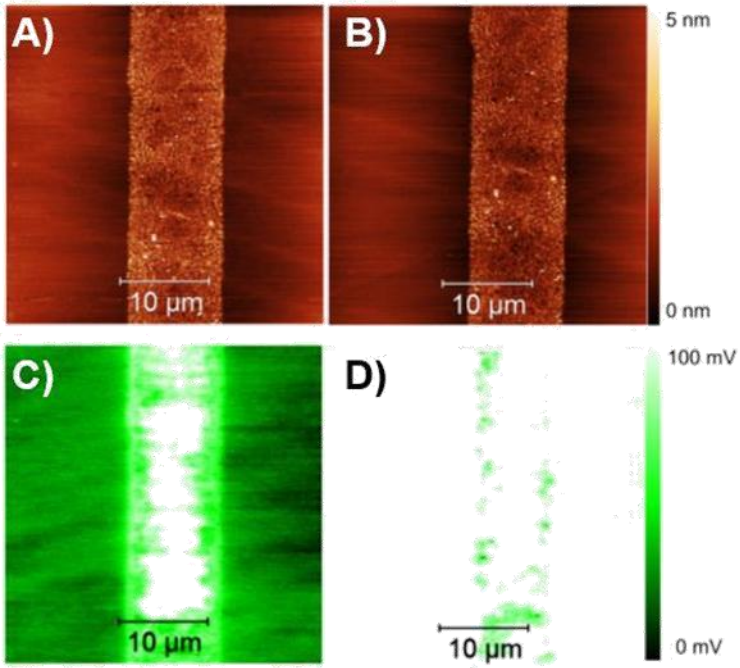

Figure 43-A presents the topographic image of the initial scan in air by KPFM, whereas figure 43-B represents the topographic image of the same area after being scanned six times. No substantial changes are revealed on the topography after six continues scans.

Nonetheless, on the potential images (43-C and 43-D), there is a clear qualitative difference observed. In order to rule out a reduction in the number of PLL molecules on the pattern as the AFM tip is repeatedly on intermittent contact, the roughness (Rq) and average height of the pattern were calculated on the topographic images. These values were found to be for the first scan Rq=.9 nm with an average height of 1.6 nm, whereas for the sixth scan Rq=.9 nm with an average height of 1.6 nm.

These numbers, remained unchanged, confirming that there is no alteration on the topography that could sensibly explain the drastic changes on the surface potential image. Figure 44 depicts a quantitative analysis corresponding to the potential difference calculated from the potential images of the six contentious scans. This result suggests that there is an electrostatic change on the surface of mica of about 60 mV, as a consequence of continuously scaning a specific area on KPFM.

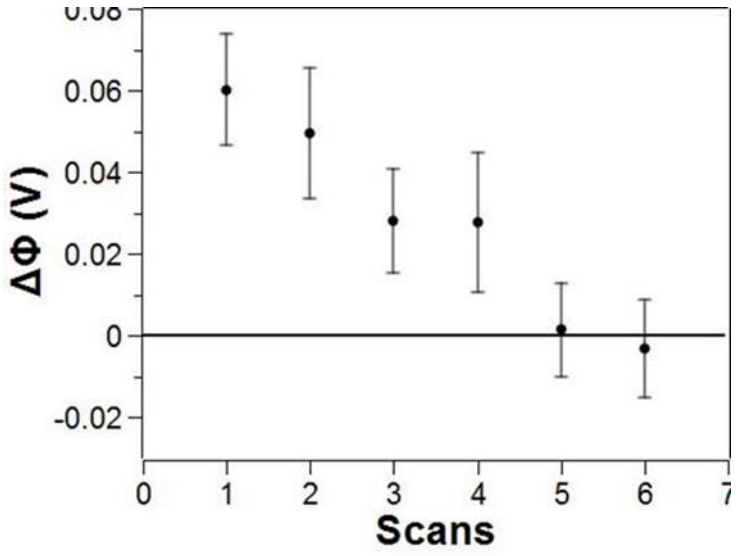

Figure 44. Continuous scans. Pattern by micro contact printing on mica.

In contrast with results obtained for a similar PLL pattern produced by micro channel filling, it can be concluded that by micro contact printing, a considerable area of the substrate (mica in this case) corresponding to the channel gap, remains untouched. Hence, there is no stamp residues or dust over the mica surface, which results in the exposure of freshly cleaved mica. According to this finding, clean freshly cleaved mica has the tendency to experience changes in surface charge faster than mica surface protected by dust or stamps residues.

4.5.2 Glass:

A similar experiment was carried out using glass as a substrate. In a previous experiment, where PLL patterns was produced on mica, it was confirmed that micro contact printing makes sample fabrication a more efficient process. However, in order to achieve good results, it is important to use freshly prepared PDMS stamps to avoid the presence of contaminants.

Since preparing a number of fresh stamps is time consuming and requires a larger amount of chemicals, recycling old used stamps was tested. To this end, stamps that were repeatedly used before were peeled off using adhesive tape. In this way, the outer layer of the stamp is removed, leaving a fresh unexposed layer of PDMS available for micro contact printing. Figure 45, represents a control experiment to confirm that peeled off stamps do not leave traces of previously adsorbed material. Similarly, serves as a control for performing further micro contact printing experiments using glass as substrate.

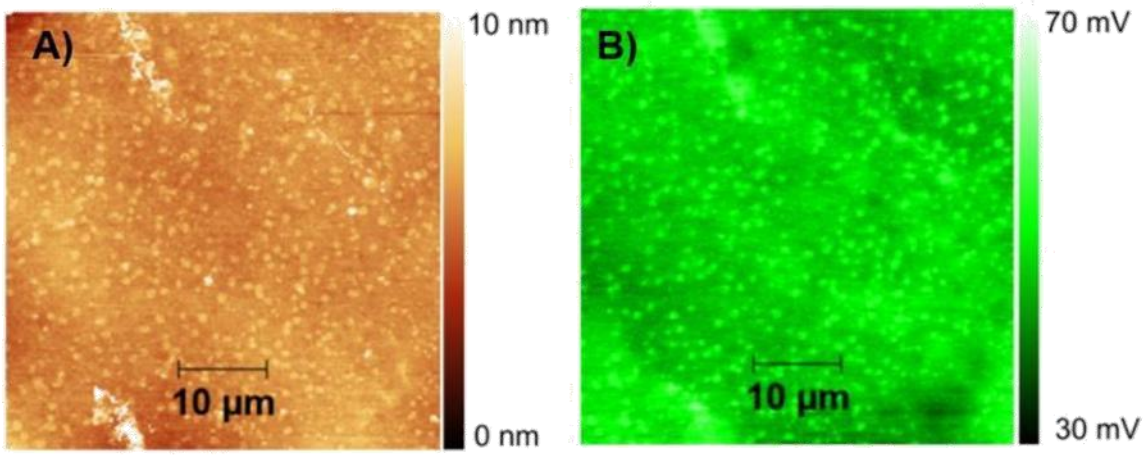

Figure 45. Control experiment of contact between a freshly peeled off stamp and glass. A) Topography and B) surface potential images.

To create this pattern, a freshly peeled off PDMS stamp was used. Due to the expected roughness of glass, the presence of PLL is not very well distinguished on the surface.

Nevertheless, they are clearly located in a pattern on the surface potential image. Figures 38-A and 38-B display the topography of an initial scan and a seventh scan respectively.

Considering the roughness of glass, the thickness of PLL films produced by micro contact printing, and the resolution of the image, any conclusion in regards changes on the topography after repeated scans cannot be made. In other words, roughness of the substrate in this case, might be higher than the actual height of the deposited layer of PLL. In the same fashion, Figures 46-C and 46-D display the surface potential of an initial scan and a seventh scan respectively.

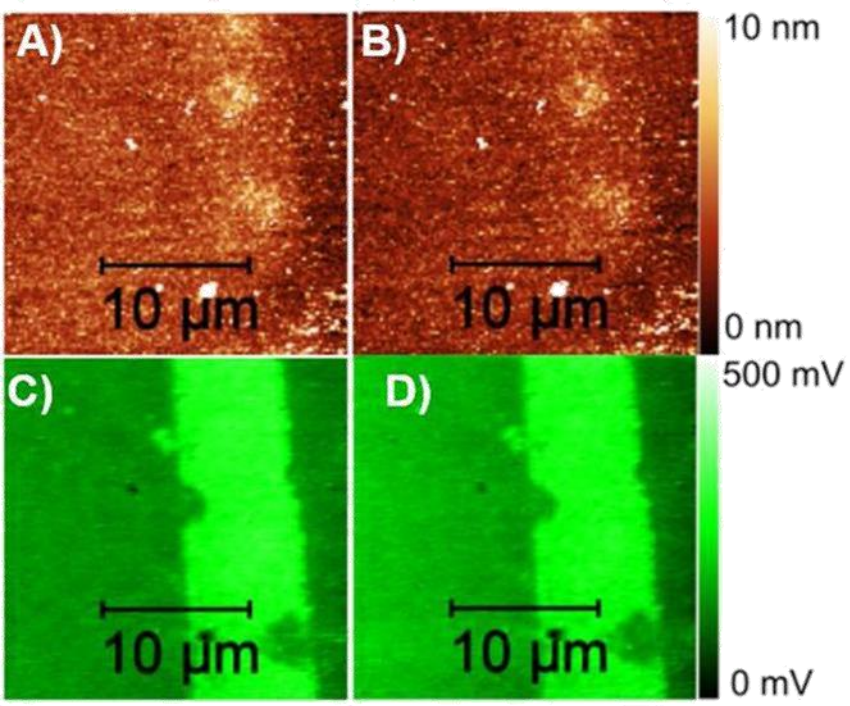

Figure 46. Continuous scans. Pattern by microcontact printing on glass. A) Topography PLL pattern on glass initial scan, B) Topography of PLL pattern on glass final scan, C) Potential of PLL pattern on glass initial scan, D) Potential of PLL pattern on glass final scan.

In figure 47 surface potential difference of each continuous scan is shown. It can be observed that after seven continuous scans there is no substantial drop on the surface potential (about 10 mV).

This data suggests that glass would be a better substrate to measure surface potential of poly-L- lysine micro patterns in contrast with mica. Although the resolution in the topography image is less clear due to the roughness of the material, the surface potential signal is clear and appears to be unaltered after repeated scans. Likewise, the process of peeling off previously used PDMS stamps, has been proven to be a reliable method to recycle stamps, reducing in this way the amount of time and materials required to successfully fabricate samples.

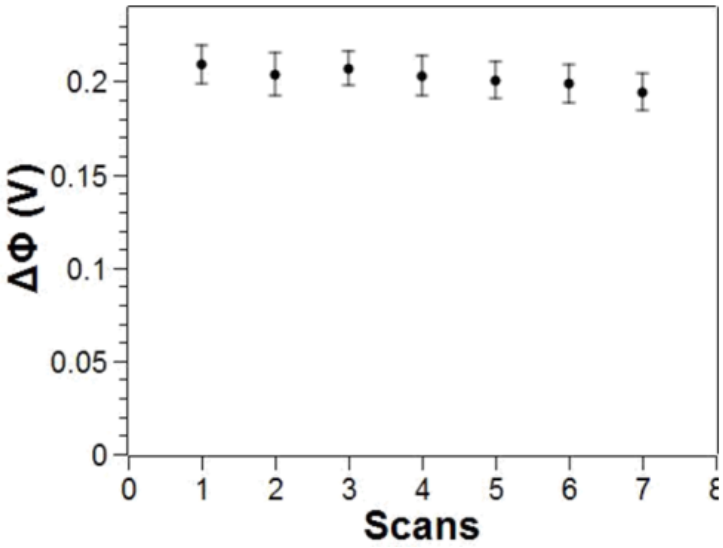

Figure 47. Continuous scans. Pattern by microcontact printing on glass.

4.5.5 Silicon dioxide:

So far, previously tested substrates present a diverse chemical composition. For instance, muscovite mica is mineral mainly composed of silicate, aluminium and potassium. Regarding borosilicate glass, is a combination of SiO_2, $B2O_3$, Na_2+K_2O

and Al_2O_3. On the other hand, silicon dioxide is composed of a linear formula of SiO_2 and arranged in a crystalline hexagonal configuration.

Furthermore, as for the case of mica and glass, silicon dioxide is expected to have a negative charge in water or at neutral pH. In terms of roughness, it is quite similar to glass. For these reasons, micro contact printing of poly-L-lysine and KPFM continuous scans were performed using silicon dioxide as substrate.

Figure 48 shows topographic and potential images of poly-L-lysine patterns on silicon dioxide, fabricated by micro contact printing using a freshly peeled off PDMS stamp.

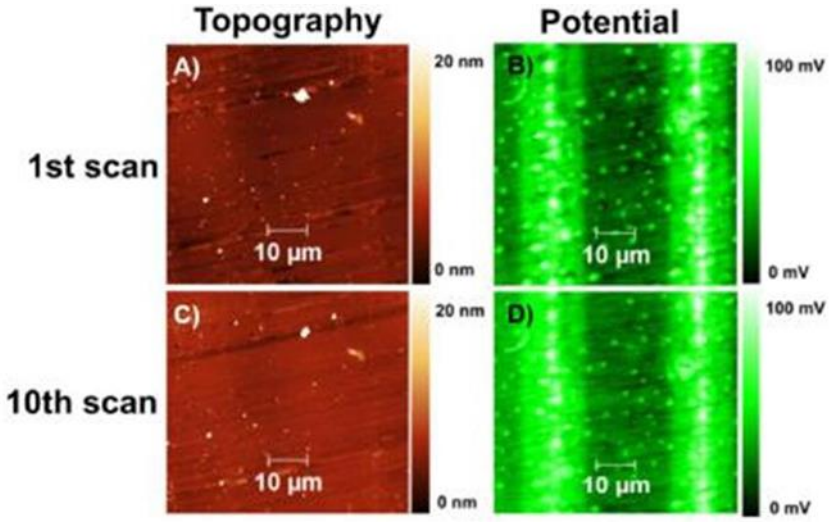

Figure 48. Continuous scans. Pattern by microcontact printing on a silicon dioxide substrate. A) Topography PLL pattern initial scan, B) Topography of PLL pattern final scan, C) Potential of PLL pattern initial scan, D) Potential of PLL pattern final scan.

A further analysis of all continuous scans is shown in figure 49. Surface potential difference remains mainly unaltered along ten continuous scans with an error of about 10 mV. This result suggests that in terms of surface potential stability, silicon dioxide could be a suitable material for surface potential studies on biomolecular patterns.

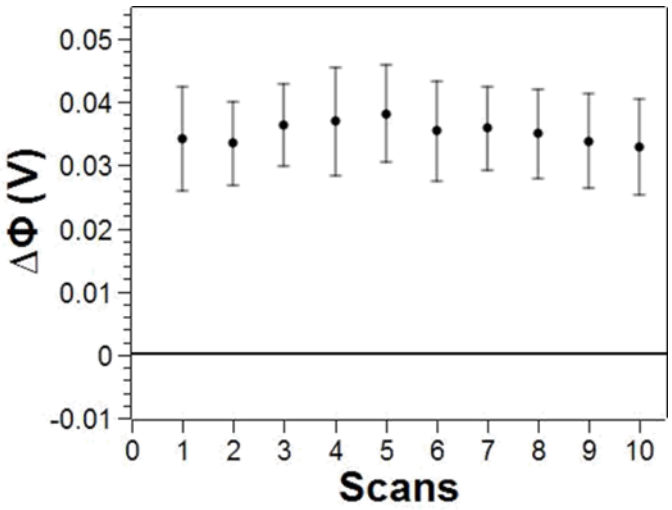

Figure 49. Continuous scans. Pattern by microcontact printing on silicon dioxide.

4.6 Micro-contact printing of proteins for surface potential mapping by KPFM

Figure 50 displays topography and surface potential map of β-lactoglobulin. On β-lactoglobulin the nature of the substrate and the pH of the solution in which is contained plays an important role on the conformation of the protein it will adopt when adsorbed [112].

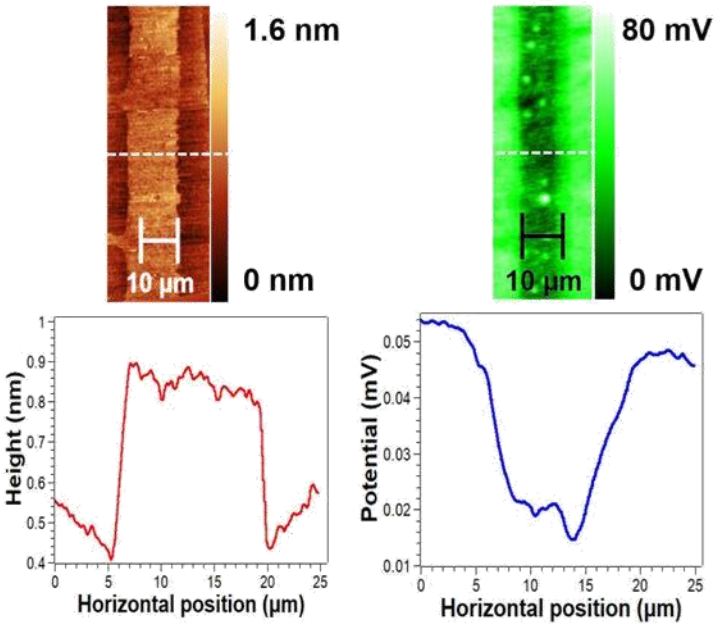

Figure 50. β-lactoglobulin topography and surface potential map with its respective profiles.

However, topographic height of single layers is not above 1 nm, as shown in the topographic profile on the same figure (50). Micro contact printing has several advantages over previously reported methods for β-lactoglobulin deposition on mica [112].

This would include the possibility of depositing a homogenous well defined layer of protein, which is for instance, essential for surface potential mapping of such sample by KPFM. Regarding the surface potential, there is no antecedents in literature of surface potential mapping of β-lactoglobulin by KPFM.

Figure 51, presents topography and surface potential map of BSA. By micro contact printing, the adsorbed protein aggregates seems not to correspond to the expected height of a single layer of protein. Nevertheless, heights of BSA aggregates above of 10 nm have been reported for adsorbed on flat surfaces by AFM [113].

Hence, it is not surprising due to the nature of BSA, to expect bigger aggregates in size than other globular proteins when adsorbed on surfaces. In contrast with β-lactoglobulin patterns, BSA seems to possess a positive charge in the order of 120 mV in respect to mica. The observed surface potential seems to be quite high compared to other globular proteins in this section. This could be explained by a higher number of molecules adsorbed, as it can be deduced by the height on the topographic image. It is not entirely sensitive to expect the same surface charge as in solution when studying complex proteins, since both pH of the solution not only affects the surface charge of the protein, but its adsorption kinetics [114]. Similarly, the nature of the surface affects in the same way, the structural conformation of the

protein when adsorbed, which not necessarily will correspond to the three-dimensional structure in solution.

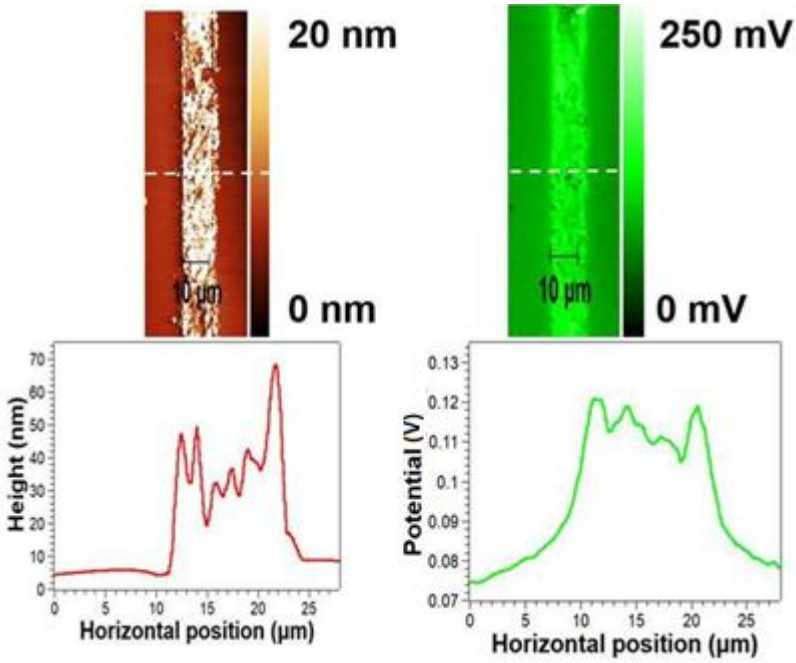

Figure 51. BSA micro pattern on mica surface.

Topography and surface potential map of micro contact printed insulin patterns are presented in figure 52. The average height for an insulin layer adsorbed on mica, as studied by AFM is in the order of 1.1 nm [115]. As it can be seen in the topography profile of patterned insulin on figure 43, the average height is in accordance with literature values, corresponding to a single layer of protein adsorbed on the substrate. The surface potential obtained by KPFM on the corresponding figure is in the order of 60 mV.

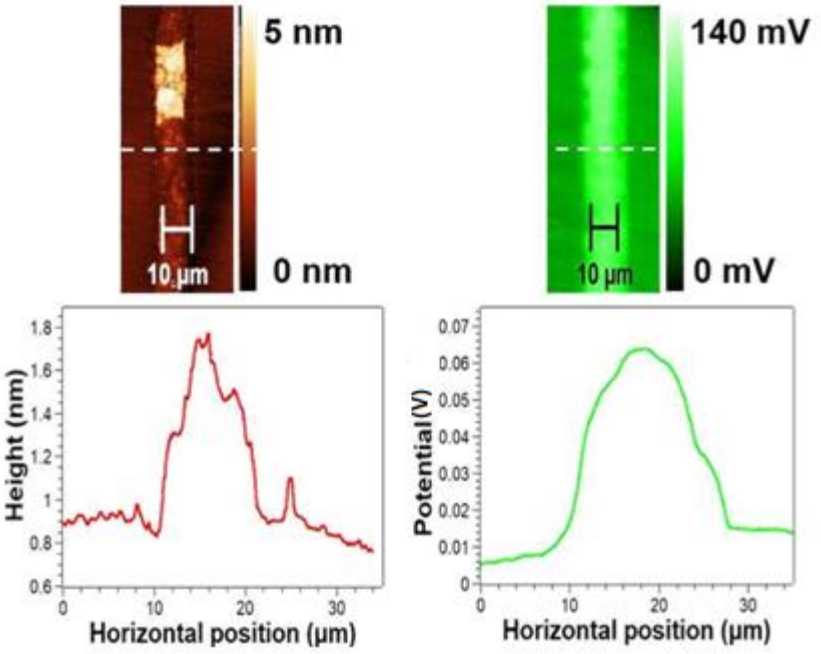

Figure 52. Insulin micro pattern on mica surface

In figure 53, β-lactoglobulin micro patterns fabricated by micro contact printing are shown. Immersion in water (neutral pH) and buffer (pH4) was performed. Surface potential images display a negative surface charge in respect to mica after the first immersion in water (near neutral pH). It was observed, however, that at pH 4 β-lactoglobulin surface charge is positive with respect to mica.

Nonetheless, the surface charge can be reversed to negative values followed by a second immersion in water (near neutral pH), showing a reversible effect. After each immersion in buffers, topographic images lose resolution.

This is due to the fact that salt contents on the buffer are deposited on the surface. Moreover, applying buffers over pH 4 resulted on detachment of the protein layers, making it unattainable to obtain results at higher pH's than 4.

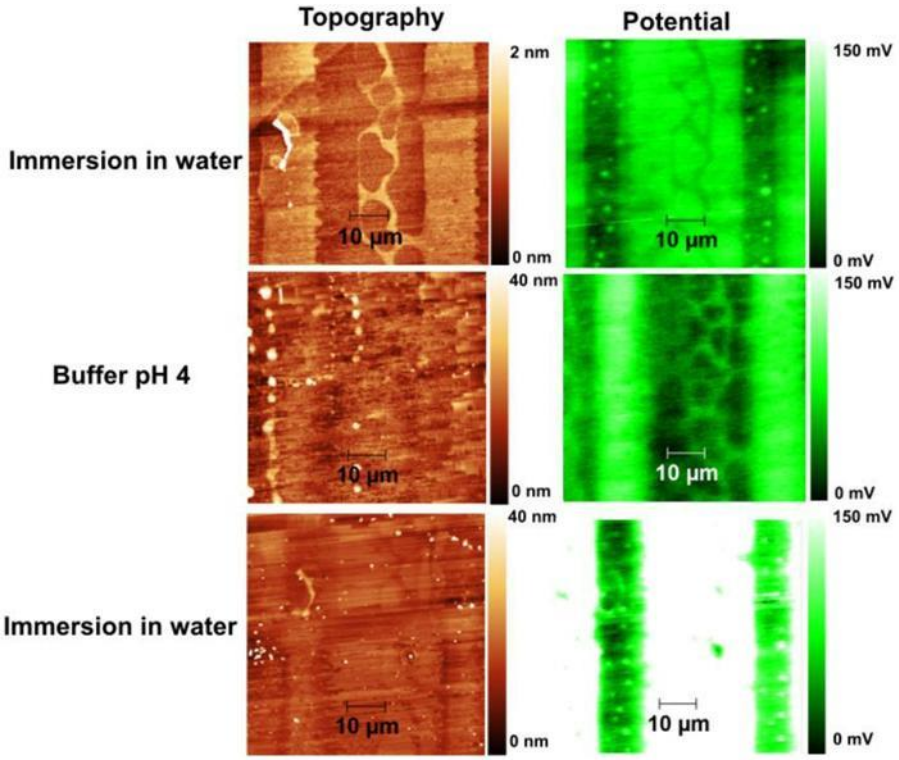

Figure 53. β-lactoglobulin on mica. Immersions in water and buffer (stamp drift observed in the middle of two patterns).

In the same fashion, immersion in water and buffer at pH 4 was applied to BSA micro patterns on mica for surface potential measurements (figure 58). In this case, all topographic images are of excellent quality and do not reveal substantial changes following immersions in water and pH 4 buffer. Moreover, surface potential images present an opposite shift on surface charge in respect to mica compared to β-lactoglobulin.

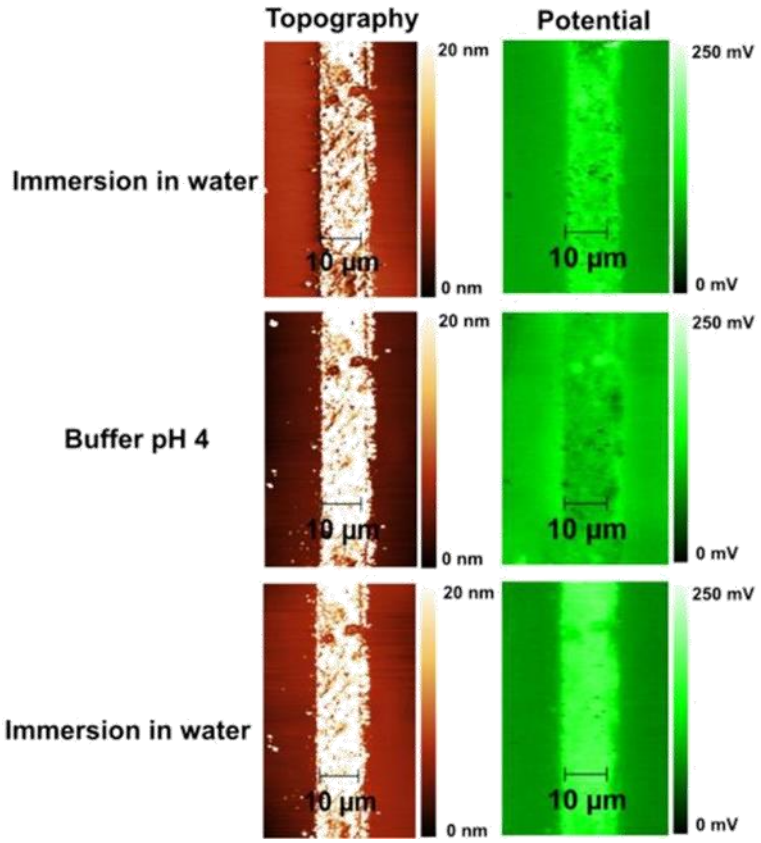

Figure 54. BSA on mica. Immersions in water and buffer

In order to understand surface potential changes on protein patterns as a result of immersions in water and pH 4 buffer, quantitative analysis was made based on the surface potential images (figure 55). In the case of β-lactoglobulin (black dots), the behaviour when reducing the pH value to 4 is as expected based on existent titration experiments [116]. In contrast, BSA (red dots) shows the opposite behaviour.

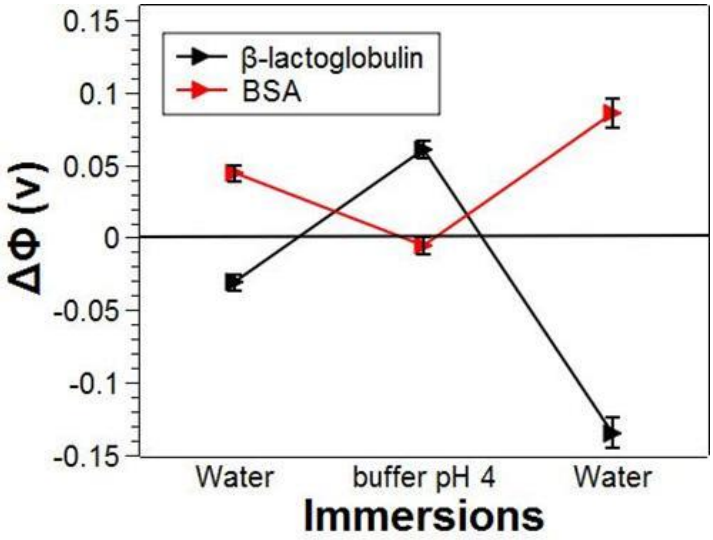

Figure 55. Surface potential difference reversible response to a pH shift of β-lactoglobulin and BSA.

This can be explained with the fact that residues on BSA can adopt different configurations depending on the substrate [117]. Immobilized proteins may not be able to re-configure and balance surface and buried charges as they would in solution.

Another possibility that could explain these results would be that mica may change its surface charge as a response to pH variations. However, these alterations are not of considerable magnitude to explain such an abrupt change on protein patterns. It is important to stress that, because of structural changes that proteins experience when adsorbed on solid substrates, zeta potential values and surface charge of immobilized proteins onto surfaces may not always correlate.

Finally, when the sample is immersed in water for the last time, there is in both cases (β-lactoglobulin and BSA) an outstanding difference in surface potential difference compared to the original value as read initially at neutral pH (last points in the graph). This could be explained by the fact that immersing in water might result on a cleaning effect on the surface by removing free charges, ions and suspended particles.

4.6.1 Cross patterning of globular proteins by micro contact printing for comparative studies of surface potential

PDMS softlithography has been used extensively to pattern proteins and cells for different purpose on various substrates [118]. However, fabrication of protein microdomains for surface potential measurements have been much more less reported [119][120]. Moreover, patterning two or more different types of proteins within the same scanning area is not described on the literature. The possibility of comparing electrostatic properties of two different proteins using the same substrate as reference could be of great importance in protein biophysics. Figure 56, shows an optical microscope image of the resulting cross patterning by micro contact PDMS soft lithography of insulin and BSA.

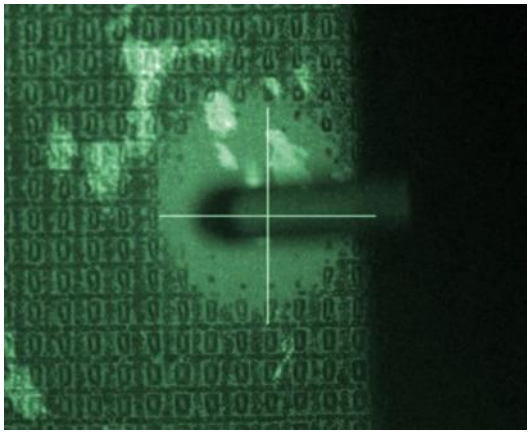

Figure 56. Cross patterned insulin and BSA observed by condensation on an optical microscope.

Obtaining AFM images of such protein cross patterns results more demanding than a single pattern.

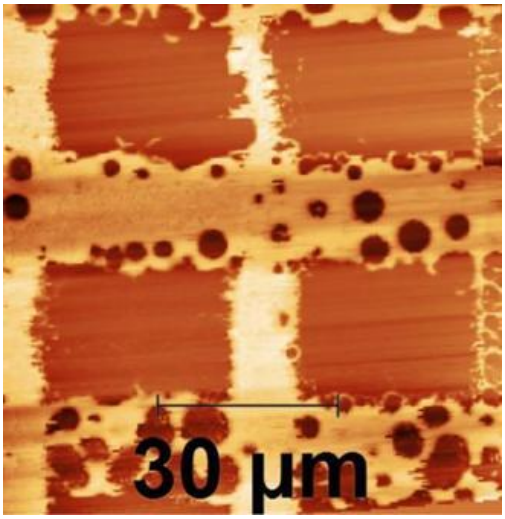

Figure 57. Phase image of the previous cross patterned insulin and BSA

Figure 57, shows for qualitative purposes, a phase image of the resulting cross patterns of insulin and BSA. Even though phase images provide only qualitative data, it is sufficient in this case to observe the presence of the proteins creating a clear contrast against the substrate (mica). In figure 58, both topographic and surface potential images of cross patterned insulin and BSA are presented.

To perform quantitative analysis, each image was recorded twice, initially at 0 º scan direction and subsequently at 90 ºso that orientation of both proteins is the same at the moment of tracing profiles and performing statistical analysis. At first stance, qualitatively, both proteins appear to have opposite charge with respect to mica.

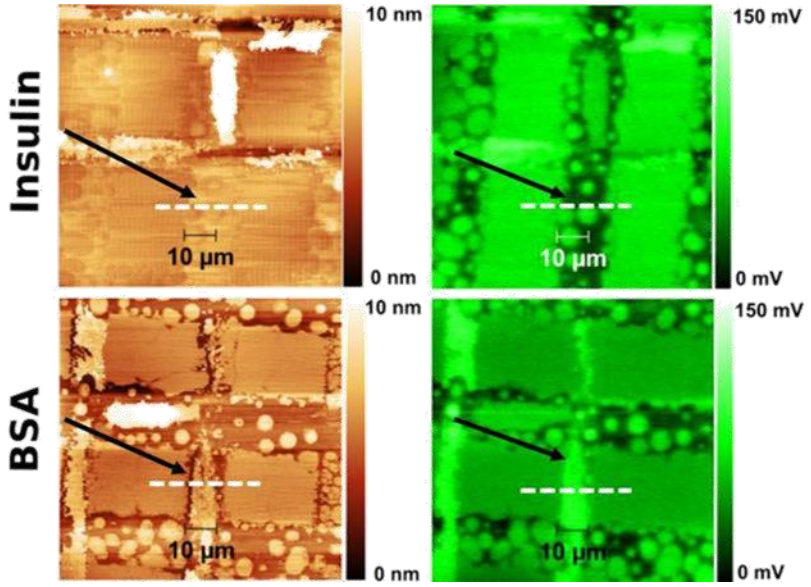

Figure 58. Topography and potential images of crossed patterned insulin and BSA scanned at 0 and 90 angles.

However, by tracing profiles (figure 59), BSA shows a clearly positive surface potential, whereas insulin shows a negative surface charge with respect to mica. Furthermore, by performing statistical analysis on the selected area (figure 60), potential difference values can be obtained.

Figure 60, represents the potential difference values obtained by calculating the average value within the pattern and subtracting the average value of the substrate. In the case of insulin an average surface potential difference around -30 mV can be observed, whereas a positive potential value of around 25 mV is obtained for BSA. As an initial stage of this experiment, no further modifications such as immersions in water or buffers were performed since the quality of the patterns and topographic images are not ideal. However, it has been shown that different proteins can be successfully cross-patterned on mica.

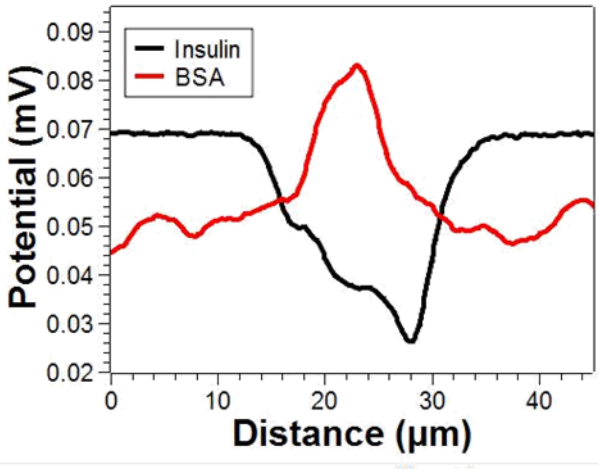

Figures 59. Surface potential cross sections of insulin and BSA obtained from the topographic image.

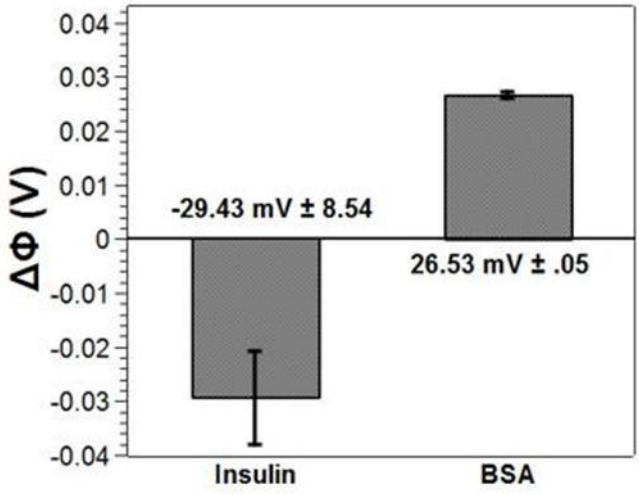

Figure 60. Statistical values obtained for the surface potential difference of Insulin and BSA when cross patterned.

4.6.2 Avidin-Biotin complex: detecting specific molecular interactions by KPFM

To demonstrate the ability of KPFM to detect specific molecular interactions, the classic avidin-biotin complex was utilised. In this case, fluorescent biotin was used in order to facilitate its detection by an alternative method (florescent optical microscopy).

However, by KPFM the use of dyes would not be necessary, since the detection is observed as a change in surface potential. Figure 61-A shows an optical microscope image of patterned avidin, fabricated by micro contact printing on glass.

The presence of the pattern is not observable by standard optical microscopy. In order to visualize the presence of the pattern by standard microscopy, condensation was induced as shown in figure 61-C. After immersing the structure patterned avidin on a fluorescent biotin solution and washing it thoroughly with ultra-pure water, the specific attachment of biotin on patterned avidin is evident as presented in figure 61-B. Avidin florescence microscopy image is not available since avidin do not produce a signal to be observed.

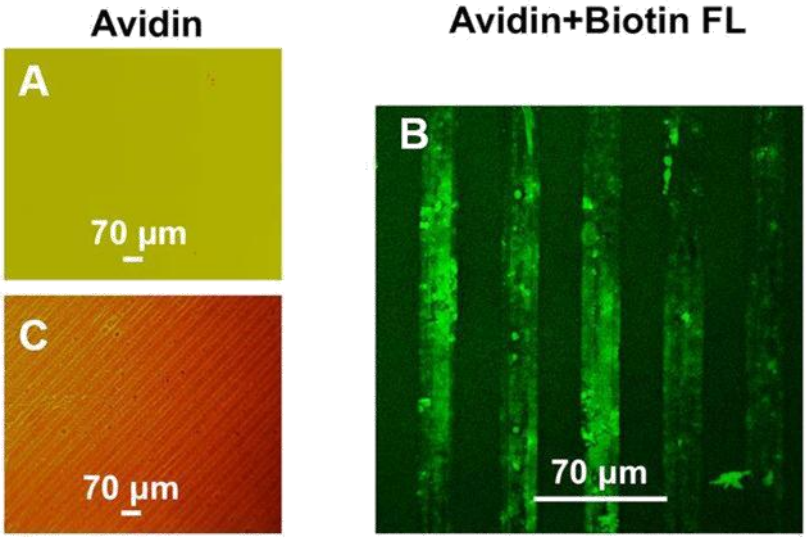

Figure 61. A) Optical image of patterned avidin on glass surface without condensation, B) optical image of patterned avidin on a glass surface observed by condensation, C) Confocal fluorescence image of patterned avidin on a glass surface, after exposure to biotin FL and washed with ultrapure water

Figure 62 represents KPFM results of an avidin pattern on glass before and after immersion in fluorescent biotin solution. Figure 62-A shows the surface potential map of avidin on glass before immersion, whereas 62-B represents the pattern in the same area after being immersed in biotin solution and washed with ultra-pure water.

These qualitative images suggest and increase on surface potential on the pattern after immersion in biotin. In order to estimate the increment on surface potential on the pattern, surface potential profiles were traced on both images (figure 62-C). According to the traced profiles, the increment on surface potential after immersion in biotin was in the order of 40 mV.

When calculating the average surface potential difference (shown in figure 62-D), the surface potential increment is in the order of 50 mV. Similar methods for label free detection of specific molecular interactions by KPFM and micro patterns have been reported previously with similar results [121]. Nonetheless, the present study utilizes much simpler micro fabrication procedures and substrates, in contrast to the use of complex surface functionalized thin films.

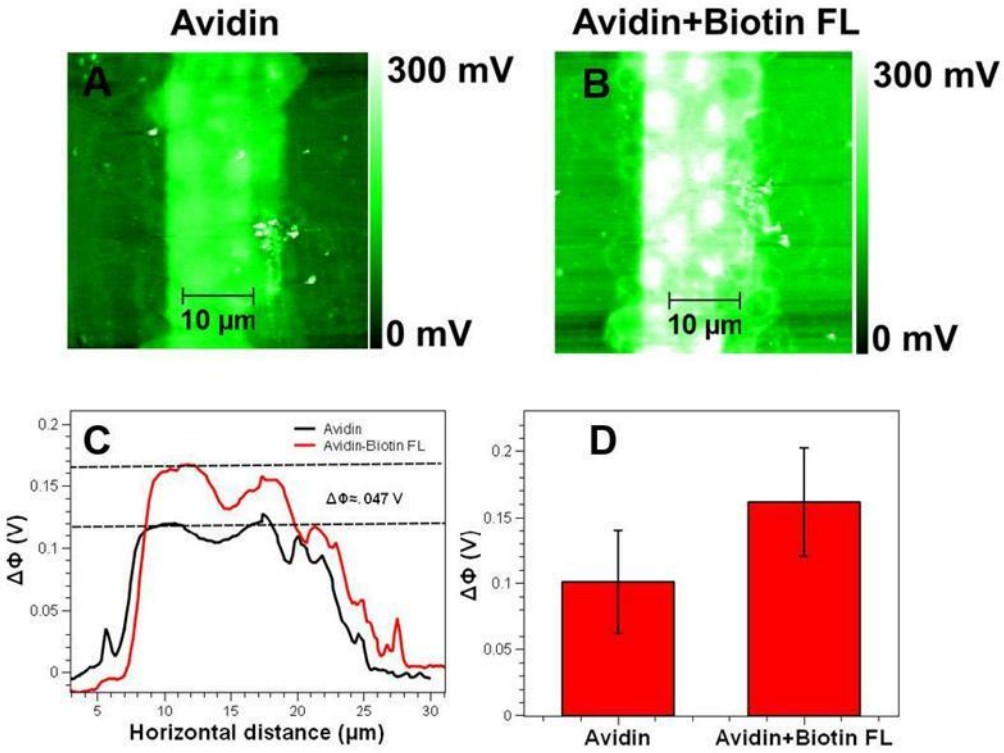

Figure 62. A) KPFM image of an avidin pattern on glass, B) KPFM image after the avidin pattern was exposed to biotin FL and washed with water, C) comparisons of potential profiles of the avidin pattern before and after exposure to biotin FL, D) surface

potential difference between the substrate and the pattern of avidin patterns on glass before and after exposure to biotin FL.

In conclusion, globular proteins were successfully adsorbed in patterns on solid substrate by micro contact printing. Moreover, both topography and surface potential maps were simultaneously produced by KPFM. After repeated immersions in water and pH buffer solution, a shift in surface potential was observed in globular protein micro patterns. The shift in surface potential results to be reversible. It was concluded that despite observing pH dependent surface potential shifts, surface potential of adsorbed proteins at certain pH do not necessarily corresponds to the expected surface potential in solution. Cross patterning two different proteins in the same surface for surface potential one to one comparison was achieved. The specific interaction between avidin and fluorescent biotin was detected using avidin micro patterns on glass by fluorescent microscopy and a change in surface potential by KPFM.

4.7 AFM tip assisted triboelectric surface charge on mica: detection by KPFM and dissipation.

Experiments on freshly cleaved mica have shown that electrostatic charges are created by friction when scanning in contact mode. This charge can be observed when re-scanning the same area on interleave mode with a potential difference in respect to mica close to 20 mV (figure 63).

Similar results have been previously reported obtaining a negative surface charge on a glass substrate [122] and silicon dioxide [123]. Scanning repeatedly the surface charge of the square did not alter significantly the surface potential difference as can be seen in figure 64. Quantitative analysis of the charge confirms that continuous scans do not

change considerably the surface potential difference. A drop can be observed during the fifth scan and it is more likely attributed to an effect of time (Figure 69). A possible explanation to this effect is discussed further.

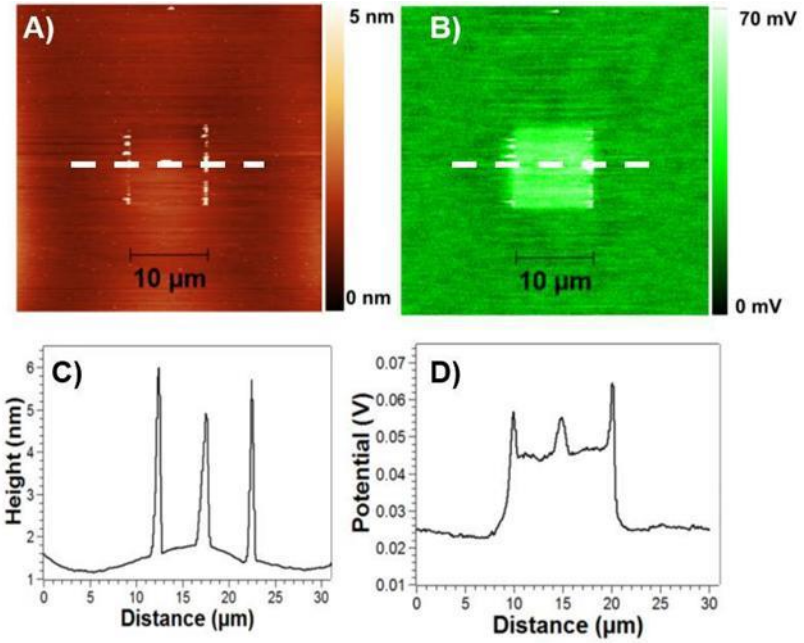

Figure 63. A) Topography image of square drawn in contact mode at time 0, B) Surface potential image of the square showing the presence of a surface charge on mica, C) height cross section corresponding to the topography image, D) surface potential cross section corresponding to the potential image.

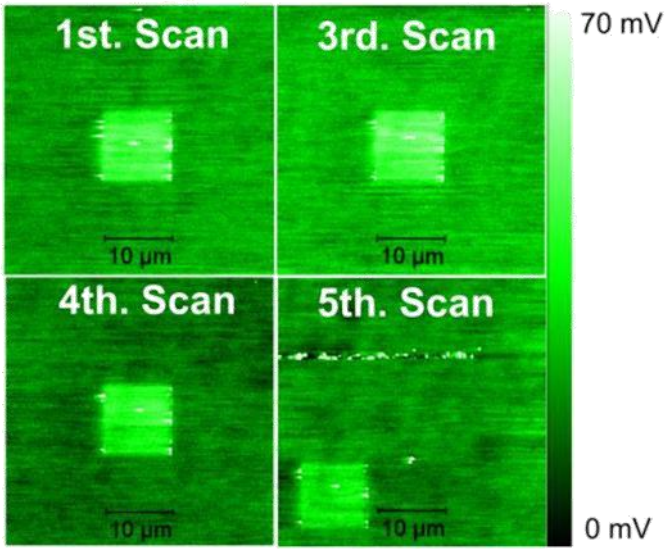

Figure 64. Shows surface charge resulting after scratching the AFM tip on the surface and performing 5 continuous scans.

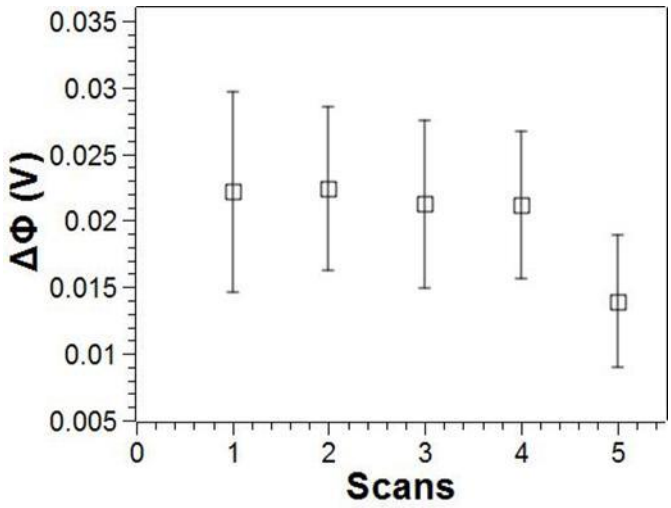

Figure 65. Surface potential difference of the square charge on mica after repeated scans.

After performing 5 consecutive scans, there was still a charge present on the surface. To understand the effect of high humidity on charge dissipation, condensation was created on the surface, and the same area was scanned. Condensation caused the positive surface charge on the surface to dissapear immediately, suggesting that humidity on the environment could play an important role on surface charge dissipation (figure 65).

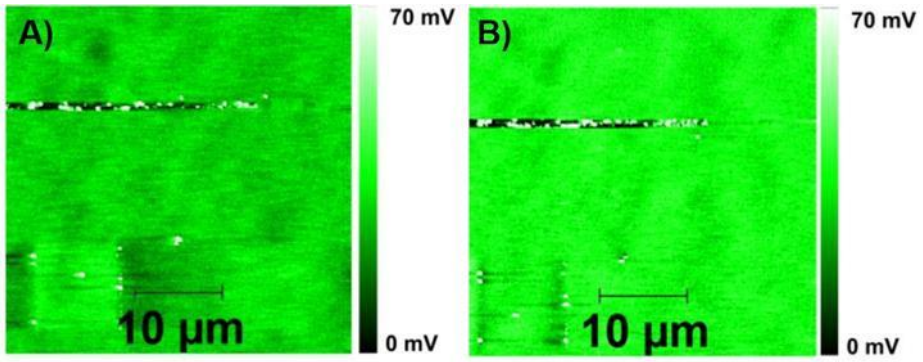

Figure 66. Shows A) surface charge after the 5th scan and B) surface charge after performing condensation on the surface.

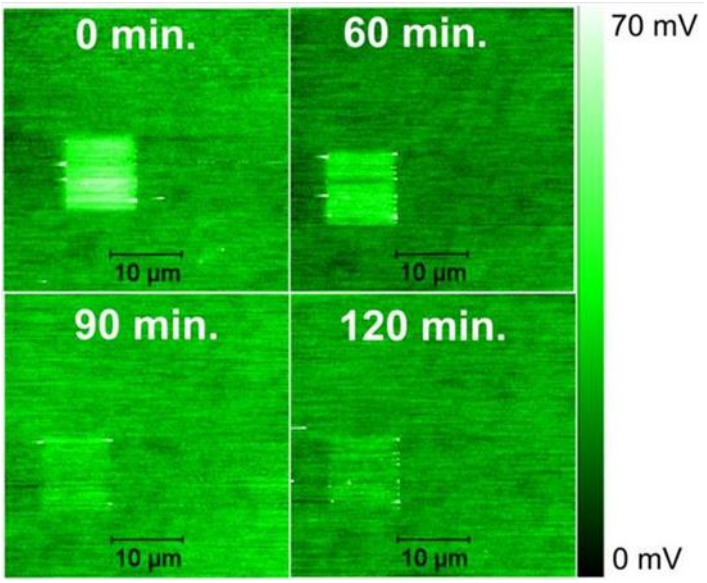

Figure 67. Potential images of the dissipation of charge over time

Furthermore, dissipation was followed when performing time resolved experiments, and contrasting the results against repeated scans on the same area. Qualitative images of time resolved experiment on charge dissipation can be seen on figure 67. In addition, quantitative analysis is presented in figure 68. Time dependence is clear on the surface potential difference. Moreover, initial drop after 60 minutes is in accordance with the surface potential drop observed after 5 continuous scans.

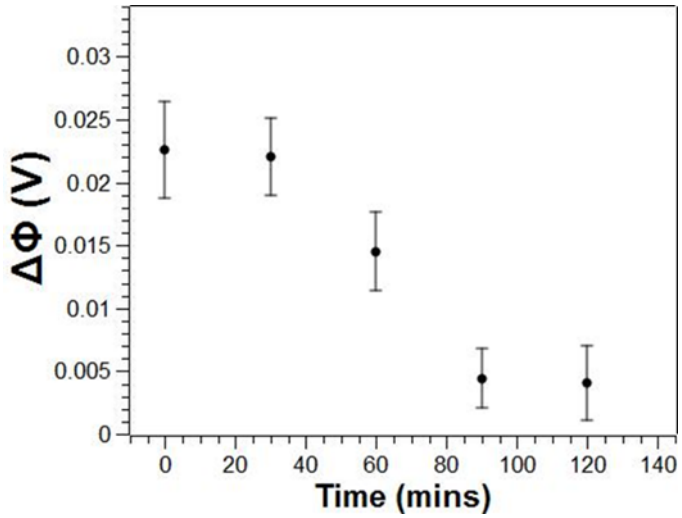

Figure 68. Surface potential difference of the square charge on mica over time.

Even though, based on the presented, results is hard to explain what is precisely causing the surface charge to dissipate over time. One explanation would be that surface free charges are displacing laterally to the surroundings by two dimensional diffusion.

Although this effect was not seen in the presented results in this section, which would have been observed by an increase on surface potential of the surroundings, it is possible indeed to be studied by means of KPFM [124]. Another explanation would be that in case there is no lateral displacement of surface charges by diffusion, free charges have the tendency to dissipate in the air due to interaction with water molecules contained in the air, which is indeed, an important variable on the decay electrostatic charges [125].

Ultimately, it is possible that both mechanisms take effect simultaneously on dissipating surface charges on mica over time. In any case, further experiments must be conducted using relative humidity as variable and possibly supporting obtained data with dynamic simulations on dissipation of surface charges on a dielectric material.

Generating free surface charges on mica by a triboelectric effect between the AFM tip and the surface is possible by using AFM in contact mode. In addition, by scanning the same area in KPFM mode, it is possible not only to observe the presence of the generated surface charge but to track down the decay over time. The density of the surface charge is not altered by the number of scans on KPFM mode, but it seems to respond to a time dependent dynamic. Also, it is suggested that relative

humidity plays an important role on charge dissipation. The behavior of the decay of charge is more similar to water adsorption on mica [126] rather than a free charge dissipating over time on an insulating surface. Finally, it is concluded that further experiments are required to determine the cause of surface charge dissipation on an insulating surface.

4.8 Insulin amyloid fibrils: Aggregation dynamics, effect of highly charged gold nanoparticles and surface potential mapping by KPFM

4.8.1 UV-Vis absorption and fibrillation kinetics:

The chosen method for following the fibrillation kinetics of insulin was UV Absorption at a fixed wavelength. This method has been previously reported and proved to be valid for tracking amyloid fibril aggregation for insulin [65]. Since a suitable absorption signal was obtained at 280 nm, this wavelength was used to follow the aggregation kinetics of incubated solutions of pure insulin and co-incubation with bPEI/AuNp's and lipoic acid/AuNp as a function of time.

Figure 69, shows the fibrillation kinetics of the mentioned solutions, where it can be observed that during the first 10 minutes of incubation, pure insulin showed the biggest absorption response which is attributed to the aggregation state of insulin and, thus, the fibrillation state of the protein.

This result suggests that bPEI/AuNp slows down aggregation in the initial state of the incubation, whereas lipoic acid/AuNp-insulin seemed to promote aggregation.

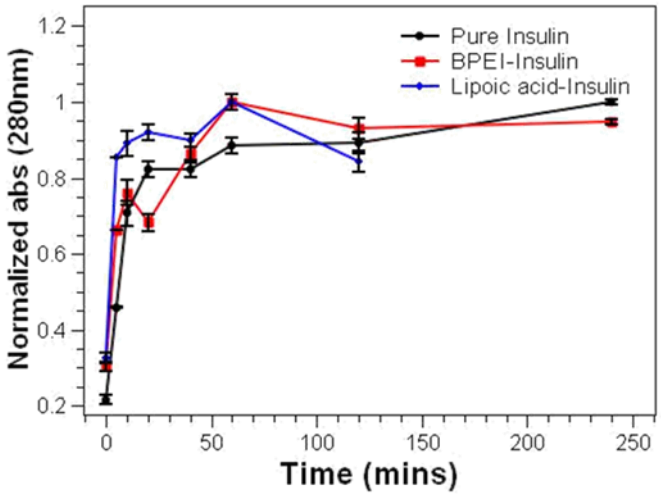

Figure 69. Aggregation Kinetics of insulin and gold nanoparticles.

All treatments reached a plateau region at 60 min. of incubation, where exponential growth seems to slow down.

Table 3 summarizes the absorption values at 280 nm reached at 60 minutes of incubation, in which can be observed how absorption was decreasing when zeta potential difference between insulin and the nanoparticles increases as well. Zeta potential values are expected to remain constant over incubation time.

Incubated solution	**ζp (mV) at pH 2**	**Normialized abs. @280**	**SD**
Pure insulin	30*	0.88	±0.0210
bPEI/AuNp-Insulin	22.3	1	±0.0050
Lipoic acid/AuNp-	13.1	1	±0.0051

Table 3. Absorption values at 280 nm reached at 60 minutes of incubation.
*Literature value of zeta potential (mV) of insulin at pH 2[127].

4.8.2 Atomic force microscopy

Atomic force microscopy was used to corroborate the results obtained by UV-Vis and to observe the morphology of insulin aggregates and fibrils. During the first 20 minutes of incubation, it is not possible to observe formation of fibrils or protofibrils. Instead, there is a presence of insulin aggregates in the form of small spheres that adsorb on mica covering the whole surface

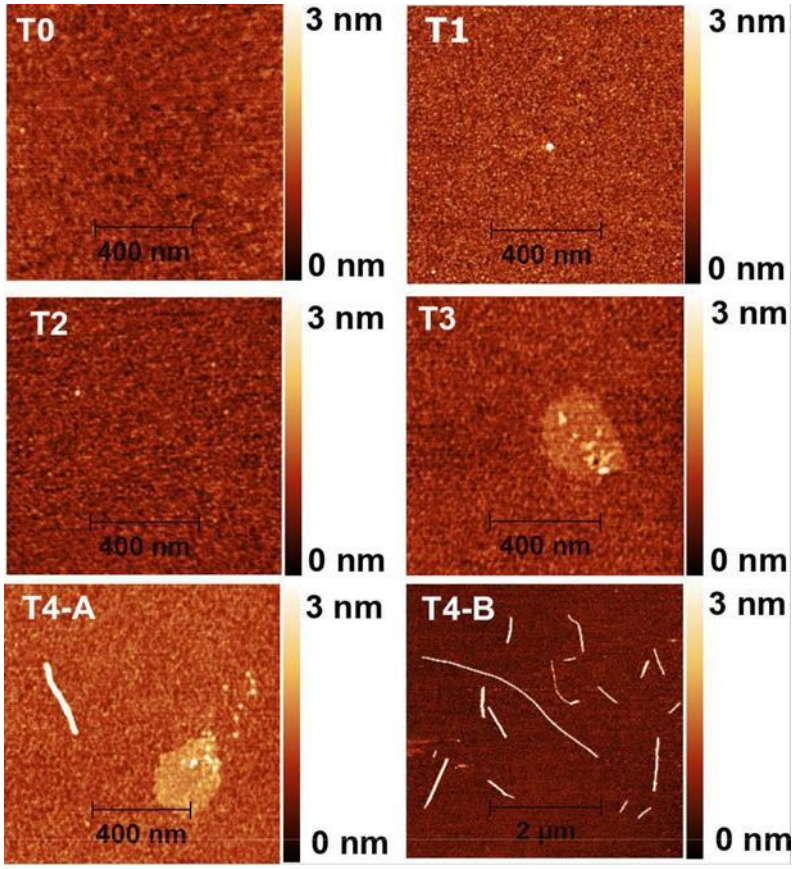

Figure 70.AFM micrographs of incubated insulin of T0= 0 mins, T1= 5 mins T2= 10 mins, T3= 20 mins, T4-A= 40mins 1 µm scan size, T4-B= 40 mins 5 µm

However, after 40 minutes the presence of small proto fibrils, rods and small fibrils is observed. Mature fibrils are formed after 60 minutes incubation as seen in figure 70.

These results are highly reproducible and demonstrate that under specific conditions of pH and temperature is possible to incubate and produce fibrils relatively rapidly.

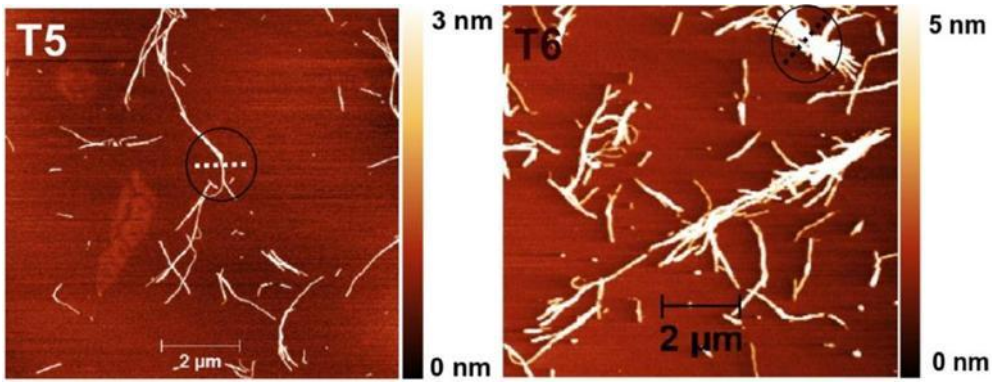

Figure 71. AFM micrographs of incubated insulin of T5= 60 mins (left) and of incubated insulin of T6= 120 mins (right).

A sample scanned after 120 minutes was utilized to test repeatability and stability of surface potential of amyloid tangles by Kelvin probe force microscopy. As shown in height profiles (Figure 72) obtained after 60 and 120 minutes of incubation, the height of insulin fibrils depends on the level of entanglement.

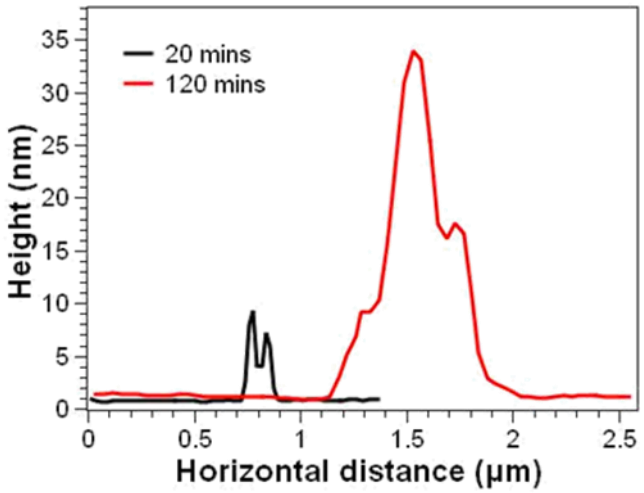

Figure 72. Height profiles of shown images of 60 and 120 minutes incubation.

The absence of mature fibrils in this treatment could be explained either by the high light absorption of insulin aggregates (optical density) over time, or by the fact

that negative surface charge of the nanoparticles prevents insulin fibrils from adsorption into mica mostly due to negatively charged surface charge.

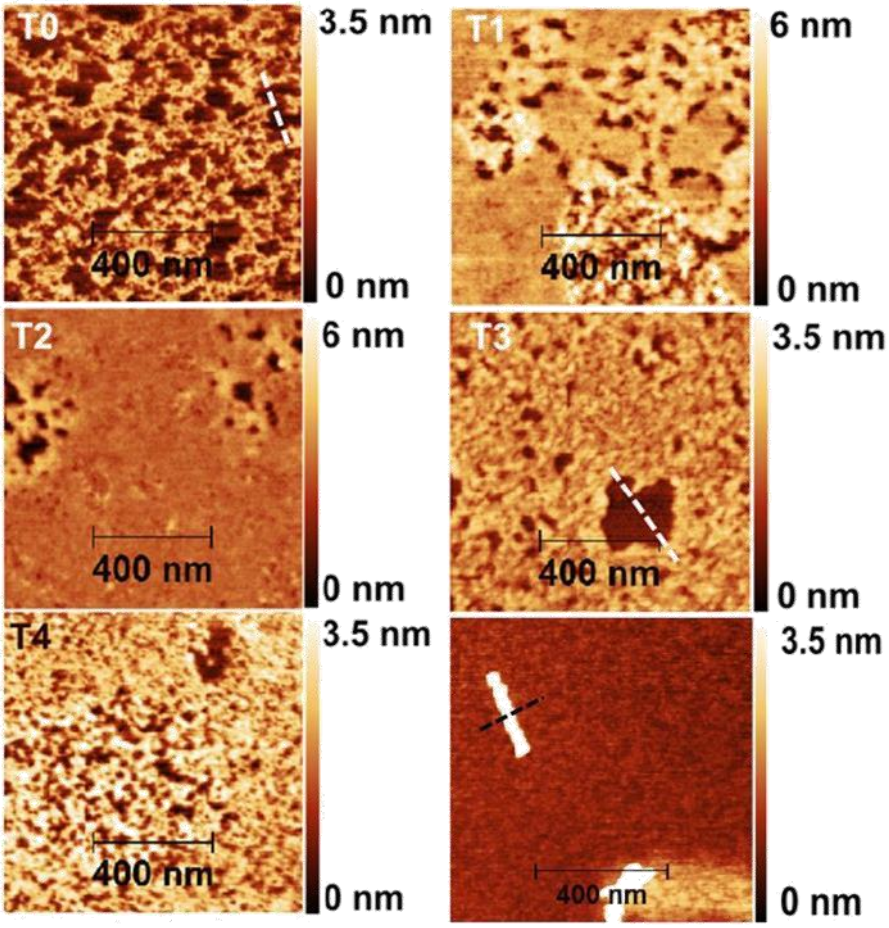

Figure 73. AFM micrographs of incubated insulin with lipoic acid gold nanoparticles of T0= 0 mins, T1= 5 mins T2= 10 mins, T3= 20 mins, T4-A= 40 mins 1 μm^2 scan size, T4-B= 40 mins 5 μm^2 scan size.

Figure 73 represents AFM topographic images on mica of incubated insulin with lipoic acid gold nanoparticles at different times. In contrast with incubation of pure insulin, in this case, there is adsorption of insulin aggregates that seems not to vary along time.

Finally, at 40 minutes of incubation it is possible to observe a protofibrils with a rod like morphology. Similarly, in figure 74, AFM topographic images of incubated insulin with bPEI/gold nanoparticles are shown. In a similar fashion, as insulin

incubated with functionalized lipoic acid gold nanoparticles, there is no evidence of the formation of mature fibrils.

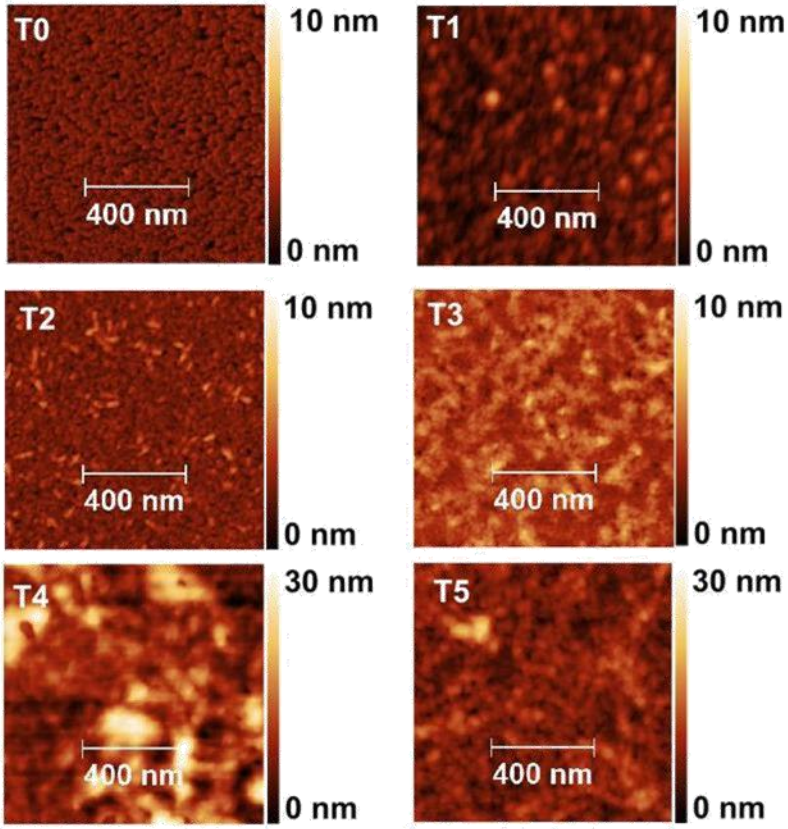

Figure 74. AFM micrographs of incubated insulin with BPEI/Gold nanoparticles of T0= 0 mins, T1= 5 mins T2= 10 mins, T3= 20 mins, T4 A= 40 mins 1 μm^2 scan size, T4-B= 40 mins 5 μm^2 scan size.

By analysing topographic images, it can only be seen the adsorption of insulin aggregates on the mica surface. This fact can only support the hypothesis that both treatments might be preventing the formation of mature fibrils and the increase on the optical density as detected by UV-Vis can be explained by the formation of larger insulin aggregates and protofribrils but no mature amyloid fibrils.

4.8.3 Kelvin probe force microscopy of amyloid fibrils

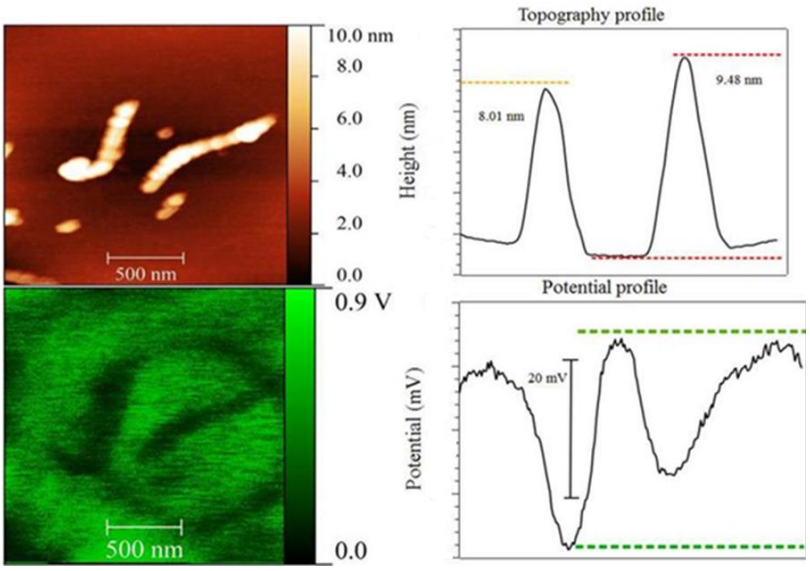

Figure 75. Surface potential map of a single insulin protofribrils by KPFM.

As shown in figure 75, it was possible to obtain an acceptable resolution for the topographic image and a good contrast on the KPFM signal as well. The observed surface potential difference for the insulin protofribrils is in the order of 20 mV with respect to mica. This results are similar to previous experiments on proteic amyloids carried out using Kelvin probe force microscopy, in which at physiological pH, the surface potential of the fibrils are negative [128]. However, as observed in previous experiments with micro contact printing, studying the stability of surface potential readings by KPFM at the nanoscale involving biomolecular structures on mica is pertinent. The effect of time and repeated scans over a biomolecular structure by KPFM is not described on the literature. Figure 76 presents the resulting images of scanning 10 over the same area a sample containing insulin tangles of mature fibrils. Figure 76 is composed after scanning the topography which is presented and marked in figure 71.

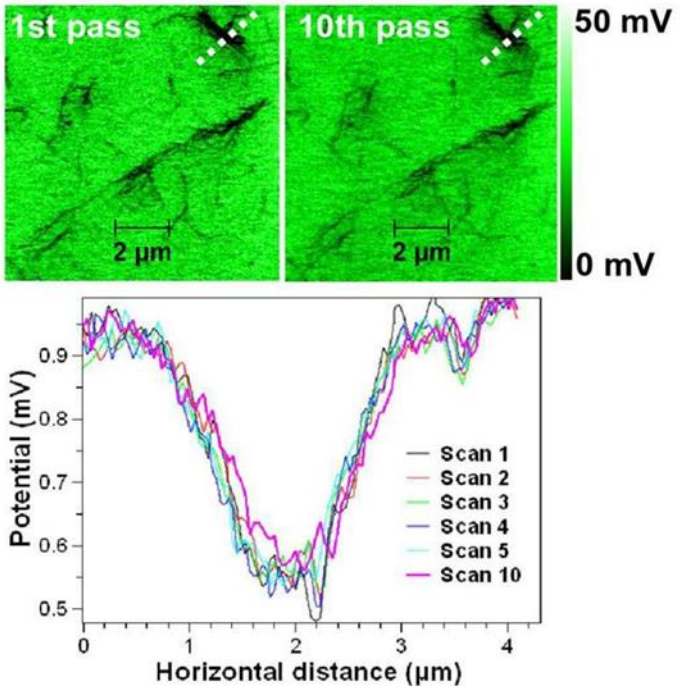

Figure 76. KPFM image of insulin tangles. Repeated scans over the same area.

Since continuous scans did not show evidence of substantial changes on surface potential (figure 80), it can be suggested that a protective layer of free insulin monomers and small aggregates were adsorbed on mica. The formation of a protein thin film could prevent mica from changing its electrostatic properties, making KPFM imaging more stable than using micro contact patterning technique. Aggregation kinetics of insulin amyloid fibrils was successfully followed by UV-Vis optical density at 280 nm as reported in literature. It was also found that the presence of highly charged colloidal gold particles do not alter significantly the aggregation behaviour of insulin fibrils. In the presence of both negatively and positively charged colloidal gold nanoparticles, evidence of the formation of mature amyloid fibrils or tangles was not found. These specific AFM based results suggest that nanoparticles might be preventing the formation of mature fibrils. In another scenario, nanoparticles might be preventing adsorption of mature fibrils and tangles

on the mica surface. Finally, the possibility of producing surface potential mappings of amyloid like structures by KPFM is demonstrated. Moreover, in contrast with the effects observed by repeated scans on biomolecular structures patterned on mica by micro contact printing, KPFM readings are stable on insulin fibrils deposited on mica. These finding suggest that a thin layer of free insulin monomers protects the mica surface from being exposed to the environment, resulting in more stable KPFM readings.

CHAPTER 5 :

General conclusions and future perspectives

It was possible to fabricate poly-L-lysine micro patterns on mica by microchannel filling for surface potential mapping by KPFM. Nevertheless, this method is time consuming and samples often present different defects such as empty channels or uneven distribution of poly-L-lysine molecules, yielding high variability. In most cases, due to the large surface area of PDMS stamps that is in contact with the substrate, the presence of undesired objects such as stamp debris or dust, hinder the possibility to track the topography of the biomolecular patterns, since poly-lysine molecules in the pattern adopt topographic heights below 2 nm. Surface potential difference of the patterns fabricated by micro channel filling showed the tendency to decay over time and continuous scans.

However, when immersed in ultrapure water they remained stable. It was demonstrated that immersion of poly-L-lysine patterns in D-ribose solutions influences the surface potential. At low concentrations (6 mM), the surface potential of poly-L-lysine patterns is inverted. Nonetheless, this effect was reversible at some extent when the sample is immersed in ultrapure water. At high sugar concentration (6 molar), the effect was no longer reversible and there was a clear deposition of D-ribose aggregates on the poly-L-lysine patterns. At this point, there is not enough evidence to attribute changes in surface potential to biochemical modifications produced by the exposure of poly-L-lysine functional groups to sugars. However, from a different perspective, the observed effect is interesting for various purposes. For instance, sugar immobilization on surfaces, accumulation of sugars on biomolecular structures, and surface charge reversibility. Colloidal gold nanoparticles are selectively adsorbed on

poly-L-lysine patterns driven by electrostatic forces. This phenomenon allows the use of nanoparticles as markers to locate the presence of poly-L-lysine. Similarly, the adsorption of nanoparticles can invert the positive surface charge of poly-L-lysine to negative. As an alternative to micro channel filling micro patterning, micro contact printing is more efficient. When patterning poly-L-lysine on different substrates, mica was found to be the most suitable substrate to reach high topographic resolution. However, mica seems to be electrostatically unstable when scanned repeatedly by KPFM. On the other hand, glass and silicon dioxide are rough materials which makes it difficult to record topographic features of small objects by AFM.

Nevertheless, these materials showed outstanding stability when performing repeated scans on KPFM of poly-L-lysine micro patterns. Patterning of a family of globular proteins on mica by micro contact printing for surface potential measurements was successfully achieved. Likewise, cross patterning offers the possibility to test and compare one to one different biomolecules to understand slight differences on surface potential, and its response to various physicochemical conditions.

Scratching mica with the AFM tip in contact mode, creating a surface charge by friction and detecting it by KPFM, confirmed once again the high sensitivity of a few millivolts and capacity for spatial resolution at micrometer scale of the technique. Similarly, the possibility to detect and track with high sensitivity the presence of electrostatic charges on dielectric substrates was successful. As for future work, it would be interesting to extend the investigation to the understanding of the relationship between relative humidity and surface potential.

Experiments of contact angle to relate it to relative humidity, hydrophobicity and surface potential values. Furthermore, it might be possible to estimate the number of layers or water molecules adsorbed on mica surface and its relation to surface potential. Another important aspect would be the understanding of concentration dependence on both adsorptions of sugar and self-assembly of colloidal nanoparticles on biomolecular patterns.

CHAPTER 6:

References

[1] G.W. Gross, B.K. Rhoades, H.M.E. Azzazy, M.C. Wu, The use of neuronal networks on multielectrode arrays as biosensors, Biosens. Bioelectron. 10 (1995) 553–567. doi:10.1016/0956-5663(95)96931-N.

[2] R.S. Kane, S. Takayama, E. Ostuni, D.E. Ingber, G.M. Whitesides, Patterning proteins and cells using soft lithography, Biomaterials. 20 (1999) 2363–2376. doi:10.1016/S0142-9612(99)00165-9.

[3] A.S. Blawas, W.M. Reichert, Protein patterning, Biomaterials. 19 (1998) 595–609. doi:10.1016/S0142-9612(97)00218-4.

[4] S. Salgin, U. Salgin, S. Bahadir, Zeta potentials and isoelectric points of biomolecules: The effects of ion types and ionic strengths, Int. J. Electrochem. Sci. 7 (2012) 12404–12414.

[5] J.D. Carbeck, I.J. Colton, J. Gao, G.M. Whitesides, Protein Charge Ladders, Capillary Electrophoresis, and the Role of Electrostatics in Biomolecular Recognition, Acc. Chem. Res. 31 (1998) 343–350. doi:10.1021/ar970255q.

[6] P.J. Kundrotas, E. Alexov, Electrostatic Properties of Protein-Protein Complexes, Biophys. J. 91 (2006) 1724–1736. doi:10.1529/biophysj.106.086025.

[7] V.C. Chappa, M.F. del Grosso, G. García-Bermúdez, R.O. Mazzei, Infrared spectroscopy analysis of physico-chemical modifications induced by heavy ions in ultra-high molecular weight polyethylene, Nucl. Instruments Methods Phys. Res. Sect. B Beam Interact. with mater. atoms 243 (2006) 58–62. doi:10.1016/j.nimb.2005.08.121.

[8] T.K. Kerppola, Visualization of molecular interactions by fluorescence complementation, Nat. Rev. Mol. Cell Biol. 7 (2006) 449–456. doi:10.1038/nrm1929.

[9] R.P. Huang, Detection of multiple proteins in an antibody-based protein microarray system, J. Immunol. Methods. 255 (2001) 1–13. doi:10.1016/S0022-1759(01)00394-5.

[10] S.R. Irani, S. Alexander, P. Waters, K.A. Kleopa, P. Pettingill, L. Zuliani, E. Peles, C. Buckley, B. Lang, A. Vincent, Antibodies to Kv1 potassium channel-complex proteins leucine-rich, glioma inactivated 1 protein and contactin-associated protein-2 in limbic encephalitis, Morvan's syndrome and acquired neuromyotonia, Brain. 133 (2010) 2734–2748. doi:10.1093/brain/awq213.

[11] H.-P. Peng, K.H. Lee, J.-W. Jian, A.-S. Yang, Origins of specificity and affinity in antibody–protein interactions, Proc. Natl. Acad. Sci. 111 (2014) E2656–E2665. doi:10.1073/pnas.1401131111.

[12] J. Gao, M. Mammen, G.M. Whitesides, Evaluating Electrostatic Contributions to Binding with the Use of Protein Charge Ladders, Science (80-.). 272 (1996) 535 LP-537. http://science.sciencemag.org/content/272/5261/535.abstract.

[13] J.A. Caravell, J.D. Carbeck, D.C. Duffy, G.M. Whitesides, B. Tidor, Long-range electrostatic contributions to protein-ligand binding estimated using protein charge ladders, affinity capillary electrophoresis, and continuum electrostatic theory, J. Am. Chem. Soc. 121 (1999) 4340–4347. doi:10.1021/ja984195a.

[14] M. Garcia-Viloca, J. Gao, M. Karplus, D.G. Truhlar, How enzymes work: analysis by modern rate theory and computer simulations., Science. 303 (2004) 186–95. doi:10.1126/science.1088172.

[15] C. Park, R.T. Raines, Quantitative analysis of the effect of salt concentration on enzymatic catalysis., J Am Chem Soc. 123 (2001) 11472–11479.

[16] S. Shazman, Y. Mandel-Gutfreund, Classifying RNA-binding proteins based on electrostatic properties, PLoS Comput. Biol. 4 (2008). doi:10.1371/journal.pcbi.1000146.

[17] S. Kumar, R. Nussinov, Salt bridge stability in monomeric proteins., J. Mol. Biol 293 (1999) 1241–55. doi:10.1006/jmbi.1999.3218.

[18] A.D.D. Stone, P. Mesquida, Kelvin-probe force microscopy of the pH-dependent charge of functional groups, Appl. Phys. Lett. 108 (2016). doi:10.1063/1.4953571.

[19]C. Leung, H. Kinns, B.W. Hoogenboom, S. Howorka, P. Mesquida, Imaging surface charges of individual biomolecules, Nano Lett. 9 (2009) 2769–2773. doi:10.1021/nl9012979.

[20]P. Seeman, The pH Concept., Science. 177 (1972) 835–836. doi:10.1126/science.177.4052.835.

[21]L.G.J. Wade, Amino acids, peptides, and proteins, Org. Chem. 2 (2009) 1320. doi:10.1039/9781847557261.

[22]E. Bombarda, G.M. Ullmann, PH-dependent pKa values in proteins-a theoretical analysis of protonation energies with practical consequences for enzymatic reactions, J. Phys. Chem. B. 114 (2010) 1994–2003. doi:10.1021/jp908926w.

[23]R.J. Hunter, B.R. Midmore, H. Zhang, Zeta Potential of Highly Charged Thin Double-Layer Systems., J. Colloid Interface Sci. 237 (2001) 147–149. doi:10.1006/jcis.2001.7423.

[24]T. Kaufmann, B.J. Ravoo, Stamps, inks and substrates: Polymers in microcontact printing, Polym. Chem. (2010). doi:10.1039/b9py00281b.

[25] a Folch, a Ayon, O. Hurtado, M. a Schmidt, M. Toner, Molding of deep polydimethylsiloxane microstructures for microfluidics and biological applications., J. Biomech. Eng. (1999). doi:10.1115/1.2798038.

[26] B.H. Jo, L.M. Van Lerberghe, K.M. Motsegood, D.J. Beebe, Three-dimensional micro-channel fabrication in polydimethylsiloxane (PDMS elastomer, J. Microelectromechanical Syst. (2000). doi:10.1109/84.825780.

[27] D.W. Lam, D. LeRoith, The worldwide diabetes epidemic, Curr. Opin. Endocrinol. Diabetes Obes. 19 (2012) 93–96. doi:10.1097/MED.0b013e328350583a.

[28] F.W. Pavy, Sugar in urine, Br. Med. J. 2 (1875) 749. doi:10.1136/bmj.2.780.749.

[29] American Diabetes Association, Diagnosis and classification of diabetes mellitus, Diabetes Care. 32 (2009) S62–S67. doi:10.2337/dc09-S062.

[30] M. Piliarik, J. Homola, Surface plasmon resonance (SPR) sensors: approaching their limits?, Opt. Express. 17 (2009) 16505. doi:10.1364/OE.17.016505.

[31] M.E. Bosch, A.J.R. Sánchez, F.S. Rojas, C.B. Ojeda, Recent Development in Optical Fiber Biosensors, Sensors. 7 (2007) 797–859. doi:10.3390/s7060797.

[32] X. Fan, I.M. White, S.I. Shopova, H. Zhu, J.D. Suter, Y. Sun, Sensitive optical biosensors for unlabeled targets: A review, Anal. Chim. Acta. 620 (2008) 8–26. doi:10.1016/j.aca.2008.05.022.

[33] W. Melitz, J. Shen, A.C. Kummel, S. Lee, Kelvin probe force microscopy and its application, Surf. Sci. Rep. 66 (2011) 1–27. doi:10.1016/j.surfrep.2010.10.001.

[34]C. Iannuzzi, G. Irace, I. Sirangelo, Differential effects of glycation on protein aggregation and amyloid formation, Front. Mol. Biosci. 1 (2014) 1–8. doi:10.3389/fmolb.2014.00009.

[35]Q. Zhang, J.M. Ames, R.D. Smith, J.W. Baynes, T.O. Metz, A perspective on the maillard reaction and the analysis of protein glycation by mass spectrometry: Probing the pathogenesis of chronic disease, J. Proteome Res. 8 (2009) 754–769. doi:10.1021/pr80085Bh.

[36] J.E. Hodge, Dehydrated Foods, Chemistry of Browning Reactions in Model Systems, J. Agric. Food Chem. 1 (1953) 928–943. doi:10.1021/jf60015a004.

[37]J.A. Gerrard, The Maillard reaction in food: Progress made, challenges ahead-Conference Report from the Eighth International Symposium on the Maillard Reaction, in: Trends Food Sci. Technol., 2006: pp. 324–330. doi:10.1016/j.tifs.2005.11.011.

[38]R.B. Nawale, V.K. Mourya, S.B. Bhise, Non-enzymatic glycation of proteins: A cause for complications in diabetes, Indian J. Biochem. Biophys. 43 (2006) 337–344.

[39]S. Ahmad, Moinuddin, R.H. Khan, A. Ali, Physicochemical studies on glycation-induced structural changes in human igg, IUBMB Life. 64 (2012) 151–156. doi:10.1002/iub.582.

[40]T. Miyata, C. Van Ypersele De Strihou, K. Kurokawa, J.W. Baynes, Alterations in nonenzymatic biochemistry in uremia: Origin and significance of “carbonyl stress” in long-term uremic complications, Kidney Int. 55 (1999) 389–399. doi:10.1046/j.1523-1755.1999.00302.x.

[41]Y.C. LIEN, W.W. NAWAR, Thermal decomposition of some amino acids. Valine, Leucine and lsoleucine, J. Food Sci. 39 (1974) 911–913. doi:10.1111/j.1365-2621.1974.tb07274.x.

[42]M. Dissanayake, L. Ramchandran, O.N. Donkor, T. Vasiljevic, Denaturation of whey proteins as a function of heat, pH and protein concentration, Int. Dairy J. 31 (2013) 93–99. doi:10.1016/j.idairyj.2013.02.002.

[43]J.-S. Chiou, T. Tatara, S. Sawamura, Y. Kaminoh, H. Kamaya, A. Shibata, I. Ueda, The α-helix to β-sheet transition in poly(l-lysine): Effects of anesthetics and high pressure, Biochim. Biophys. Acta - Protein Struct. Mol. Enzymol. 1119 (1992) 211–217. doi:https://doi.org/10.1016/0167-4838(92)90394-S.

[44]M. Yamauchi, M. Sricholpech, Lysine post-translational modifications of collagen, Essays Biochem. 52 (2012) 113–133. doi:10.1042/bse0520113.

[45]W. De Poel, S. Pintea, J. Drnec, F. Carla, R. Felici, P. Mulder, J.A.A.W. Elemans, W.J.P. Van Enckevort, A.E. Rowan, E. Vlieg, Muscovite mica: Flatter than a pancake, Surf. Sci. 619 (2014) 19–24. doi:10.1016/j.susc.2013.10.008.

[46] J. Rodríguez-Hernández, M. Gatti, H.A. Klok, Highly branched poly(L-lysine), Biomacromolecules. 4 (2003) 249–258. doi:10.1021/bm020096k.

[47] R.A. Quirk, W.C. Chan, M.C. Davies, S.J.B. Tendler, K.M. Shakesheff, Poly(L-lysine)-GRGDS as a biomimetic surface modifier for poly(lactic acid), Biomaterials. 22 (2001) 865–872. doi:10.1016/S0142-9612(00)00250-7.

[48] M. Morga, Z. Adamczyk, S. Gödrich, M. Oćwieja, G. Papastavrou, Monolayers of poly-L-lysine on mica--Electrokinetic characteristics., J. Colloid Interface Sci. 456 (2015) 116–24. doi:10.1016/j.jcis.2015.05.044.

[49] P.F. Luckham, J. Klein, Forces between mica surfaces bearing adsorbed polyelectrolyte, poly-L-lysine, in aqueous media, J. Chem. Soc. Faraday Trans. 1. 80 (1984) 865. doi:10.1039/f19848000865.

[50] B. Moores, J. Simons, S. Xu, Z. Leonenko, AFM-assisted fabrication of thiol SAM pattern with alternating quantified surface potential., Nanoscale Res. Lett. 6 (2011) 185. doi:10.1186/1556-276X-6-185.

[51] K.W. Sun, C.C. Chang, Patterned self-assembly of magnetic biomolecules on semiconductor substrates, J. Phys. Chem. Solids. 68 (2007) 1211–1214. doi:10.1016/j.jpcs.2007.01.035.

[52] C.T. Lin, S.L. Chung, C.H. Lin, P.L. Kuo, C.H. Li, The configurable-biomolecular nano pattern controlled by surface potential, in: Microelectron. Eng., 2011: pp. 1785–1788. doi:10.1016/j.mee.2010.12.041.

[53] P. Mesquida, A. Stemmer, Attaching silica nanoparticles from suspension onto surface charge patterns generated by a conductive atomic force microscope tip, Adv. Mater.13(2001)1395–1398.doi:10.1002/1521-4095(200109)13:18<1395

[54] P. Mesquida, A. Stemmer, Guiding self-assembly with the tip of an atomic force microscope, Scanning. 24 (2002) 117–120. doi:10.1002/sca.4950240302.

[55] P. Mesquida, A. Stemmer, Maskless nanofabrication using the electrostatic attachment of gold particles to electrically patterned surfaces, in: Microelectron. Eng., 2002: pp. 671–674. doi:10.1016/S0167-9317(02)00441-0.

[56] J. Huang, F. Kim, A.R. Tao, S. Connor, P. Yang, Spontaneous formation of nanoparticle stripe patterns through dewetting, Nat. Mater. 4 (2005) 896–900. doi:10.1038/nmat1517.

[57] K. Shen, J. Qi, L.C. Kam, Microcontact printing of proteins for cell biology., J. Vis. Exp. (2008) 8–10. doi:10.3791/1065.

[58] A. Offenhäusser, S. Böcker-Meffert, T. Decker, R. Helpenstein, P. Gasteier, J. Groll, M. Möller, A. Reska, S. Schäfer, P. Schulte, A. Vogt-Eisele, Microcontact printing of proteins for neuronal cell guidance, Soft Matter. 3 (2007) 290–298. doi:10.1039/B607615G.

[59]O.S. Makin, L.C. Serpell, Structures for amyloid fibrils, FEBS J. 272 (2005) 5950–5961. doi:10.1111/j.1742-4658.2005.05025.x.

[60]J.D. Sipe, A.S. Cohen, Review: history of the amyloid fibril., J. Struct. Biol. 130 (2000) 88–98. doi:10.1006/jsbi.2000.4221.

[61]M.F.B.G. Gebbink, D. Claessen, B. Bouma, L. Dijkhuizen, H.A.B. Wösten, Amyloids--a functional coat for microorganisms., Nat. Rev. Microbiol. 3 (2005) 333–341. doi:10.1038/nrmicro1127.

[62]E.B. Sawyer, D. Claessen, S.L. Gras, S. Perrett, Exploiting amyloid: how and why bacteria use cross-β fibrils, Biochem. Soc. Trans. 40 (2012) 728–734. doi:10.1042/BST20120013.

[63]R. Wetzel, Kinetics and thermodynamics of amyloid fibril assembly, Acc. Chem. Res. 39 (2006) 671–679. doi:10.1021/ar050069h.

[64]S. Kumar, J. Walter, Phosphorylation of amyloid beta (Abeta) peptides - a trigger for formation of toxic aggregates in Alzheimer's disease, Aging (Albany NY). 3 (2011) 803–812.

[65]C.-C. Lee, A. Nayak, A. Sethuraman, G. Belfort, G.J. McRae, A three-stage kinetic model of amyloid fibrillation., Biophys. J. 92 (2007) 3448–3458. doi:10.1529/biophysj.106.098608.

[66] S. Kumar, J. Walter, Phosphorylation of amyloid beta (A??) peptides - A trigger for formation of toxic aggregates in Alzheimer's disease, Aging (Albany. NY). 3 (2011) 803–812. doi:100362 [pii].

[67] J. Hardy, D. Allsop, Amyloid deposition as the central event in the aetiology of Alzheimer's disease, Trends Pharmacol. Sci. 12 (1991) 383–388. doi:10.1016/0165-6147(91)90609-V.

[68] L.F. Lue, Y.M. Kuo, A.E. Roher, L. Brachova, Y. Shen, L. Sue, T. Beach, J.H. Kurth, R.E. Rydel, J. Rogers, Soluble amyloid beta peptide concentration as a predictor of synaptic change in Alzheimer's disease., Am. J. Pathol. 155 (1999) 853–862. doi:10.1016/S0002-9440(10)65184-X.

[69] J. Näslund, V. Haroutunian, R. Mohs, K.L. Davis, P. Davies, P. Greengard, J.D. Buxbaum, Correlation between elevated levels of amyloid beta-peptide in the brain and cognitive decline., JAMA. 283 (2000) 1571–7.

[70] J. Wang, D.W. Dickson, J.Q. Trojanowski, V.M. Lee, The levels of soluble versus insoluble brain Abeta distinguish Alzheimer's disease from normal and pathologic aging., Exp. Neurol. 158 (1999) 328–337. doi:10.1006/exnr.1999.7085.

[71] S.E. Kahn, D.A. D'Alessio, M.W. Schwartz, W.Y. Fujimoto, J.W. Ensinck, G.J. Taborsky, D. Porte, Evidence of Cosecretion of Islet Amyloid Polypeptide and Insulin by β-Cells, Diabetes . 39 (1990) 634–638. doi:10.2337/diab.39.5.634.

[72]E. Masliah, E. Rockenstein, I. Veinbergs, Y. Sagara, M. Mallory, M. Hashimoto, L. Mucke, beta-amyloid peptides enhance alpha-synuclein accumulation and neuronal deficits in a transgenic mouse model linking Alzheimer's disease and Parkinson' disease., Proc. Natl. Acad. Sci. U. S. A. 98 (2001) 12245–12250. doi:10.1073/pnas.211412398.

[73]L.K. Clinton, M. Blurton-Jones, K. Myczek, J.Q. Trojanowski, F.M. LaFerla, Synergistic Interactions between Abeta, tau, and alpha-synuclein: acceleration of neuropathology and cognitive decline., J. Neurosci. 30 (2010) 7281–7289. doi:10.1523/JNEUROSCI.0490-10.2010.

[74]R. Vasita, D.S. Katti, Nanofibers and their applications in tissue engineering, Int. J. Nanomedicine. 1 (2006) 15–30. doi:10.2147/nano.2006.1.1.15.

[75]D. Gottlieb, S.A. Morin, S. Jin, R.T. Raines, Self-assembled collagen-like peptide fibers as templates for metallic nanowires, J. Mater. Chem. 18 (2008) 3865–3870. doi:10.1039/B807150K.

[76]V. Leung, F. Ko, Biomedical applications of nanofibers, Polym. Adv. Technol. 22 (2011) 350–365. doi:10.1002/pat.1813.

[77]O. Hassan, S. Sajjad, M. Dina, N.-G. Mohsen, Insulin aggregation and amyloid fibril formation accelerated by the presence of the PVP-coated nanoparticles, Clin. Biochem. 44 (2011) S218–S218. doi:10.1016/j.clinbiochem.2011.08.970.

[78]R. Jansen, W. Dzwolak, R. Winter, Amyloidogenic self-assembly of insulin aggregates probed by high resolution atomic force microscopy, Biophys J. 88 (2005) 1344–1353. doi:10.1529/biophysj.104.048843.

[79]P. Westermark, C. Wernstedt, E. Wilander, D.W. Hayden, T.D. O'Brien, K.H. Johnson, Amyloid fibrils in human insulinoma and islets of Langerhans of the diabetic cat are derived from a neuropeptide-like protein also present in normal islet cells, Proc Natl Acad Sci U S A. 84 (1987) 3881–3885.

[80]S. Sardar, S. Pal, S. Maity, J. Chakraborty, U.C. Halder, Amyloid fibril formation by beta-lactoglobulin is inhibited by gold nanoparticles, Int. J. Biol. Macromol. 69 (2014) 137–145. doi:10.1016/j.ijbiomac.2014.05.006.

[81]A. Donald, Aggregation in b-lactoglobulin, Soft Matter. 4 (2008) 1147–1150. doi:10.1039/b800106e.

[82]M.R.H. Krebs, G.L. Devlin, A.M. Donald, Amyloid fibril-like structure underlies the aggregate structure across the pH range for ??-lactoglobulin, Biophys. J. 96 (2009) 5013–5019. doi:10.1016/j.bpj.2009.03.028.

[83]D. Hamada, C.M. Dobson, A kinetic study of beta-lactoglobulin amyloid fibril formation promoted by urea., Protein Sci. 11 (2002) 2417–2426. doi:10.1110/ps.0217702.

[84] S. Budavari, The Merck Index: An Encyclopedia of Chemicals, Drugs, and Biologicals, Ann. Intern. Med. 113 (2006) 487-a-.

[85] S. Wohlfart, S. Gelperina, J. Kreuter, Transport of drugs across the blood-brain barrier by nanoparticles, J. Control. Release. 161 (2012) 264–273. doi:10.1016/j.jconrel.2011.08.017.

[86] E. Araya, I. Olmedo, N.G. Bastus, S. Guerrero, V.F. Puntes, E. Giralt, M.J. Kogan, Gold Nanoparticles and Microwave Irradiation Inhibit Beta-Amyloid Amyloidogenesis, Nanoscale Res. Lett. 3 (2008) 435–443. doi:10.1007/s11671-008-9178-5.

[87] S. Hsieh, C. Chang, H. Chou, Gold nanoparticles as amyloid-like fibrillogenesis inhibitors, Colloids and Surfaces B-Biointerfaces. 112 (2013)525–529. doi:10.1016/j.colsurfb.2013.08.029.

[88] S. Linse, C. Cabaleiro-Lago, W.-F. Xue, I. Lynch, S. Lindman, E. Thulin, S.E. Radford, K.A. Dawson, Nucleation of protein fibrillation by nanoparticles, Proc Natl Acad Sci U S A. 104 (2007) 8691–8696. doi:10.1073/pnas.0701250104.

[89] S. Palmal, A.R. Maity, B.K. Singh, S. Basu, N.R. Jana, N.R. Jana, Inhibition of Amyloid Fibril Growth and Dissolution of Amyloid Fibrils by Curcumin-Gold Nanoparticles, Chem. Eur. J. 20 (2014) 6184–6191. doi:10.1002/chem.201400079.

[90] M.J. Kogan, N.G. Bastus, R. Amigo, D. Grillo-Bosch, E. Araya, A. Turiel, A.

Labarta, E. Giralt, V.F. Puntes, Nanoparticle-mediated local and remote manipulation of protein aggregation, Nano Lett. 6 (2006) 110–115. doi:10.1021/nl0516862.

[91] H. Skaat, M. Sorci, G. Belfort, S. Margel, Effect of maghemite nanoparticles on insulin amyloid fibril formation: Selective labeling, kinetics, and fibril removal by a magnetic field, J. Biomed. Mater. Res. Part A. 91A (2009) 342–351. doi:10.1002/jbm.a.32232.

[92] E.P. O'Brien, J.E. Straub, B.R. Brooks, D. Thirumalai, Influence of Nanoparticle Size and Shape on Oligomer Formation of an Amyloidogenic Peptide, J. Phys. Chem. Lett. 2 (2011) 1171–1177. doi:10.1021/jz200330k.

[93] M. Chanana, M.A. Correa-Duarte, L.M. Liz-Marzan, Insulin-coated gold nanoparticles: a plasmonic device for studying metal-protein interactions, Small. 7 (2011) 2650–2660. doi:10.1002/smll.201100735.

[94] Y.D. Álvarez, J.A. Fauerbach, J. V Pellegrotti, T.M. Jovin, E.A. Jares-Erijman, F.D. Stefani, Influence of Gold Nanoparticles on the Kinetics of α-Synuclein Aggregation, Nano Lett. 13 (2013) 6156–6163. doi:10.1021/nl403490e.

[95] Y.H. Liao, Y.J. Chang, Y. Yoshiike, Y.C. Chang, Y.R. Chen, Negatively charged gold nanoparticles inhibit Alzheimer's amyloid-beta fibrillization, induce fibril dissociation, and mitigate neurotoxicity, Small. 8 (2012) 3631–3639. doi:10.1002/smll.201201068.

[96] S.H. Brewer, W.R. Glomm, M.C. Johnson, M.K. Knag, S. Franzen, Probing BSA binding to citrate-coated gold nanoparticles and surfaces, Langmuir. 21 (2005) 9303–9307. doi:10.1021/la050588t.

[97] Q. Ma, G. Wei, X. Yang, Influence of Au nanoparticles on the aggregation of amyloid-β-(25-35) peptides., Nanoscale. 5 (2013) 10397–403. doi:10.1039/c3nr02973e.

[98] I.T. Lucas, S. Durand-Vidal, E. Dubois, J. Chevalet, P. Turq, Surface Charge Density of Maghemite Nanoparticles: Role of Electrostatics in the Proton Exchange, J. Phys. Chem. C. 111 (2007) 18568–18576. doi:10.1021/jp0743119.

[99] H. Skaat, G. Shafir, S. Margel, Acceleration and inhibition of amyloid-β fibril formation by peptide-conjugated fluorescent maghemite nanoparticles, J. Nanoparticle Res. 13 (2011) 3521–3534. doi:10.1007/s11051-011-0276-4.

[100] J.A. Loureiro, S. Rocha, C. Pereira Mdo, Charged surfactants induce a non-fibrillar aggregation pathway of amyloid-beta peptide, J Pept Sci. 19 (2013) 581–587. doi:10.1002/psc.2535.

[101] K.L. Berkowski, K.N. Plunkett, Q. Yu, J.S. Moore, Introduction to Photolithography: Preparation of Microscale Polymer Silhouettes, J. Chem. Educ. 82 (2005) 1365–1369. doi:10.1021/ed082p1365.

[102] R. Leuschner, G. Pawlowski, Photolithography, in: Handb. Semicond. Technol., 2000: pp. 177–263. doi:10.1002/9783527621828.ch4.

[103] H.O. Jacobs, H.F. Knapp, A. Stemmer, Practical aspects of Kelvin probe force microscopy, Rev. Sci. Instrum. 70 (1999) 1756–1760. doi:10.1063/1.1149664.

[104] P. Mesquida, D.L. Ammann, C.E. MacPhee, R.A. McKendry, Microarrays of peptide fibrils created by electrostatically controlled deposition, Adv. Mater. 17 (2005) 893–897. doi:10.1002/adma.200401229.

[105] N. Anand, P. Ramudu, K.H.P. Reddy, K.S.R. Rao, B. Jagadeesh, V.S.P. Babu, D.R. Burri, Gold nanoparticles immobilized on lipoic acid functionalized SBA-15: Synthesis, characterization and catalytic applications, Appl. Catal. A Gen. 454 (2013) 119–126. doi:10.1016/j.apcata.2013.01.006.

[106] I. Turcu, I. Zarafu, M. Popa, M. Chifiriuc, C. Bleotu, D. Culita, C. Ghica, P. Ionita, Lipoic Acid Gold Nanoparticles Functionalized with Organic Compounds as Bioactive Materials, Nanomaterials. 7 (2017) 43. doi:10.3390/nano7020043.

[107] R. Ginter, Ultraviolet and visible spectroscopy, Spectrochim. Acta Part A Mol. Biomol. Spectrosc. 53 (1997) 2189. doi:10.1016/S1386-1425(97)00090-5.

[108] P.S. Pourhosseini, A.A. Saboury, F. Najafi, M.N. Sarbolouki, Interaction of insulin with a triblock copolymer of PEG-(fumaric-sebacic acids)-PEG:

Thermodynamic and spectroscopic studies, Biochim. Biophys. Acta Proteins Proteomics. 1774 (2007) 1274–1280. doi:10.1016/j.bbapap.2007.08.007.

[109] Determination of Insulin Concentration in Camel Milk Using Ultra Violet Visible Absorption Spectroscopy, J. Food Biosci. Technol. 03 (2013). http://jfbt.srbiau.ac.ir/?_action=articleInfo&article=1376.

[110] K. Kaja, N. Chevalier, D. Mariolle, F. Bertin, G. Feuillet, A. Chabli, E.M. Secula, D.G. Seiler, R.P. Khosla, D. Herr, C. Michael Garner, R. McDonald, A.C. Diebold, Effects of Experimental Parameters on the Work Function Measurement: A Kelvin Force Microscopy Study, AIP Conf. Proc. 1173 (2009) 224–228. doi:10.1063/1.3251225.

[111] L. Liu, R. Wu, J. Zhang, N. Shang, P. Li, D-ribose interferes with quorum sensing to inhibit biofilm formation of Lactobacillus paraplantarum L-ZS9, Front. Microbiol. 8 (2017). doi:10.3389/fmicb.2017.01860.

[112] B. Rizzuti, B. Zappone, M.P. De Santo, R. Guzzi, , Langmuir. 26 (2010) 1090–1095. doi:10.1021/la902464f.

[113] Z.H. Wu, X.H. Zhang, X.D. Zhang, J.L. Sun, Y.M. Dong, J. Hu, In situ AFM observation of BSA adsorption on HOPG with nanobubble, Chinese Sci. Bull. 52 (2007) 1913–1919. doi:10.1007/s11434-007-0288-8.

[114] H.T.M. Phan, S. Bartelt-Hunt, K.B. Rodenhausen, M. Schubert, J.C. Bartz, Investigation of bovine serum albumin (BSA) attachment onto self-assembled

monolayers (SAMs) using combinatorial quartz crystal microbalance with dissipation (QCM-D) and spectroscopic ellipsometry (SE), PLoS One (2015). doi:10.1371/journal.pone.0141282.

[115] A. Podestà, G. Tiana, P. Milani, M. Manno, Early events in insulin fibrillization studied by time-lapse atomic force microscopy, Biophys. J. 90 (2006) 589–597. doi:10.1529/biophysj.105.068833.

[116] K. Engelhardt, M. Lexis, G. Gochev, C. Konnerth, R. Miller, N. Willenbacher, W. Peukert, B. Braunschweig, pH Effects on the Molecular Structure of β-Lactoglobulin Modified Air–Water Interfaces and Its Impact on Foam Rheology, Langmuir. 29 (2013) 11646–11655. doi:10.1021/la402729g.

[117] P. Rubio-Pereda, J.G. Vilhena, N. Takeuchi, P.A. Serena, R. Pérez, Albumin (BSA) adsorption onto graphite stepped surfaces, J. Chem. Phys. 146 (2017) 214704. doi:10.1063/1.4984037.

[118] R.S. Kane, S. Takayama, E. Ostuni, D.E. Ingber, G.M. Whitesides, Patterning proteins and cells using soft lithography, Biomaterials. 20 (1999) 2363–2376. doi:10.1016/S0142-9612(99)00165-9.

[119] T. Plecenik, S. Robin, M. Gregor, M. Truchly, S. Lang, A. Gandhi, M. Zahoran, F. Laffir, T. Soulimane, M. Vargova, G. Plesch, P. Kus, A. Plecenik, S.A.M. Tofail, Directly created electrostatic micro-domains on hydroxyapatite: Probing with a

Kelvin Force probe and a protein, in: J. Mater. Sci. Mater. Med., 2012: pp. 47–50. doi:10.1007/s10856-011-4498-x.

[120] E. Macarena Blanco, M.A. Horton, P. Mesquida, Simultaneous investigation of the influence of topography and charge on protein adsorption using artificial nanopatterns, Langmuir. 24 (2008) 2284–2287. doi:10.1021/la702957f.

[121] A.K. Sinensky, A.M. Belcher, Label-free and high-resolution protein/DNA nanoarray analysis using Kelvin probe force microscopy, Nat. Nanotechnol. 2 (2007) 653. http://dx.doi.org/10.1038/nnano.2007.293.

[122] W. Cai, N. Yao, Dynamic nano-triboelectrification using torsional resonance mode atomic force microscopy, Sci. Rep. 6 (2016). doi:10.1038/srep27874.

[123] Y.S. Zhou, Y. Liu, G. Zhu, Z.H. Lin, C. Pan, Q. Jing, Z.L. Wang, In situ quantitative study of nanoscale triboelectrification and patterning, Nano Lett. 13 (2013) 2771–2776. doi:10.1021/nl401006x.

[124] R.W. Herfst, P.G. Steeneken, J. Schmitz, A.J.G. Mank, M. Van Gils, Kelvin probe study of laterally inhomogeneous dielectric charging and charge diffusion in RFMEMS capacitive switches, in: IEEE Int. Reliab. Phys. Symp. Proc., 2008: pp. 492–495. doi:10.1109/RELPHY.2008.4558935.

[125] A. Elajnaf, P. Carter, G. Rowley, The Effect of Relative Humidity on Electrostatic Charge Decay of Drugs and Excipient Used in Dry Powder Inhaler

Formulation, Drug Dev. Ind. Pharm. 33 (2007) 967 974.doi:10.1080/03639040601134207.

[126] G. Zhao, Q. Tan, L. Xiang, D. Cai, H. Zeng, H. Yi, Z. Ni, Y. Chen, Structure and properties of water film adsorbed on mica surfaces, J. Chem. Phys. 143 (2015). doi:10.1063/1.4930274.

[127] A.K. K. WAIZUMI, S. NAWATA, Effects of pH and Particle Size on Zeta Potential of Insulin Crystals in their Growth Solutions, Int. J. Microgravity Sci. Appl. (2008) 593.

[128] W. Lee, H. Lee, Y. Choi, K.S. Hwang, S.W. Lee, G. Lee, D.S. Yoon, Nanoelectrical characterization of amyloid-β-42 aggregates via Kelvin probe force microscopy, Macromol. Res. (2017). doi:10.1007/s13233-017-5155-0.